Generalized Likelihood Commutation Signaling for Indoor Communications

Kai Ming Cheung, B. Eng.

Department of Electrical Engineering

McGill University, Montréal

October, 1992.

A Thesis submitted to the Faculty of Graduate Studies and Research
in partial fulfillment of the requirements for the degree of Master of Engineering

©Kai Ming Cheung, 1992

To my parents

Abstract

Using the Generalized Likelihood (GL) principle, a receiver structure of relatively low complexity is developed for indoor wireless communication channels. The receiver, which is robust against channel models, provides a performance close to optimal in the GL sense. The GL receiver combines naturally both channel estimation and data detection and therefore it is ideal for transmission systems which operate over unknown channels. The effects of multipath induced intersymbol interference (ISI) on the channel estimation process are mitigated by employing the technique of commutation signaling. In addition, by union bounding technique, it is shown that with sufficient bandwidth expansion, the probability of having significant ISI on the data detection process can be made arbitrarily small. Furthermore, a simplified GL receiver is proposed to combine binary commutation signaling with DPSK modulation scheme. The error performance of such a receiver under perfect channel estimation over multipath Rayleigh and Lognormal fading channels is presented and the performance degradation due to incorrect channel estimation is investigated via computer simulations.

Résumé

Basée sur le principe de vraisemblance généralisée (VG), une structure de récepteur de complexité relativement faible est developpée pour la radiocommunication dans des canaux intérieurs. Ce récepteur, robuste par rapport aux modèles de canaux, a une performance presque idéale en terme de VG. Le récepteur à base de VG combine de façon naturelle estimation de canal ainsi que détection des données, et par conséquent, il est idéal pour des systèmes de transmission qui opèrent dans des canaux inconnus. Les effets de l'interférence entre symboles (IES) induites par multi-routes au procédé d'estimation du canal sont atténuées par l'emploi de techniques de signaux commutés. À l'aide de technique de borne à union, il est démontré également qu'en utilisant une expansion de largeur de bande suffisante, la probabilité d'avoir de l'IES lors du procédé de detection des données peut-être réduite de façon arbitraire. De plus, un récepteur à base de VG simplifié est proposé et combine les signaux commutés binaires et la technique de modulation DPSK. La performance d'erreur de ce récepteur dans des conditions parfaites d'estimation de canal est présentée lorsque le canal exhibe des caractéristiques Rayleigh multi-routes ainsi que Lognormal. De même, la dégradation de performance dûe a une estimation incorrecte de canal est étudiée à l'aide de simulation par ordinateur.

Acknowledgement

I would like to express my most sincere gratitude and appreciation to my supervisor, Prof. Harry Leib for his initiation, persistent interest, continuous encouragement, patient guidance and support throughout the course of this research and in the preparation of this thesis. I also thank him for his understanding and concern during moments of my personal problems.

I also wish to acknowledge the administration of Canadian Institute for Telecommunications Research (CITR) on Project B-2.3 for the financial assistantships provided without which this research would not have done.

I would like to extend my deepest thanks to my family especially my parents for their continuous encouragement and support throughout my studies.

Thanks are extended to all my friends in the Communications group for their friendship. My knowledge in the field of Communications has been enriched by their readiness to share their expertise in their areas of specialty and provide me help whenever they could. It has been my pleasure and privilege to be associated with them. Special thanks are due to Nagi Abboud who helped me translating the abstract into French.

I wish to acknowledge Information and Network Systems Laboratory (INSL) for providing the computer facilities and Telecommunications and Signal Processing (TSP) Laboratory for using the workstations where most of the computer simulations were performed.

Last but not least, I would like to thank all my best friends for their support. Their companionship during my limited leisure time will always remain cherished.

Contents

List of Figures

List of Symbols

Symbol		Meaning
t	:	Time in seconds
$\tilde{h}(t)$	:	Channel impulse response
α_i	:	Amplitude of the i-th delayed path
θ_i	:	Phase shift of the i-th delayed path
τ_i	:	Propagation time delay of the i-th delayed path
$\delta(t)$	:	Dirac delta function
$\tilde{s}(t)$	:	Transmitted signal
$\tilde{n}(t)$	:	Additive white Gaussian noise
$\tilde{r}(t)$	:	Received input signal
R_i	:	Rayleigh-distributed factor of the i-th tap
L_i	:	Lognormally-distributed factor of the i-th tap
W_i	:	Weight coefficient of the i-th tap
T_i	:	Arrival time of the i-th cluster
τ_{ij}	:	Arrival time of the i-th ray as measured from the beginning of the j-th
	:	cluster or the difference of τ_i and τ_j.
α_{ij}	:	Amplitude of the i-th ray of the j-th cluster
H_1	:	Hypothesis 1
H_0	:	Hypothesis 0
r_i	:	The i-th observable
$\mathbf{r}$	:	An observable vector
$\Lambda(\mathbf{r})$	:	Likelihood ratio

Symbol		Meaning
$p_{\mathbf{R}\|H_1}(\mathbf{r})$	:	Conditional probability density induced by H_1
$p_{\mathbf{R}\|H_0}(\mathbf{r})$	:	Conditional probability density induced by H_0
η	:	Threshold of the likelihood ratio test
A_i	:	The i-th random parameter
$\mathbf{A}$	:	A vector of random parameters
$p_{\mathbf{A}\|H_i}(\mathbf{a})$	:	Joint prior probability density function of $\mathbf{A}$ on H_i
$\hat{\mathbf{A}}$	:	Maximum of $\mathbf{A}$
$\Lambda_{GL}(\mathbf{r})$	:	Generalized Likelihood ratio
$\mathbf{A}_i$	:	A vector of random parameters on H_i
$\hat{\mathbf{A}}_i$	:	Maximum Likelihood estimates on $\mathbf{A}_i$
T_o	:	Observation interval
$*$	:	Convolution operator or conjugate operator
I	:	Number of delayed paths in the channel impulse response
N_o	:	Noise power in [Watts/Hz]
$n_R(t)$	:	Real component of the noise
$n_I(t)$	:	Imaginary component of the noise
C	:	A positive constant
T_c	:	Autocorrelation time or width
W	:	Transmitted signal bandwidth
$\hat{\alpha}_i$	:	Maximum Likelihood estimate of α_i
E_i	:	Symbol energy
$\hat{\theta}_i$	:	Maximum Likelihood estimate of θ_i
$\hat{\tau}_i$	:	Maximum Likelihood estimate of τ_i
z	:	A decision variable of the GL receiver
T_D	:	Time-delay module
J	:	Number of taps on the RAKE combiner
Δ	:	Multipath *time delay spread*

Symbol		Meaning
Δ_i	:	Time delay between the i-th and $(i+1)$-th delayed path
T	:	Symbol of signaling interval
M	:	Number of signal points in constellation
N	:	Number of distinct signaling sets or number of commutation signals
R	:	Information bit rate
$\tilde{u}(t)$	:	Shaping filter impulse response
$\tilde{u}^*(-t)$	:	Matched filter impulse response to $\tilde{u}(t)$
$\Phi(t)$	:	Autocorrelation function
$\tilde{y}(t)$	:	Output signal of the matched filter $\tilde{u}^*(-t)$ for single pulse transmission
$\Phi_u(t)$	:	Autocorrelation function of the signal $\tilde{u}(t)$
$\tilde{g}(t)$	:	Maximum gain RAKE combiner impulse response
$\tilde{z}(t)$	:	Output signal of the maximum gain or equal weight RAKE combiner
P	:	Probability of having significant ISI at the output of the RAKE combiner
λ	:	The Poisson process rate
K	:	The integral number of Δ/T
$\tilde{\Delta}$	:	The integral number of Δ
G_p	:	The bandwidth expansion factor or the processing gain
$\tilde{I}_{max}$	:	Average number of channel delayed paths
$\tilde{P}$	:	Upper bound of the probability of having significant ISI
L	:	Order of antenna diversity
$\tilde{x}(t)$	:	Output signal of the square-law device
$\tilde{v}(t)$	:	Output signal of the matched filter $\tilde{u}^*(-t)$ for sequential transmissions
$\tilde{f}(t)$	:	Equal weight RAKE combiner impulse response
$z_1(t)$	:	Sum of the square of $\Phi_u(t)$ with different delays
$z_2(t)$	:	Sum of the multiplication of $\Phi_u(t)$ with its conjugate of different delays
P_1	:	Probability of having significant ISI in $z_1(t)$
P_2	:	Probability of having significant ISI in $z_2(t)$

Symbol		Meaning
T_c'	:	Width of the square of $\Phi_u(t)$
$\tilde{P}_2$	:	Upper bound of P_2
$a(k)$	:	Binary data sequence
$b(k)$	:	Differentially encoded binary data sequence
$\tilde{u}_m(t)$	:	The m-th commutation signal
$\tilde{s}_m(t)$	:	The m-th transmitted signal
$Z_m{}^-$	:	A decision variable of GL receiver on H_0
$Z_m{}^+$	:	A decision variable of GL receiver on H_1
$\hat{\tau}_i^-$	:	The estimate of the i-th path delay on H_0
$\hat{\tau}_i^+$	:	The estimate of the i-th path delay on H_1
$\hat{\tau}_i$	:	The estimate of the i-th path delay
$z_m(t)$	:	Output signal of the matched filter $\tilde{u}_m^*(-t)$
$z_m{}^-(t)$	:	Output signal of the square-law device on H_0
$z_m{}^+(t)$	:	Output signal of the square-law device on H_1
E_b	:	Bit energy
α	:	Attenuation factor
γ_b	:	Signal-to-Noise ratio per bit
$\overline{\gamma}_b$	:	Average signal-to-noise ratio per bit
P_e, $P_b(\gamma_b)$	:	Probability of error
$\overline{\gamma}_c$	:	Average signal to-noise ratio per channel
$p(x)$	:	Probability density function of normally-distributed random variable x
μ	:	Mean of a probability distribution
σ^2	:	Variance of a probability distribution
E[x]	:	Expectation of x
e^x, $exp(x)$	:	Exponent of x
c	:	A positive constant E_b/N_o
$f(x)$	:	Equation of a straight line

Symbol		Meaning
a	:	Slope of a straight line
b	:	y-intercept of a straight line
P_U	:	Upper-bounded error probability
ϵ	:	A positive number
$Q(x)$	:	Error function
P_L	:	Lower-bounded error probability
x_i	:	A normally-distributed random variable
$p(x_i)$	:	Probability density function of normally-distributed random variable x_i
$p(x_0, .., x_{L-1})$	:	Joint probability density function of the random variable $x_o, .., x_{L-1}$
μ_i	:	Mean of the probability distribution of the random variable x_i
σ_i	:	Variance of the probability distribution of the random variable x_i

Chapter 1

Introduction

Owing to the increasing demand for personal communication services in recent years, the use of radio for wireless access in many indoor environments, such as within an office building, a factory, a supermarket, etc, has been widely investigated. Wireless access not only provides the users with true mobility by not having the wires attached to particular locations, but also avoids all the expensive rewiring when changing or installing other communications services in existing indoor environments. However, a wireless indoor radio system has to cope with harsh communication channels. The multiple paths propagations phenomenon in indoor environments can be a major impairment to radio communications. This impairment is due to multipath fading and multipath induced intersymbol interference (ISI). As a result, a complete knowledge of the channel characteristics likely to be encountered is required to design a reliable indoor wireless communications system.

In order to gain some insights into the wideband propagation characteristics of different indoor environments, many researches pertaining to the indoor or urban multipath propagation measurements [1]-[5], [26]-[29] and modeling of the indoor channel [6]-[8] using radio signals at different carrier frequencies have been done. Based on the measurements results on the channel parameters such as the signal power variations and multipath delays, statistical models of the indoor radio channel were developed. As a result, the statistical behaviour of the channel parameters becomes the main concern when designing optimal indoor communications schemes and it is often that an *a-priori* probability model for the unknown parameters which determine the channel impulse response is needed.

The Bayesian approach has been considered as one of the decision strategies for signal detection when the prior probability distributions of the parameters are available [10]. The extend to which a Bayesian approach may yield good results depends on the availability of good *a-priori* models. In this work, we propose the use of the Generalized Likelihood (GL) principle to obtain receiver structures which are robust against channel models for indoor communications. Therefore, an *a-priori* probability model for the channel parameters is not required. In addition, these receivers possess a relative low-complexity structure which employs the square-law equal weight combining. Unlike the maximum gain combining which requires the estimations of the signal amplitude, phase and multipath propagation delays, the square-law equal weight combining requires only the multipath delays estimates. This advantage further advocates the use of GL receiver for indoor applications since phase tracking is difficult to perform in multipath fading channels.

As the GL principle combines naturally both channel estimation and data detection, one of the difficulties that the receiver encounters is the estimation of the multipath delays from the received signal. The existence of multipath induced ISI especially in high-rate transmissions may complicate the channel multipath estimation process. However, by employing the technique of commutation signaling [11], the effects of multipath induced ISI on the channel estimation process can be reduced.

Adaptive equalization techniques have been used for combating ISI effects on data detection for communication over multipath fading channels such as those found in HF and troposcatter systems [12] where bandwidth expansion is not possible. M-ary signaling which enlarges the transmission alphabet can also be used to avoid ISI. However, it usually leads to complicated receiver structures When bandwidth expansion is possible, the inherent capability of the RAKE receiver to suppress multipath induced ISI has been pointed out in [14]. In this work, we investigate this issue, and consider the tradeoff between the ISI suppression capability of general RAKE receivers and bandwidth expansion. In addition, we also consider the ISI effects on the GL receiver when commutation signaling is employed.

Carrier phase tracking is a difficult task in many communication systems especially over multipath fading channels. Furthermore, at extremely high frequencies, oscillators may suffer from significant phase noise, making phase coherent communications very difficult. Therefore, we propose to combine binary commutation signaling with differential phase shift keyed (DPSK) modulation as the signaling scheme for the GL receiver. The structure of a simplified GL receiver for this signaling scheme is derived and shown to employ differentially coherent detection. In order to evaluate the performance of the simplified GL receiver for differentially encoded binary commutation signaling under perfect channel estimation, we model the indoor radio transmission medium as a Rayleigh-distributed and a Lognormally-distributed fading channels It is obvious that incorrect channel estimation may cause degradation in the performance of the receiver, therefore, in this work, we also investigate the effects of multipath time delay estimation errors.

The organization of this thesis is as follows. Chapter 2 presents different indoor channel models obtained from the results of many indoor multipath propagation measurements. The disparity of these models shows the need for the GL approach Then, the structure of the GL receiver for indoor radio channels is derived. In Chapter 3, the technique of commutation signaling for mitigating the effects of multipath induced ISI on channel estimation process is described, and the tradeoff between the ISI suppression capability of general RAKE receivers and GL receivers with commutation signaling and bandwidth expansion is presented. Chapter 4 shows how the commutation signaling scheme for GL receiver can be integrated with differential phase keyed (DPSK) modulation, reveals the advantages of such an implementation, and derives a simplified GL receiver structure. In Chapter 5, the performance of the simplified GL receiver with differentially encoded binary commutation signaling over Rayleigh or Lognormal fading channels is presented and the performance degradation due to incorrect channel estimation is explored. Finally, Chapter 6 presents the conclusions. A bibliography and two appendices are then followed. Appendix A presents an overview of the simulation program with perfect channel estimation. Appendix B presents an overview of the simulation program under practical channel estimation, that is, when estimation errors are taken into account.

Chapter 2

Generalized Likelihood Demodulation over Indoor Channels

This chapter considers the concept of the Generalized Likelihood test for demodulation over indoor radio channels. Section 2.1 gives a survey of different indoor channel models developed from the results of indoor multipath propagation measurements using radio signal at different carrier frequencies such as 900 MHz, 1.5 GHz and 20-60 GHz. Based on the channel model described in section 2.1, the structure of the Generalized Likelihood receiver for indoor radio channel is derived in section 2.2. It is shown that the Generalized Likelihood concept advocates the use of square-law equal weight combining for the exploitation of multipath diversity.

2.1 Indoor Channel Models

Wireless communication systems have to operate in very harsh radio environments, characterized by fading multipath channels. As a result of multipath propagation, the received signal consists of many echoes having different and randomly varying delays. amplitudes and carrier phases. One characteristic of a multipath radio environment is the *time delay spread* introduced in the signal which is transmitted through the channel. The channel *time delay spread* is the time delay between the first and last significantly large echoes. One effect of multipath on the indoor radio communication systems is signal fading. Signal fading is a result of the time variations in the phases of the Fourier components delivered to the receiving antenna via various paths Since the total received signal is a vector sum of each of the delayed components, when they add destructively, the resulting received signal is small or practically zero. On the other hand, the received signal is becoming large when the delayed Fourier components add constructively. Consequently, this amplitude attenuations or variations in the received Fourier components cause the fading phenomenon.

Another effect of multipath is time dispersion or frequency selectivity. Frequency selective distortion occurs when the bandwidth of the transmitted signal is greater than the coherence bandwidth, the reciprocal of the multipath *time delay spread*, of the channel. In this case, two Fourier components with frequency separation larger than the coherence bandwidth will be attenuated differently and the channel is then called *frequency-selective*. Wideband transmission is appropriate for this type of channel because diversity advantage can be obtained. In wideband transmission, the transmitted signal is normally having a bandwidth much greater than the coherence bandwidth of the channel. This wideband signal is then able to resolve the multipath signal components which provide the receiver with several independently fading signal replicas which can be combined. Therefore, the use of wideband signaling can also be considered as another way to obtain frequency diversity. On the other hand, if the transmitted signal bandwidth is smaller than the coherence bandwidth of the channel, the transmitted signal will not be severely distorted by the channel; it will only be attenuated. In this case, the channel is called *frequency-nonselective* Thus, with a multipath channel, if the transmitted signal bandwidth is less than the coherence bandwidth, then it can be modelled as *frequency-nonselective* fading. Both the signal fading and frequency selectivity are considered as two different types of distortion due to the multipath effects on the indoor wireless communication systems. The signal fading is mainly caused by the time variations of the channel while the frequency selectivity is related to the bandwidth of the transmitted signal relative to the coherence bandwidth of the channel or equivalently, the multipath *time delay spread* of the channel.

The fading multipath nature of the indoor radio channel imposes fundamental limitations on the performance of the communication systems. In order to properly estimate the performance limits, a parametric channel model is useful. A common technique of estimating multipath channel parameters is channel sounding [15]-[17] The channel sounding technique is used in both narrowband and wideband channel characterization For narrowband transmissions where the reciprocal of the transmitted signal bandwidth is much greater than the multipath *time delay spread*, the channel characterization is usually done by exciting the channel with an unmodulated single tone radio frequency carrier. From the measurement results of the variations in the amplitude and phases of the received signal, an appropriate model is then derived to describe the behaviour of the channel. In the case of wideband transmissions, there are several wideband channel sounding techniques. One of them is the periodic pulse sounding method in which a short duration, periodic pulse is used to excite the channel. The period of the sounding pulse is chosen such that the time-varying response of the propagation paths can be observed and all echoes due to multipath have faded out between successive impulses The received signal is simply the convolution of the channel impulse response with the sounding pulse. This technique results in a series of snapshots, in real time, of the channel impulse response. Since pulse transmitters are generally peak power limited, one of the major limitations of the periodic pulse sounding technique is the high peak-to-mean power requirement as needed for detecting weak echoes. Other sounding methods which provide pulse compression can overcome this limitation. With pulse compression sounding, the channel is excited with a maximal-length pseudorandom binary sequence which possesses the characteristics of white noise. After pulse compression of the receiver, the channel impulse response convolved with the sounding pulse, autocorrelation is obtained. Because of the excellent periodic autocorrelation properties of the pseudorandom sequences [18], pulse compression is commonly employed for channel sounding purposes and it is implemented via two techniques. One technique known as the matched-filtering uses a filter which is matched to the sounding waveform to produce pulse compression. The matched filter is usually realized by a surface acoustic wave (SAW) device Since the matched filter is matched to a particular pseudorandom sequence used in the transmitter, the local generation of the sequence at the receiver is unnecessary. Thus, this asynchronous sounding technique reduces the complexity of the receiver. In addition, this method operates in real time because the matched filter output gives a series of snapshots of the channel response and a one-to-one mapping of time delays in the time domain. However, because of the inherent deficiencies in the devices such as multiple reflections and scattering of the surface acoustic waves, the performance of practical SAW devices is then limited. Another pulse compression sounding technique employs swept time-delay crosscorrelation. This method uses correlation instead of convolution to obtain pulse compression. The correlation processing is practically done with a single correlator, using a swept time-delay correlation technique in such a way that the incoming signal is correlated with a specific pseudorandom sequence identical to the one being transmitted, but clocked at a slightly slower frequency. The difference of the clock rates at the transmitter and receiver produces time-scaling of the crosscorrelation where the scaling factor is the ratio of the highest clock rate to the frequency difference.

The indoor channel can be characterized by a multipath fading channel. As stated earlier, when the transmitted signal bandwidth is smaller than the coherence bandwidth of the multipath channel, the received signal is not distorted severely by the channel and it appears at the receiver via a single fading path. As a result, the multipath components in the received signal are not resolvable. However, if the transmitted signal bandwidth is expanded such that it becomes larger than the coherence bandwidth of the multipath channel, it has been shown in [19] that the multipath components in the received signal are then resolvable with a resolution in time delay of the reciprocal of the transmitted signal bandwidth. Therefore, two paths are resolvable when the time difference between them is greater than the reciprocal of the transmitted signal bandwidth. With the usage of wideband signaling, more paths can be resolvable than the case when narrowband signaling is employed. The indoor channel is often modelled as a linear filter with the complex, lowpass impulse response expressed as [19]:

$$\tilde{h}(t) = \sum_{i=0}^{\infty} \alpha_i e^{j\theta_i} \delta(t - \tau_i) \tag{2.1}$$

where α_i is the amplitude of the ith resolvable path, τ_i is the propagation time delay, θ_i is the associated phase shifts, i is the path index and in principle, is extending from 0 to ∞ ,$\delta(\cdot)$ is simply the Dirac delta function and $j = \sqrt{-1}$. The model of the indoor channel is depicted in Fig. 2.1. It can be employed for obtaining the channel response to the transmission of any signal $\tilde{s}(t)$ by the convolution of $\tilde{s}(t)$ and $\tilde{h}(t)$. As a result of the movement of people and equipment around the indoor environment, the amplitude attenuations $\{\alpha_i\}$, propagation delays $\{\tau_i\}$ and phases $\{\theta_i\}$ are randomly time-varying functions and these parameters must be described in terms of some random processes. However, since these parameters are changing slowly as compared to any signaling rates to be considered, they will be therefore considered as virtually time-invariant random variables.

In order to design optimum transceivers for indoor radio communication systems, we need an *a-priori* probability model for the parameters which determine the channel impulse response. The statistical behaviour of the set of random variables $\{\alpha_i\}$, $\{\tau_i\}$ and $\{\theta_i\}$ has become the primary motivating factor behind many researches in recent years

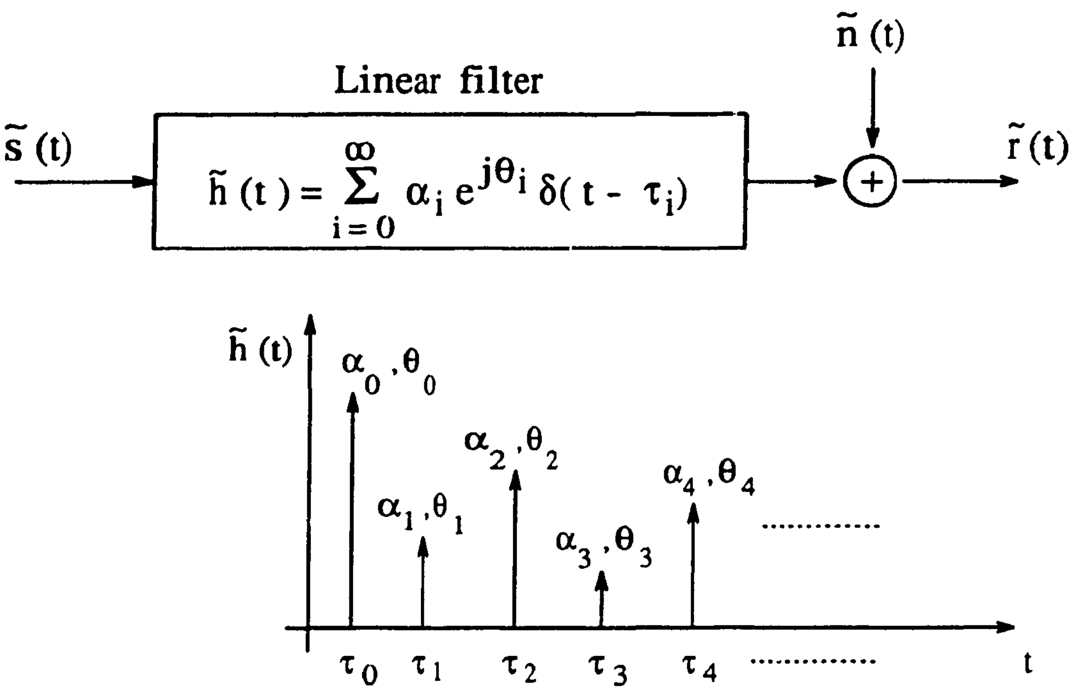

Figure 2.1: The model of the indoor channel.

A reasonable assumption which has long been universally accepted is that the phases $\{\theta_i\}$ of the various paths are assumed *a priori* to be a set of statistically independent random variables which are uniformly distributed over the range $(0,2\pi)$ [20]-[22]. Therefore, the measurement of $\{\theta_i\}$ was not carried out in most of the multipath propagation experiments.

Various measurements for the signal attenuation of radio waves propagating into buildings [1] or within buildings [2]-[3] at 900 MHz reported that the spatial distribution of signal strength adhered closely to Rayleigh fading characteristics. Time delay spread measurements of 850 MHz wideband radio signals due to multipath propagation in and around building environments were carried out and reported by Devasirvatham [4]-[5]. These measurements showed that the root mean square (RMS) time delay spread was in the order of magnitude of few hundred nanoseconds and was smaller in case of the presence of a LOS path between the transmitter and receiver.

In the work of Turkmani *et al.* [23], which measured the complex bandpass impulse response of urban mobile radio channels at 900 MHz, all the coefficients required to describe a simple and realistic tapped-delay line model for wideband mobile radio channel can be obtained from the wideband channel measurements. Their work used a two-stage model proposed in [20]. With this two-stage model, the amplitude fluctuations of different paths are basically characterized in terms of small-scale and large-scale signal variations. A small-scale characterization is obtained over a short period of time during which the characteristic of the radio channel is assumed not to change significantly. Thus, the mean signal level of the delayed paths remains constant. A large-scale characterization is then obtained by averaging all the small-scale channel statistics

Employing the two-stage analysis on the wideband propagation data, the tapped-delay line model for wideband mobile radio channel as described by Turkmani *et al.* is shown in Fig. 2.2. Each time-delay cell along the tapped-delay line introduces fixed time delays into the input signal. This is different from the model given in Fig. 2.1 which assumes that the propagation time delays are random. The small-scale signal fluctuations in each time-delay cell were well modelled by uncorrelated Rayleigh fading distribution $\{R_i\}$ while the large-scale signal fluctuations were well modelled by a zero-mean, Lognormal distribution $\{L_i\}$. Unlike small-scale signal fluctuations which were found to be almost completely uncorrelated, the large-scale amplitude variations in adjacent time-delay cells possessed a significant degree of correlation. The tap weights $\{W_i\}$ were simply the mean signal strength of the delayed paths The existence of an echo in a particular time-delay cell was determined by the effects of the small-scale and large-scale signal fluctuations in that time-delay cell. As the small-scale signal variations had zero-means, the means and standard deviations of the large-scale amplitude fluctuations were then used for identifying all significant propagation time delays. The measurement results showed that the large-scale mean signal was decreasing monotonically with increasing excess time delay. The signal variation was large when the excess time delay was small, and the signal strength approached asymptotically to a constant when the

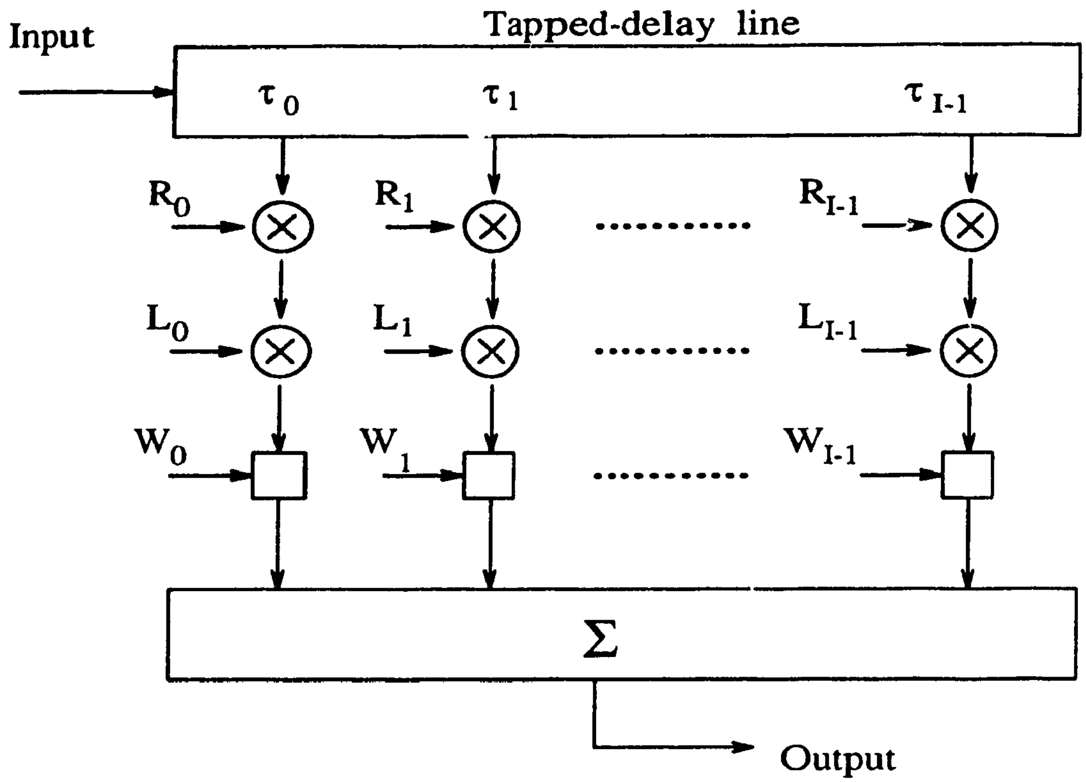

Figure 2.2: The tapped-delay model for wideband mobile radio channel.

excess time delay was becoming large. In general, when using this model with limited numbers of time-delay cells, more time-delay cells were assigned to the period during which the large-scale signal variation was the greatest or the standard deviation was large. Therefore, in this model, the distribution of time delays was described in terms of the large-scale mean signal strength because the selection of time delays was based on the signal amplitude characteristics, but not on the actual statistical distribution of the propagation time delays.

Another statistical multipath model of the indoor radio channel was presented by Saleh and Valenzuela [6]. Their indoor multipath propagation measurements within a medium-size office building were done using 1.5 GHz radarlike pulses. Several researchers [7],[22] have conjectured that the statistical distributions of the propagation time delays $\{\tau_i\}$ formed a Poisson arrival-time sequence with some mean arrival rate. However, from the measurement results, these researchers observed that the statistical distributions of the propagation time delays were not consistent with a simple Poisson arrival-time model with fixed rate. A refined model which is similar to a Markov-type model was then developed [21]-[22]. Although the refined model was able to match the features of the experimental data, it is quite complicated to use because of its Markovian nature. Saleh and Valenzuela were able to come up with a multipath model of indoor radio channel which fitted their measurement results reasonably well while keeping the basic features of a simple Poisson arrival-time process with constant rate.

With this model, the rays of the received signal are presumed to arrive in clusters. The arrival times of the first rays of clusters, that is, the cluster arrival times, are modelled as a simple Poisson arrival-time process with some constant rate. Moreover, the arrival times of the subsequent rays within each cluster are also modelled as a Poisson process with another fixed rate. There are normally many rays within each cluster. If the arrival time of the lth cluster is denoted by T_l and that of the ith ray as measured from the beginning of the lth cluster is denoted by τ_{il}, where $i, l = 0, 1, 2, ..,$ then the first cluster and the first ray within the lth cluster are $T_0 = 0$ and $\tau_{0l} = 0$ respectively. In this model, the complex, low-pass impulse response of the indoor channel differs from (2.1) and is given as:

$$\tilde{h}(t) = \sum_{l=0}^{\infty}\sum_{i=0}^{\infty} \alpha_{il} e^{j\theta_{il}} \delta(t - T_l - \tau_{il}) \tag{2.2}$$

where α_{il} is the positive gain of the ith ray of the lth cluster, θ_{il} is its corresponding phase shift which is assumed to be uniformly distributed over the range $(0,2\pi)$, and both T_l and τ_{il} are distributed according to the interarrival exponential probability density functions. This model is shown in Fig. 2.3. The physical interpretation of the formation of clusters is that they result from reflections from the building superstructures such as large metalized walls and doors. On the other hand, the main cause of individual rays within a cluster is due to the multiple reflections from all the objects in the neighborhood of the transmitter and the receiver such as room walls and furnitures. From their measurement results on the path gain $\{\alpha_{il}\}$, Saleh and Valenzuela observed that the

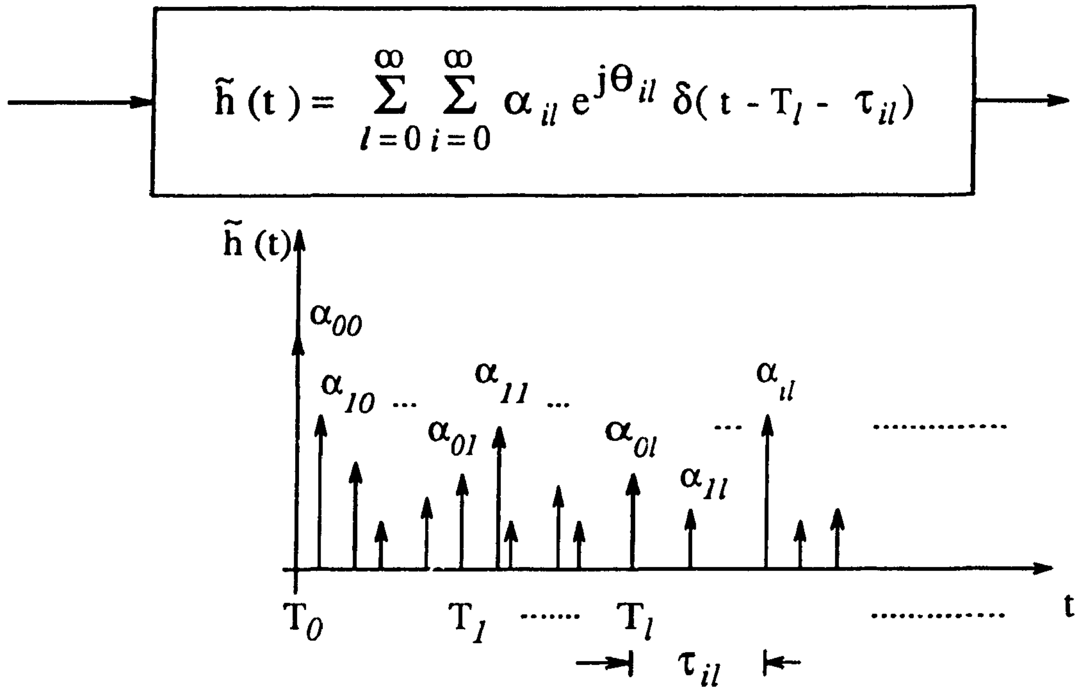

Figure 2.3: The model of the indoor channel as described by Saleh and Valenzuela.

amplitudes of the received rays were well fitted by Rayleigh distribution with variances that decayed exponentially with the cluster delays and the ray delays within the clusters. They also claimed that, to certain extent, their model was close to the physical reality. Furthermore, it could be extended to other types of buildings.

The use of radio in manufacturing environment has also been considered recently. Based on the propagation measurements results from five factory buildings, Rappaport *et al.* [8] characterized the statistical radio channel impulse responses for factories and open plan buildings at 1.3 GHz. Their measurements showed that the number of delayed paths which arrived at the receiver over a 1 m local area was Gaussian distributed having the mean in the range of 9 to 36, and the standard deviation linearly related to the mean In addition, the distribution of the amplitude of individual multipath component within a local area was found to be Lognormally-distributed, the amplitudes of the multipath components were correlated when the distance separations were less than three times the wavelength of the radio signal and the temporal separations were less than 100 ns. With an insensitive receiver which had high threshold, the measurements results showed that the arrival time of each multipath component adhered roughly to a Poisson distribution with a constant mean arrival rate. However, when the sensitivity of the receiver was increased, the results deviated from the Poisson-distributed arrival time model

In order to accomodate large numbers of users for indoor wireless services and to avoid severe congestion of radio spectrum in the future, many studies have been investigated to use higher carrier frequencies than 900 MHz or 1.5 GHz for providing wide range of digital services to mobile users. Because of the large amount of bandwidth that it can offer and its sparse usage currently, the millimeter-wave band between 20 GHz and 60 GHz seems to be an appropriate choice. Such applications as a radio local area network (RALAN) at 30 GHz [24] and a local cellular radio network (LCRN) at 60 GHz [25] were proposed for both digital voice and data transmissions in an indoor wireless environment.

From their results of a survey on the propagation characteristics of 60 GHz radio signals within buildings, Alexander and Pugliese [26] presented that the use of the radio signals at 60 GHz was restricted to a small coverage area due to the attenuation loss caused by oxygen absorption. The atmospheric oxygen absorption attenuates the power of the received signals from distant reflections considerably, thus reducing the associated RMS delay spreads. This characteristics of short range propagation allows the region of radio spectrum around 60 GHz to be applicable for microcellular indoor wireless communications.

The results of the envelope distribution measurements conducted within buildings using phase-locked oscillators at 60 GHz [27] showed that when a LOS path was not existed between the transmitter and receiver, the envelope distribution followed approximately the Rayleigh distribution. However, if there was a LOS path, the signal received was possibly much stronger than the received signal via the reflected paths, so the received signal envelope was no longer Rayleigh distributed, but tended to become a Rician distribution.

Kalivas *et al.* [28] has recently reported their measurement results for the indoor radio channel at 21.6 GHz and 37.2 GHz. They observed that the envelope distribution of the received signal for the two millimeter-wave frequencies followed closely the Rayleigh distribution. Moreover, the same result was obtained when the technique of selection diversity was applied at the receiver where the stronger signal between the two diversity channels was chosen.

So far, there has not been much literature discussing the wideband propagation characteristics of the indoor radio channel for radio signals operating at frequencies in the millimeter-wave band between 20 GHz and 60 GHz. Nevertheless, it is likely that the characterization and modelling of the indoor channel at this frequency band will be as complicated as the ones at 900 MHz and 1.5 GHz which have been described earlier. One can even conjecture that a model similar to that of Saleh and Valenzuela, when adequately adjusted, can be used for the millimeter-wave band. Because of the conclusion from [26] that reflections from distant objects are significantly reduced, the impulse response from (2.2) then contains only one cluster, and therefore it reduces to (2.1) where the time delays $\{\tau_i\}$ are the arrival times of a Poisson process with some fixed rate. Smulders and Wagemans [29] have recently observed, from their results of wideband measurements at 58 GHz in eight different indoor environments, that the RMS delay spread seemed to be independent of the separation distance between a base station and a remote station. The values of the RMS delay spread were found to be in the range of 13-98 ns. When channel equalization is not applied, this worst-case RMS delay spread of 98 ns will limit the symbol rate to about 2 M symbols/second.

Since reflections in the millimeter-wave band are more likely to be generated in the vicinity of the receiver and the transmitter area, the time delays are then bound to be close. This may generate a flat fading effect and thus the natural time diversity associated with multipath propagation is lost. However, this time diversity can be

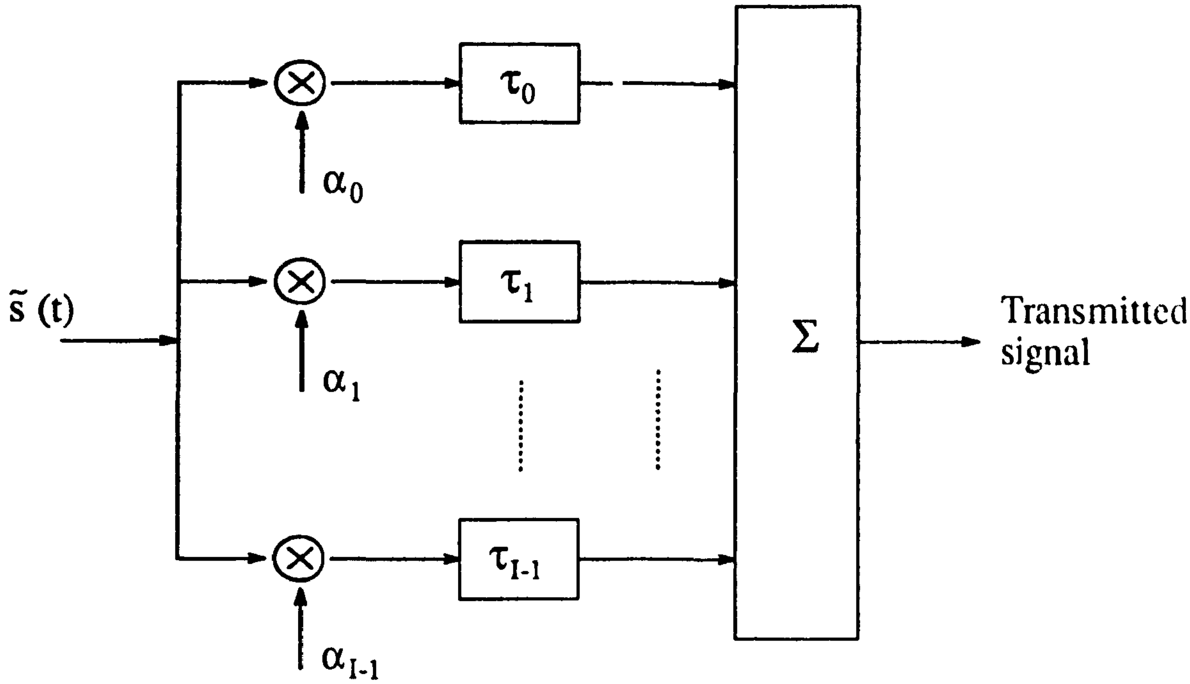

Figure 2.4: Artificial multipath time spread transmission.

regained by inserting artificial multipath in the transmitter as shown in Fig. 2.4 This time spread scheme can be very efficient against fast flat fading. When the time delays $\{\tau_i\}$ are chosen such that $\tau_i - \tau_{i-1}$ is larger than the channel coherent time, the fading of different echoes is uncorrelated. Thus, if an echo is faded, the receiver can still detect the signal from other echoes which might be strong. The channel for this case is still modelled by (2.1), however, the time delays $\{\tau_i\}$ are now known to the receiver.

The work of Smulders and Wagemans [30] presented a method to obtain near uniform coverage for indoor radio networks operating in the millimeter frequency range. It was achieved by employing a pair of biconical horn antennas which were properly designed such that the radiation pattern would provide the antennas with high gains in compensation for the path loss. By using those antennas, if the remote station was located near the base station antenna, the direct ray would have a low path loss and a small antenna gain. However, if the remote station was located far away from the base station, the direct ray would suffer a high path loss, but both antennas would have a higher antenna gain due to the reflected rays. Therefore, a near uniform coverage was maintained. The measurements results under both line-of-sight (LOS) and obstructed (OBS) conditions also exhibited the significance of reflected rays in maintaining the signal coverage under OBS conditions. This indicates that the artificial multipaths are also needed in some situations where necessary for maintaining satisfactory signal coverage for indoor radio communications.

The task of exploitation of the inherent diversity associated with natural or artificial multipath relies on the receiver. Receiver structures for this purpose is the main subject of this thesis. Of considerable interest are receivers which exploit the time-diversity inherent in multipath and are robust against the channel model, that is, perform well over a large class of channel models. A framework for the derivation of such receivers is provided by the Generalized Likelihood principle, explored in the next section.

2.2 Generalized Likelihood (GL) Receiver for Wideband Signaling

Statistical decision theory plays an important role in the optimum design of detection and estimation schemes for radio communications. One of the most significant applications of the theory is in the analysis and design of optimum receiver structures for detection of signals in the presence of noises [9]. The first step in using the statistical decision framework is to establish a system performance criterion. When a particular performance criterion is chosen, then the theory gives the corresponding processing technique which will optimize this system performance.

One of the decision criteria commonly used in classical detection theory is the Bayes criterion. For a simple binary hypothesis-testing problem, the Bayes criterion requires a prior probability for both hypotheses H_1 and H_0, and also a cost to be assigned to each possible course of action. The decision rule for this test is then designed so that the expected value of the cost or the average risk is minimized. Such a test can be reduced to a *likelihood ratio test* [9, pp. 26]. For each observation $\mathbf{r} = [r_1, r_2, .., r_n]$ of n observables, the *likelihood ratio* denoted as:

$$\Lambda(\mathbf{r}) = \frac{p_{\mathbf{R}|H_1}(\mathbf{r})}{p_{\mathbf{R}|H_0}(\mathbf{r})} \tag{2.3}$$

where $p_{\mathbf{R}|H_1}(\mathbf{r})$ and $p_{\mathbf{R}|H_0}(\mathbf{r})$ are the conditional probability density induced by the hypothesis H_1 and H_0 respectively, is computed. This quantity is then compared with the threshold of the test, denoted by η, and decided for hypothesis H_0 if $\Lambda(\mathbf{r}) < \eta$ and for hypothesis H_1 if $\Lambda(\mathbf{r}) > \eta$. In general, the threshold η is a function of the prior probabilities of the two hypotheses and the costs assigned to each course of action. Since the Bayes decision criterion has been proved to give minimum average risk [10, pp. 83], it is used in situations where the prior probabilities for the hypotheses and the costs for each possible actions are known.

The Bayes method can also be applied to detect signals with unknown parameters provided that a prior probability distribution of the parameters is available. In this case the likelihood ratio is given by:

$$\Lambda(\mathbf{r}) = \frac{p_{\mathbf{R}|H_1}(\mathbf{r})}{p_{\mathbf{R}|H_0}(\mathbf{r})} = \frac{\int p_{\mathbf{R}|\mathbf{A},H_1}(\mathbf{r}|\mathbf{a})p_{\mathbf{A}|H_1}(\mathbf{a})d^m\mathbf{A}}{\int p_{\mathbf{R}|\mathbf{A},H_0}(\mathbf{r}|\mathbf{a})p_{\mathbf{A}|H_0}(\mathbf{a})d^m\mathbf{A}} \tag{2.4}$$

where $\mathbf{A} = [A_1, A_2, .., A_m]$ is a vector having m random parameters with joint prior probability density functions on the two hypotheses as $p_{\mathbf{A}|H_0}(\mathbf{a})$ and $p_{\mathbf{A}|H_1}(\mathbf{a})$, and $d^m\mathbf{A} = dA_1\, dA_2 ..\, dA_m$ and the m-fold integration is taken over the entire space of the m parameters $A_1, A_2, .., A_m$. In some situations where the joint prior probability density functions of the unknown parameters are not known, the Bayes approach is no longer applicable. In these cases, it was suggested that those joint prior probability density functions were replaced by the "least favorable distribution" of the parameters $\mathbf{A}$ for the two hypotheses [10, pp. 151]. The receiver could then make the decision based on the likelihood ratio averaged with respect to those least favorable distributions according to

(2.4). However, the least favorable prior probability density functions of the unknown parameters do not necessarily exist as they are obtained when the Bayes risk is being maximized with the proper value of the prior probabilities for the two hypotheses. As a result, this approach is not as promising and another decision criterion should be used if all the least favorable prior probability density functions cannot be found.

If the ranges of the unknown parameters are broad and finite, the signals will be bound to a finite region called the expected domain of the parameter space. When the expected domain of the parameters $\mathbf{A}$ is very wide, the prior probability density function $p_{\mathbf{A}|H_0}(\mathrm{a})$ or $p_{\mathbf{A}|H_1}(\mathrm{a})$ will change slowly with respect to $\mathbf{A}$. If there exists a sharp maximum point at $\mathbf{A} = \hat{\mathbf{A}}$ in the likelihood function, the results of the integrations in (2.4) will be confined to the vicinity of $\hat{\mathbf{A}}$. Therefore, the average likelihood ratio will be proportional to the likelihood ratio evaluated at the maximum point $\mathbf{A} = \hat{\mathbf{A}}$. As a consequence, the Bayes decision strategy is equivalent to a likelihood ratio test with the maximum likelihood estimator of the parameters used as they would be the true parameters [10, pp. 291]. This is commonly called a *generalized likelihood* (GL) *test*.

For GL detection, the decision requires the receiver to compare the GL ratio

$$\Lambda_{GL}(\mathrm{r}) = \frac{max_{\mathbf{A_1}}\ p_{\mathbf{R}|\mathbf{A_1}}(\mathrm{r}|\mathrm{a}_1)}{max_{\mathbf{A_0}}\ p_{\mathbf{R}|\mathbf{A_0}}(\mathrm{r}|\mathrm{a}_0)} \tag{2.5}$$

with an appropriate threshold level and decide for hypothesis H_1 if the level is exceeded and hypothesis H_0 if it is not. In this GL ratio test, the maximum likelihood estimate of the parameters $\mathbf{A}$ corresponding to each hypothesis is evaluated by assuming that each hypothesis is true. The maximum likelihood estimated parameters $\hat{\mathbf{A}}_1$ and $\hat{\mathbf{A}}_0$ are then used in the likelihood functions $p_{\mathbf{R}|\mathbf{A_1}}(\mathrm{r}|\mathrm{a}_1)$ and $p_{\mathbf{R}|\mathbf{A_0}}(\mathrm{r}|\mathrm{a}_0)$ respectively to form the the GL ratio,

$$\Lambda_{GL}(\mathrm{r}) = \frac{p_{\mathbf{R}|\mathbf{A_1}}(\mathrm{r}|\hat{\mathrm{a}}_1)}{p_{\mathbf{R}|\mathbf{A_0}}(\mathrm{r}|\hat{\mathrm{a}}_0)} \tag{2.6}$$

As mentioned in previous section, the design of reliable receivers for indoor radio channels is extremely difficult unless the details of the propagation characteristics of the channel is known. Because of the random nature of the unknown parameters such as the signal variations, carrier phases and the multipath delay spread of the indoor channel, it is appropriate that the idea of GL detection is employed to design an optimal receiver structure for this channel. It seems that this technique will produce a receiver which is robust to channel models, since it estimates the channel parameters from the received signal itself and it does not require any *a-priori* model. The GL principle combines naturally channel parameter estimation and data detection.

Using the indoor channel impulse response $\tilde{h}(t)$ as given in (2.1) with modulated signals represented by the Complex Envelope (CE) notation, the CE of the received signal is:

$$\begin{aligned} \tilde{r}(t) &= \tilde{s}(t) * \tilde{h}(t) + \tilde{n}(t) \quad ,0 \le t \le T_o \\ &= \sum_{i=0}^{I-1} \alpha_i e^{j\theta_i} \tilde{s}(t-\tau_i) + \tilde{n}(t) \end{aligned} \tag{2.7}$$

where $*$ denotes as the convolution, $\tilde{s}(t)$ is the CE of the transmitted signal, α_i, θ_i and τ_i are the ith path gain, phase and propagation time delay, respectively which are treated as unknown parameters to the receiver. In this work, we assume that the number of delayed paths I in the channel impulse response is fixed and known

The channel additive noise is zero mean Gaussian with two-sided power spectral density of $\frac{N_o}{2}$ [Watt/Hz]. This noise can be represented at baseband by its CE as

$$\tilde{n}(t) = n_R(t) + jn_I(t) \tag{2.8}$$

where $n_R(t)$ and $n_I(t)$ are the real and imaginary components respectively, with zero mean, that is, $\overline{n_R(t)} = \overline{n_I(t)} = 0$, and uncorrelated, that is, $\overline{n_R(t)n_I(t-\tau)} = 0$. In addition, the power spectral density of the real and imaginary components of the noise is N_o [Watt/Hz], that is, $\overline{n_R(t)n_R(t-\tau)} = \overline{n_I(t)n_I(t-\tau)} = N_o\delta(\tau)$.

The likelihood functional of $\{\tilde{r}(t), 0 \le t \le T_o\}$ conditioned on the set of unknown parameters $\{\alpha_i, \theta_i, \tau_i \; ; \; i = 0, 1, .., I-1\}$ is given by.

$$p\left[\ \{\tilde{r}(t), 0 \le t \le T_o\} \mid \{\alpha_i, \theta_i, \tau_i \; ; \; i = 0, 1, .., I-1\}\ \right]$$

$$
\begin{aligned}
&= C \cdot exp\,[\,-\frac{1}{N_o}\int_0^{T_o} |\tilde{r}(t) - \sum_{i=0}^{I-1} \alpha_i e^{j\theta_i}\tilde{s}(t-\tau_i)|^2\, dt\,] \\
&= C \cdot exp\,[\,-\frac{1}{N_o}\int_0^{T_o} |\tilde{r}(t)|^2 dt\,] \cdot exp\,[\,\frac{2}{N_o}\, Re\,\{\int_0^{T_o} \tilde{r}(t)\sum_{i=0}^{I-1} \alpha_i e^{-j\theta_i}\tilde{s}^*(t-\tau_i)\, dt\,\}\,] \\
&\quad \cdot exp\,[\,-\frac{1}{N_o}\int_0^{T_o} \sum_{i=0}^{I-1}\sum_{k=0}^{I-1} \alpha_i\alpha_k e^{j(\theta_i-\theta_k)}\tilde{s}(t-\tau_i)\tilde{s}^*(t-\tau_k)\, dt\,] \qquad (2.9)
\end{aligned}
$$

where C is a positive constant, T_o is the observation interval and $Re(\cdot)$ is taking the real part of the argument.

The CE of the transmitted signal $\tilde{s}(t)$ is assumed to be a wideband signal with autocorrelation function characterized by a narrow main lobe of duration T_c called the autocorrelation time. The autocorrelation of a wideband pulse is shown in Fig. 2.5 For $T_c << T_o$, we have that the probability that $|\tau_i - \tau_k| < T_c$, for $i \neq k$, is very small. This probability tends to zero when T_c tends to zero or when W, the bandwidth of $\tilde{s}(t)$, increases, since $W \approx \frac{1}{T_c}$. Therefore we have, for large bandwidth signals, and sufficiently large observation intervals:

$$
\int_0^{T_o} \tilde{s}(t-\tau_i)\tilde{s}^*(t-\tau_k)dt = \begin{cases} E_{\tilde{s}} & , i = k \\ 0 & , i \neq k \end{cases} \qquad (2.10)
$$

where $E_{\tilde{s}} = \int_0^{T_o} |\tilde{s}(t)|^2 dt$. This is a statement of the multipath resolvability condition [14]. With this wideband signaling property, the likelihood functional becomes:

$$
\begin{aligned}
&p\,[\,\{\tilde{r}(t), 0 \le t \le T_o\} \mid \{\alpha_i, \theta_i, \tau_i\,;\, i = 0,1,..,I-1\}\,] \\
&= C \cdot exp\,[-\frac{1}{N_o}\int_0^{T_o} |\tilde{r}(t)|^2 dt\,] \cdot \prod_{i=0}^{I-1} exp\,[\frac{2\alpha_i}{N_o}\, Re\{e^{-j\theta_i}\int_0^{T_o}\tilde{r}(t)\tilde{s}^*(t-\tau_i)\, dt\,\} - \frac{E_{\tilde{s}}}{N_o}{\alpha_i}^2\,] \qquad (2.11)
\end{aligned}
$$

The GL functional of $\tilde{r}(t)$ is:

$$
p\,[\,\{\tilde{r}(t), 0 \le t \le T_o\} \mid \{\hat{\alpha}_i, \hat{\theta}_i, \hat{\tau}_i\,;\, i = 0,1,..,I-1\}\,] \qquad (2.12)
$$

where $\hat{\alpha}_i$, $\hat{\theta}_i$, and $\hat{\tau}_i$ are the maximum likelihood (ML) estimates of the channel parameters α_i, θ_i, and τ_i from $\{\tilde{r}(t), 0 \le t \le T_o\}$. Now, we need to find the ML estimates of

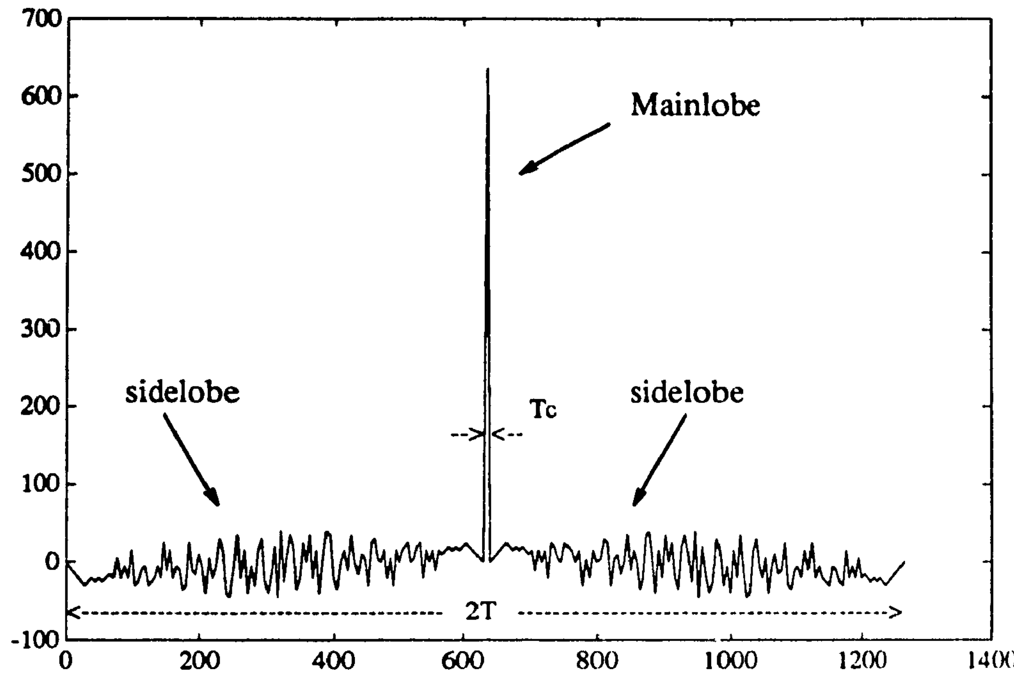

Figure 2.5: The autocorrelation of a wideband pulse.

each channel parameter such that the likelihood functional is being maximized. In order for the channel parameter θ_i to maximize the likelihood functional, the terms

$$Re\ \{e^{-j\theta_i} \int_0^{T_o} \tilde{r}(t)\tilde{s}^*(t-\tau_i)\ dt\ \} \tag{2.13}$$

in (2.11) have to be maximized for $i = 0, 1, .., I-1$. It is obvious that the maximum possible values of these terms are obtained when:

$$\hat{\theta}_i = \arg\ [\int_0^{T_o} \tilde{r}(t)\tilde{s}^*(t-\tau_i)\ dt\ ] \tag{2.14}$$

By substituting (2.14) into (2.13), we have the following:

$$Re\ \{e^{-j\hat{\theta}_i} \int_0^{T_o} \tilde{r}(t)\tilde{s}^*(t-\tau_i)\ dt\ \}\ =\ |\int_0^{T_o} \tilde{r}(t)\tilde{s}^*(t-\tau_i)\ dt\ | \tag{2.15}$$

Now, (2.15) has to be maximized over τ_i. The maximum likelihood estimates $\hat{\tau}_i$ are obtained by choosing the $I-1$ instants $\hat{\tau}_1, .., \hat{\tau}_{I-1}$ which give the largest values of $|\int_0^{T_o} \tilde{r}(t)\tilde{s}^*(t-\tau_i)\,dt\,|$ and with the constraint that $|\hat{\tau}_i - \hat{\tau}_k| \geq T_c$, where T_c is the autocorrelation time of $\tilde{s}(t)$. Therefore, the likelihood functional is further reduced to:

$$p\,[\,\{\tilde{r}(t), 0 \leq t \leq T_o\}\,|\,\{\alpha_i, \hat{\theta}_i, \hat{\tau}_i\,;\, i = 0,1,..,I-1\}\,]$$
$$= C \cdot exp\,[-\frac{1}{N_o}\int_0^{T_o} |\tilde{r}(t)|^2 dt\,] \cdot \prod_{i=0}^{I-1} exp\,[\,\frac{2}{N_o}\,|\int_0^{T_o} \tilde{r}(t)\tilde{s}^*(t-\hat{\tau}_i)\,dt\,|\,\alpha_i - \frac{E_s}{N_o}\alpha_i^2\,] \tag{2.16}$$

From (2.16), the remaining unknown parameter to be estimated is α_i. This can be achieved by considering the term

$$\frac{2}{N_o}\,|\int_0^{T_o} \tilde{r}(t)\tilde{s}^*(t-\hat{\tau}_i)\,dt\,|\,\alpha_i - \frac{E_s}{N_o}\alpha_i^2 \tag{2.17}$$

in (2.16). The estimate $\hat{\alpha}_i$ which maximizes (2.17) can be obtained as follows:

$$\frac{\partial}{\partial \alpha_i}\,\{\,\frac{2}{N_o}\,|\int_0^{T_o} \tilde{r}(t)\tilde{s}^*(t-\hat{\tau}_i)\,dt\,|\,\alpha_i - \frac{E_s}{N_o}\alpha_i^2\,\}\,|_{\alpha_i=\hat{\alpha}_i} = 0 \tag{2.18}$$

which gives:

$$\hat{\alpha}_i = \frac{1}{E_s}\,|\int_0^{T_o} \tilde{r}(t)\tilde{s}^*(t-\hat{\tau}_i)\,dt\,| \tag{2.19}$$

Since the second derivative of (2.17) with respect to α_i is $-E_s/N_o$ which is negative, the estimate $\hat{\alpha}_i$ as obtained in (2.19) is indeed maximizing (2.17). By substituting (2.19) into (2.16), we have the GL functional as follows:

$$p\,[\,\{\tilde{r}(t), 0 \leq t \leq T_o\}\,|\,\{\hat{\alpha}_i, \hat{\theta}_i, \hat{\tau}_i\,;\, i = 0,1,..,I-1\}\,]$$
$$= C \cdot exp\,[\,-\frac{1}{N_o}\int_0^{T_o} |\tilde{r}(t)|^2 dt\,] \cdot \prod_{i=0}^{I-1} exp\,[\,\frac{1}{E_s N_o}\,|\int_0^{T_o} \tilde{r}(t)\tilde{s}^*(t-\hat{\tau}_i)\,dt\,|^2\,]$$
$$= C \cdot exp\,[\,-\frac{1}{N_o}\int_0^{T_o} |\tilde{r}(t)|^2 dt\,] \cdot exp\,[\,\frac{1}{E_s N_o}\sum_{i=0}^{I-1}\,|\int_0^{T_o} \tilde{r}(t)\tilde{s}^*(t-\hat{\tau}_i)\,dt\,|^2\,] \tag{2.20}$$

Therefore, the decision variable of the GL receiver for the indoor channel is:

$$z = \sum_{i=0}^{I-1}\,|\int_0^{T_o} \tilde{r}(t)\tilde{s}^*(t-\hat{\tau}_i)\,dt\,|^2 \tag{2.21}$$

It is seen that the only channel parameters required to be estimated are the multipath delays.

This GL receiver is shown in Fig. 2.6. It is realized by a matched filter followed by a square-law device, a fixed time-delay module T_D allowing time for channel estimation process to activate the appropriate taps of the RAKE receiver, then the equal weight RAKE combiner. The path delays $\tau_0, \tau_1, .., \tau_{I-1}$ estimated from the output of the matched filter are used to activate the I coefficients of the tapped delay lines. For each delayed path, there is a corresponding peak appeared at the matched filter output. The estimation of the path delays is done by locating where these multipath peaks are. Each of the activated taps is of unity weight while all other taps not being activated are set to zero. The number of taps J along the RAKE combiner depends on the maximum multipath *time delay spread*, Δ, of the channel. In general, J is truncated at $\frac{\Delta}{T_c} + 1$.

It is seen that the optimal receiver in the GL sense is a matched filter with square-law equal weight RAKE combiner. The operation of the square-law equal weight RAKE combiner is illustrated in Fig. 2.7. Here, we assume that the multipath channel consists of four delayed paths. Thus, there are four multipath peaks at the output of the matched filter. The time delays between the first and the second delayed path, the second and the third delayed path, and the third and the last delayed path, as indicated in Fig 2.7 are Δ_1, Δ_2 and Δ_3 respectively. The taps along the RAKE combiner that allow the multipath peaks to align together will be activated with equal weight coefficients. The four waveforms at the top of the figure are the signals appeared at the four activated taps. From the output of the RAKE combiner, it can be seen that the multipath contributions due to each delayed path are added at $t = T + \Delta$ where the sampling is done.

Square-law equal weight combining is not new. It has been shown by Pierce [31] that this form of combining diversity is optimal in the absence of any phase and amplitude information in the diversity branches. In this work, it is shown that square-law equal weight combining is the optimal receiver in the GL sense for multipath channels.

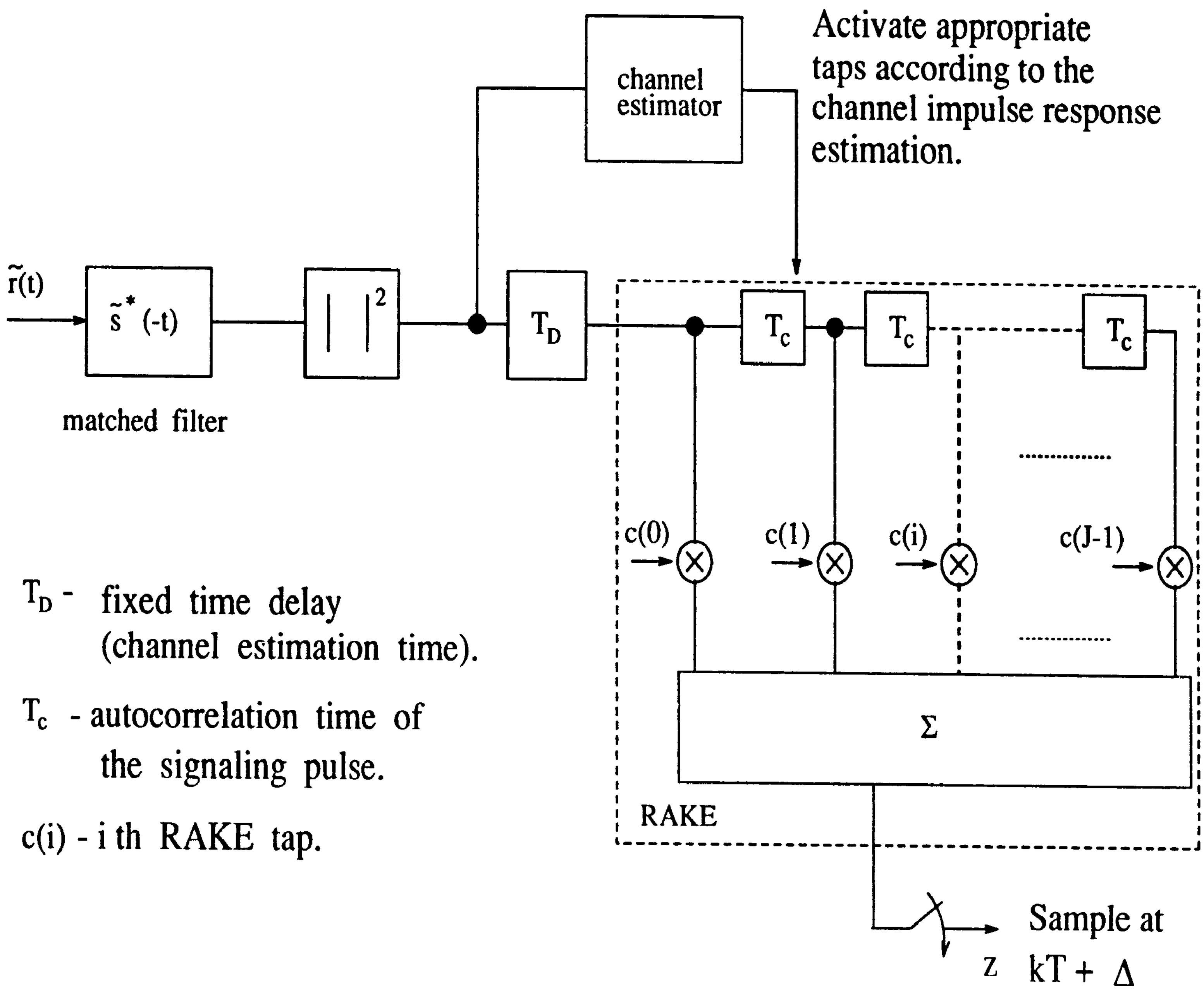

Figure 2.6: The Generalized Likelihood receiver for indoor channel.

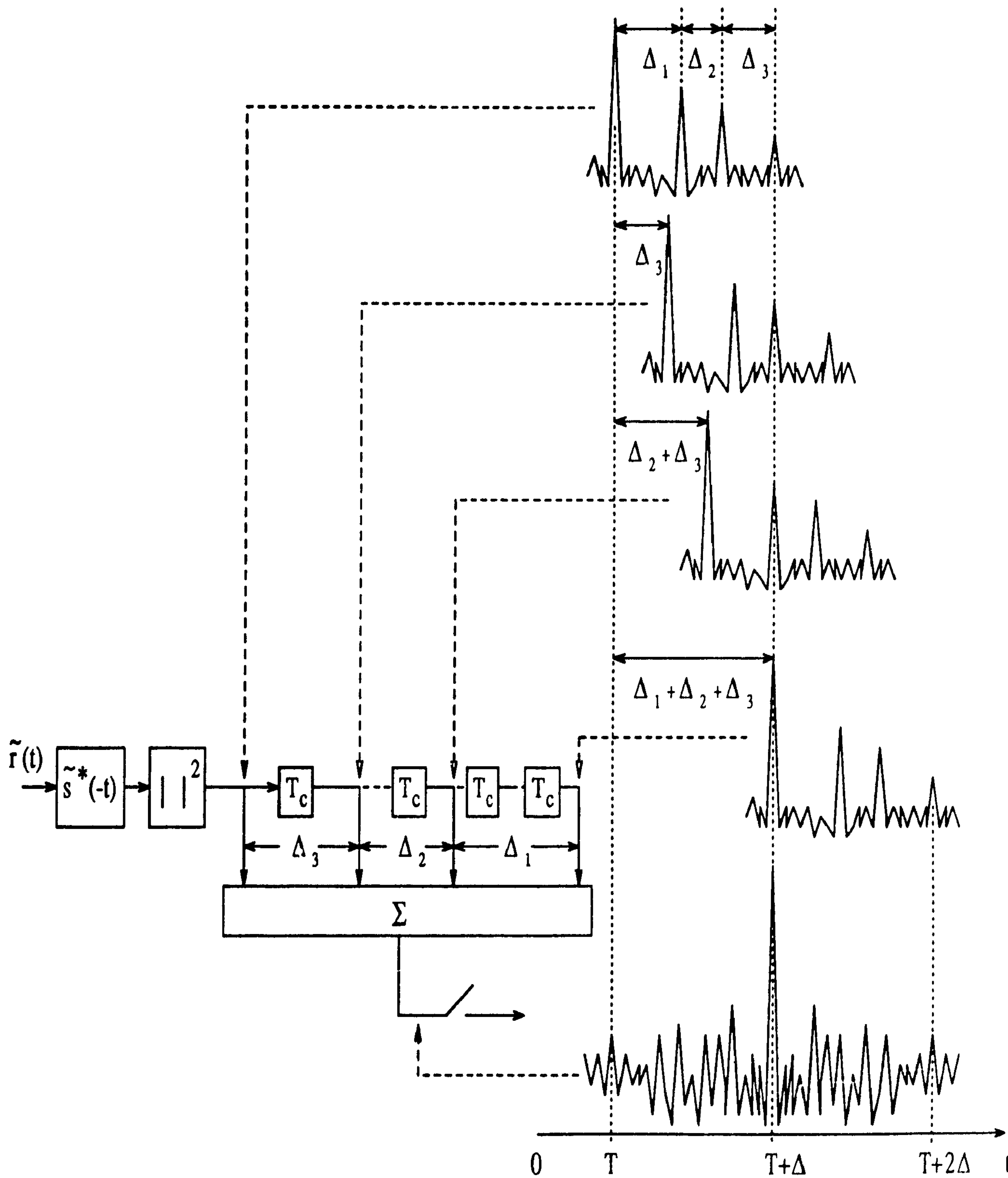

Figure 2.7: The operation of a square-law equal weight RAKE combiner.

This relation to GL seems to be a result not found in the technical literature. From [31], we also have that square-law equal weight combining is 3 dB poorer in performance than maximum gain coherent combining. However, maximum gain coherent combining requires phase and amplitude estimates. When the errors of these estimates are taken into account, the degradation which is obtained in practice is less than 3 dB. Thus, we see that the GL receiver not only is of low complexity, but also provides a performance close to optimal.

Chapter 3

Multipath Induced Intersymbol Interference (ISI)

This chapter considers the effects of multipath induced intersymbol interference (ISI) in bandwidth expanding digital communications. Section 3.1 gives a qualitative analysis of the multipath induced ISI effects on the channel estimation process To mitigate the effects of multipath induced ISI which may complicate the channel estimation process, an antimultipath technique called commutation signaling is then described. In section 3.2, we consider the effects of multipath induced ISI on the data detection process. By employing union bounding techniques, an upper bound to the event of having significant ISI at the output of the maximum gain RAKE receiver and the square-law equal weight RAKE receiver is derived. It is shown that with sufficient bandwidth expansion, the ISI effects due to multipath are reduced. Finally, by incorporating commutation signaling with the maximum gain RAKE combiner and square-law equal weight RAKE combiner it is shown in Section 3.3 that the effects of multipath induced ISI on the data detection process are significantly reduced.

3.1 ISI Effects on Channel Estimation - Commutation Signaling

The GL receiver in chapter 2 which was derived assuming a single pulse transmission, requires the estimation of the path delays in order to activate the appropriate taps of the equal weight RAKE combiner. This channel estimation process is performed by estimating the location of the multipath peaks from the output of the matched filter. However, in the case of high-rate sequential transmission of pulses, the occurrence of multipath induced ISI at the matched filter output may complicate the channel estimation process As a result, wrong RAKE taps may be activated causing a degradation in performance.

To understand the multipath induced ISI effects on the channel estimation process, we find it useful to examine how the ISI occurs at the output of the matched filter when sequences of pulses are transmitted over a multipath channel. The transmitted signal is given by:

$$\tilde{s}(t) = \sum_{k=-\infty}^{\infty} a(k)\tilde{u}(t-kT) \tag{3.1}$$

where $a(k)$ are the information symbols, $\tilde{u}(t)$ is the signaling pulse and $1/T$ is the information symbol rate. The impulse response of the multipath fading channel as given in (2.1) is:

$$\tilde{h}(t) = \sum_{i=0}^{\infty} \alpha_i e^{j\theta_i}\delta(t-\tau_i) \tag{3.2}$$

where α_i is the amplitude of the ith delayed path, τ_i is the propagation time delay, θ_i is the associated phase shifts.

We first consider a single pulse transmission and examine the output of the matched filter. When a single spread-spectrum pulse is transmitted over the multipath fading channel with no delayed path, Fig. 3.1 shows the matched filter response As the signaling pulse is of bandwidth expanding type, the matched filter output, that is, the autocorrelation of the signaling pulse, is characterized by a narrow mainlobe of duration T_c, the autocorrelation time, and some small autocorrelation sidelobes. When the same bandwidth expanding pulse is transmitted over a multipath fading channel with four delayed paths and with a *time delay spread* Δ, the four mainlobes corresponding to each delayed path at the matched filter output are of different amplitudes and are spreaded over the interval between $t = T$ and $t = T + \Delta$. This can be seen in Fig. 3.2.

Now, consider a successive transmission of two data symbols, which both are equal to one, over a multipath channel with *time delay spread* smaller than the symbol interval, that is $\Delta < T$. The matched filter response for this case, Fig 3.3, shows that the multipath peaks are not interlaced. Therefore, no significant ISI is occurred and the channel estimation can be easily performed by observing the peaks within a symbol time interval. In the case of high-rate transmission when the *time delay spread* is larger than the symbol interval , that is, $\Delta > T$, the interlacing of multipath peak at the matched filter output causes the occurrence of multipath induced ISI. This phenomenon can be seen in Fig. 3.4. As a result of the presence of the interlaced peaks, the channel estimation becomes complicated. The interlaced peaks may cause activation of wrong RAKE taps. One simple method to avoid the occurrence of this peak interlacing is to transmit the information in such a low symbol rate that $\Delta < T$. For a fixed information bit rate, this implies that an M-ary signaling scheme has to be used. Another approach is based on **commutation signaling** [11].

Commutation signaling was introduced by Turin [11] to mitigate the effects of the multipath induced ISI – the interlacing of multipath mainlobes. The principle of this signaling technique is to avoid the occurrence of the interlaced mainlobes, in high-rate transmission when the *time delay spread* is larger than the symbol interval, (i.e. when $\Delta > T$), by commutating the signal sets effectively among a number of shift quasi-orthogonal signaling alphabets in such a way that any signals that are still "ringing" in the multipath channel will not be used again until they have faded away.

The concept of $M \times N$ commutation signaling [11] is to switch among N distinct M-ary signal sets. To illustrate the utility of this technique, we consider an example. The

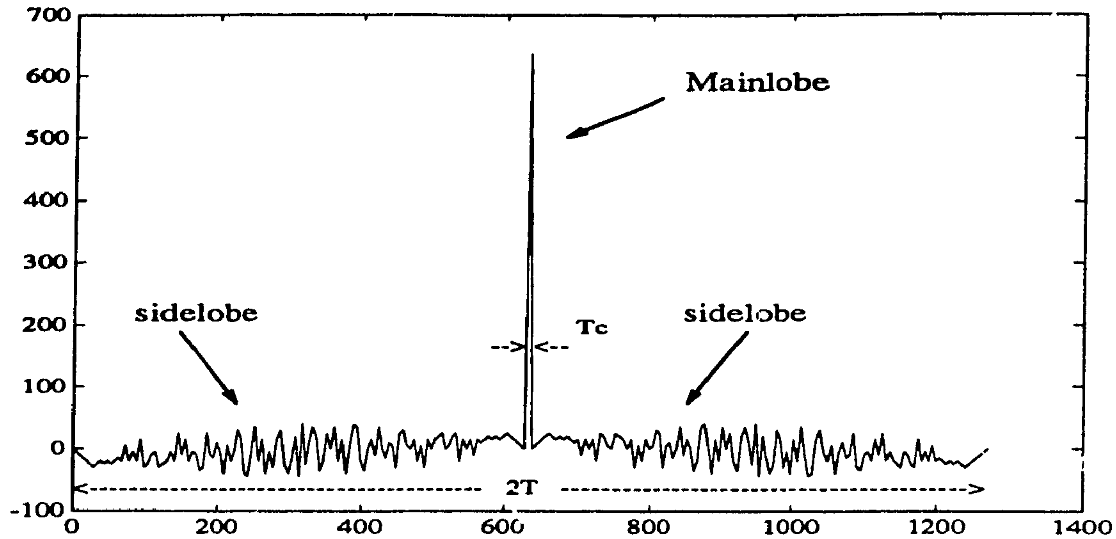

Figure 3.1: Matched filter response to single spread-spectrum pulse transmission over a direct path channel.

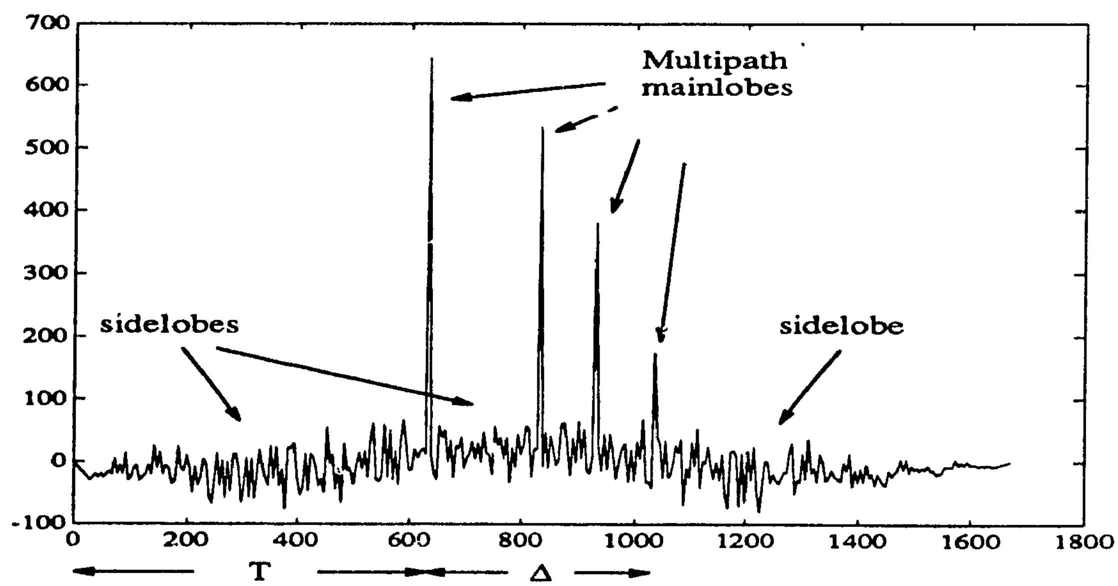

Figure 3.2: Matched filter response to single spread-spectrum pulse transmission over a multipath channel with four delayed paths.

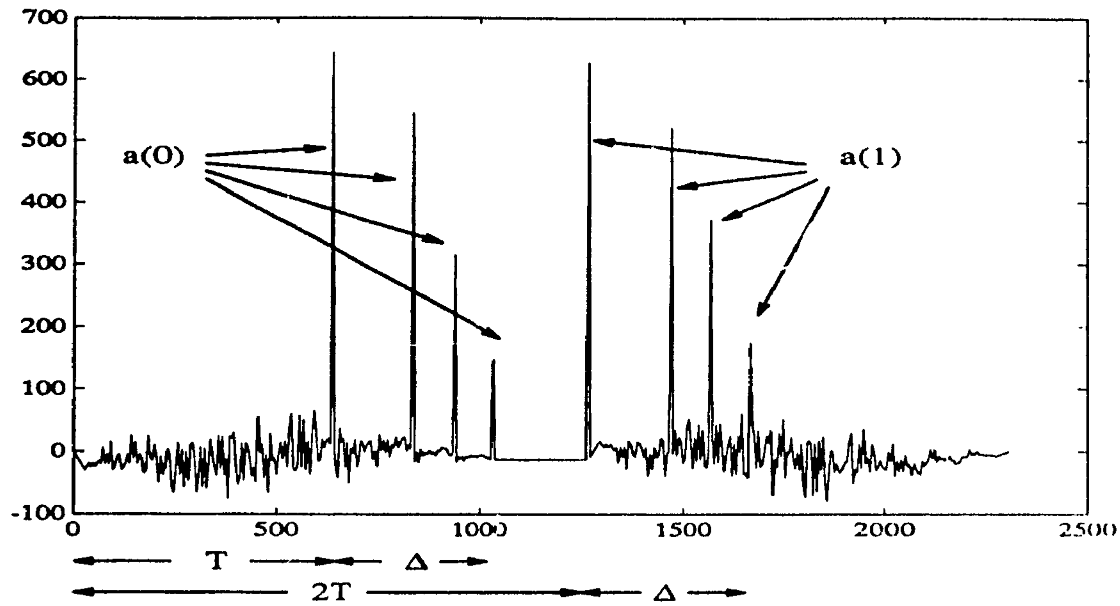

Figure 3.3: Matched filter response to successive transmission over a multipath channel with $\Delta < T$.

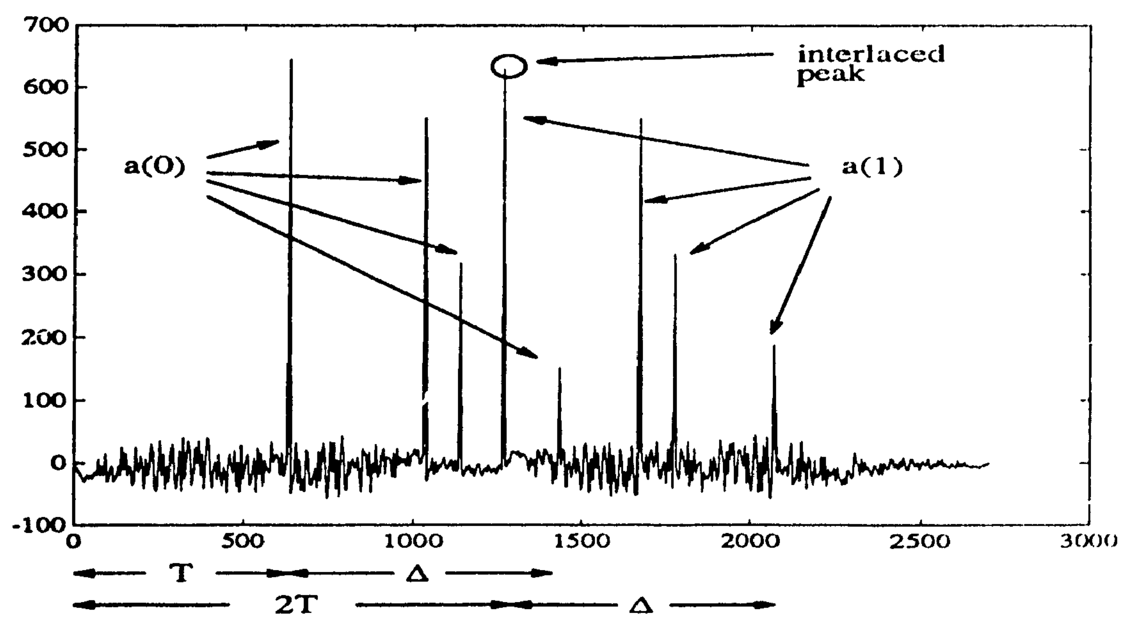

Figure 3.4: Matched filter response to successive transmission over a multipath channel with $\Delta > T$.

2×4 signaling scheme commutes among 4 different signal sets of 2 signals each. Suppose that the four signal sets are $\pm\tilde{s}_1(t), \pm\tilde{s}_2(t), \pm\tilde{s}_3(t)$ and $\pm\tilde{s}_4(t)$. The waveforms $s_i(t)$ are shift orthogonal spread-spectrum pulses, and the data sequence is $a(0), a(1), a(2)\ldots$ with $a(i) = \pm 1$. These spread-spectrum pulses have the property that they are mutually orthogonal to each other, that is, their autocorrelations are characterized by a narrow mainlobe and some low-level sidelobes, while their crosscorrelations are characterized by some low-level sidelobes only, even when any of the pulses is being shifted by a certain time duration. With this signaling technique, the transmitted signals are $a(0)\tilde{s}_1(t)$, $a(1)\tilde{s}_2(t)$, $a(2)\tilde{s}_3(t)$, $a(3)\tilde{s}_4(t)$, $a(4)\tilde{s}_1(t)$, $a(5)\tilde{s}_2(t)$, $a(6)\tilde{s}_3(t)$, $a(7)\tilde{s}_4(t)$,.. etc The matched filter responses for this 2×4 signaling scheme is shown in Fig. 3.5. Since no signal in the signal set repeats itself in less than the *time delay spread* Δ, the major part of ISI, interlacing of multipath mainlobes, is avoided. As a result of employing this signaling scheme, the channel estimation can be done safely because there is always no interlaced peaks appeared at the matched filter outputs.

The total number of signals required for $M \times N$ signaling is MN; therefore this signaling scheme may require MN matched filters. In order to reduce the total number of matched filters to be used in a commutation signaling scheme, it is important to minimize the values of M and N. As mentioned earlier, $M \times N$ signaling is based on switching among N distinct M-ary signal sets. The value of N is normally chosen large enough such that no signal set is repeated before the ringing of its previous use has diminished. In other words, the value of N depends on the *time delay spread* Δ. In fact, $N = \lceil \frac{\Delta}{T} \rceil$ where $\lceil x \rceil$ is the smallest integer larger than x. If R is the information bit rate in bits/second, then the M-ary signal duration is $T = log_2 M \,/\, R$. Therefore. $N = \lceil R\Delta \,/\, log_2 M \rceil$ and the total number of signals required is $MN = M\lceil R\Delta \,/\, log_2 M \rceil$. It is easily seen that for $M = 2$, we have a minimum number of signals. In a commutation signaling scheme, the value of N increases linearly with $R\Delta$. Thus, the total number of matched filters required also grows linearly with $R\Delta$.

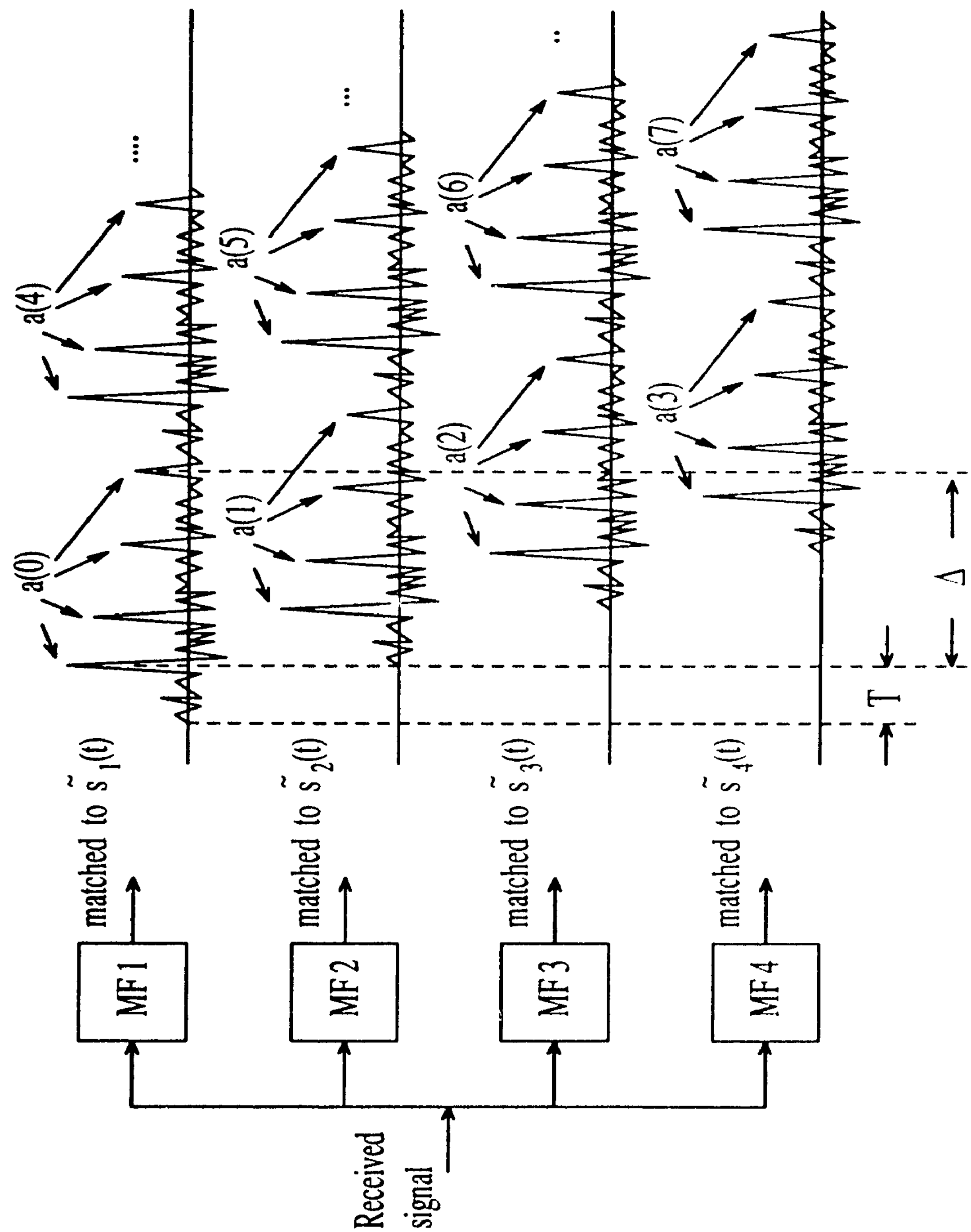

Figure 3.5: Matched filter responses for 2 × 4 signaling scheme.

Other M-ary signaling techniques can be used for increasing the symbol time and thus reducing ISI. Commutation signaling, however, offers a good trade-off between the number of matched filters employed by the receiver and SNR performance. For M-ary orthogonal signaling, the receiver consists of a bank of M filters matched to each of the orthogonal signals. In order to prevent from the occurrence of interlaced multipath peaks, the total number of matched filters required for M-ary orthogonal signaling is $M = 2^{\lceil R\Delta \rceil}$, where R is the information bit rate in bits/second and Δ is the *time delay spread* in seconds. Similarly, M-ary biorthogonal signaling can be obtained from $M/2$ orthogonal signals by simply employing the negatives of the orthogonal signals as well. Therefore, M-ary biorthogonal signaling requires $M/2$ orthogonal signals and $2^{\lceil R\Delta \rceil - 1}$ matched filters to avoid the interlacing of multipath peaks For M-ary two-dimensional signaling, two orthogonal signals are needed. One for the in-phase component and the other for the quadrature component. The components of the signals are selected from the M-point two dimensional signal constellation. Therefore, this scheme needs only two matched filters.

A comparison on the number of orthogonal signals and matched filters required for each of the aboved signaling schemes is shown in Table 3.1. The total number of matched filters required increases exponentially with $R\Delta$ for both the M-ary orthogonal and biorthogonal signaling, but linearly with $R\Delta$ for $M \times N$ commutation signaling. For M-ary two-dimensional signaling, the number of matched filters required is 2; however, the SNR performance deteriorates with increasing M. For an $M \times N$ commutation signaling, the number of matched filters required increases linearly with $\lceil R\Delta \rceil$. while the SNR performance is identical to that of an M-ary signaling scheme. For $M = 2$, we minimize the number of required matched filters and maximize the SNR efficiency. Thus, binary commutation signaling which requires $2\lceil R\Delta \rceil$ matched filters seems most appropriate. With binary commutation signaling, we use $\lceil R\Delta \rceil$ binary signal sets. The optimal scheme in terms of maximizing SNR performance while minimizing the number of matched filters is obtained when each signal set is antipodal. In this case, we need

Signaling scheme	Number of orthogonal signals required	Number of matched filters required to avoid the interlacing of multipath peaks.
M-ary orthogonal signaling	M	$2^{\lceil R\Delta \rceil}$
M-ary biorthogonal signaling	M/2	$2^{\lceil R\Delta \rceil - 1}$
M-ary two-dimensional signaling	2	2
M x N commutation signaling	MN	$M\left\lceil \frac{R\Delta}{\log_2 M} \right\rceil$

Table 3.1: Comparison of M-ary orthogonal, biorthogonal, two-dimensional signaling and $M \times N$ commutation signaling schemes.

only $\lceil R\Delta \rceil$ matched filters. This can be combined with differentially encoding to bypass the need for a phase reference at the receiver. Receivers for such a signaling scheme will be considered in the next chapter. In the next section, we consider the effects of multipath induced ISI on data detection, the role that wideband signaling, in general, plays in reducing these effects.

3.2 ISI Effects on Data Detection

Multipath fading has been a troublesome condition in many communication channels One of its influence on data detection in a high-rate communication system is via multipath induced ISI. The occurrence of the interference as explained in section 3.1 is due to different and randomly varying delays and amplitudes of the transmitted signal after travelling along not one, but many paths, to the receiver The two main approaches commonly used for combating the multipath induced ISI are : equalization techniques and bandwidth expanding signaling with RAKE receivers.

Adaptive equalization techniques have been considered for communication over multipath fading channels such as those found in HF and troposcatter systems [12]. This communication medium is characterized by a large number of scatters located at random points within the propagation path and by lack of spectrum which does not allow for bandwidth expansion. The dispersion on these channels can be quite large and the equalization techniques which can overcome this dispersion must be of the nonlinear type. Adaptive decision feedback equalizers have been found appropriate for these systems [13].

When spectrum is available and bandwidth expansion is possible, it has been observed that by using RAKE receivers, the multipath contribution to ISI is insignificant. This is attributed to the inherent capability of the RAKE receiver to suppress multipath induced ISI [14]. This ISI suppression capability is due to the bandwidth expansion and the discrete nature of the impulse response of wideband multipath channels. In this section, we examine the effects of multipath induced ISI on the data detection process. In particular, we first consider the trade-off between the ISI suppression capability of general RAKE receivers and bandwidth expansion, which has been reported in [32]. Then, we extend the analysis to the GL receiver as derived in section 2.2.

The analysis is based on a general CE model of a communication system as shown in Fig. 3.6. A direct spread spectrum system fits this model as well as other bandwidth expanding schemes which are based on linear FM modulation such as chirp signaling. In this model, the source produces data sequences which pass through an impulse generator, then a shaping filter with impulse response $\tilde{u}(t)$ of a wideband type. The transmitted signal $\tilde{s}(t)$ is then sent through a multipath fading channel perturbed by additive noise. On the receiving side, we first have a filter $\tilde{u}^*(-t)$ matched to the signaling pulse, then followed by a maximum gain RAKE combining receiver. This RAKE receiver, in fact,

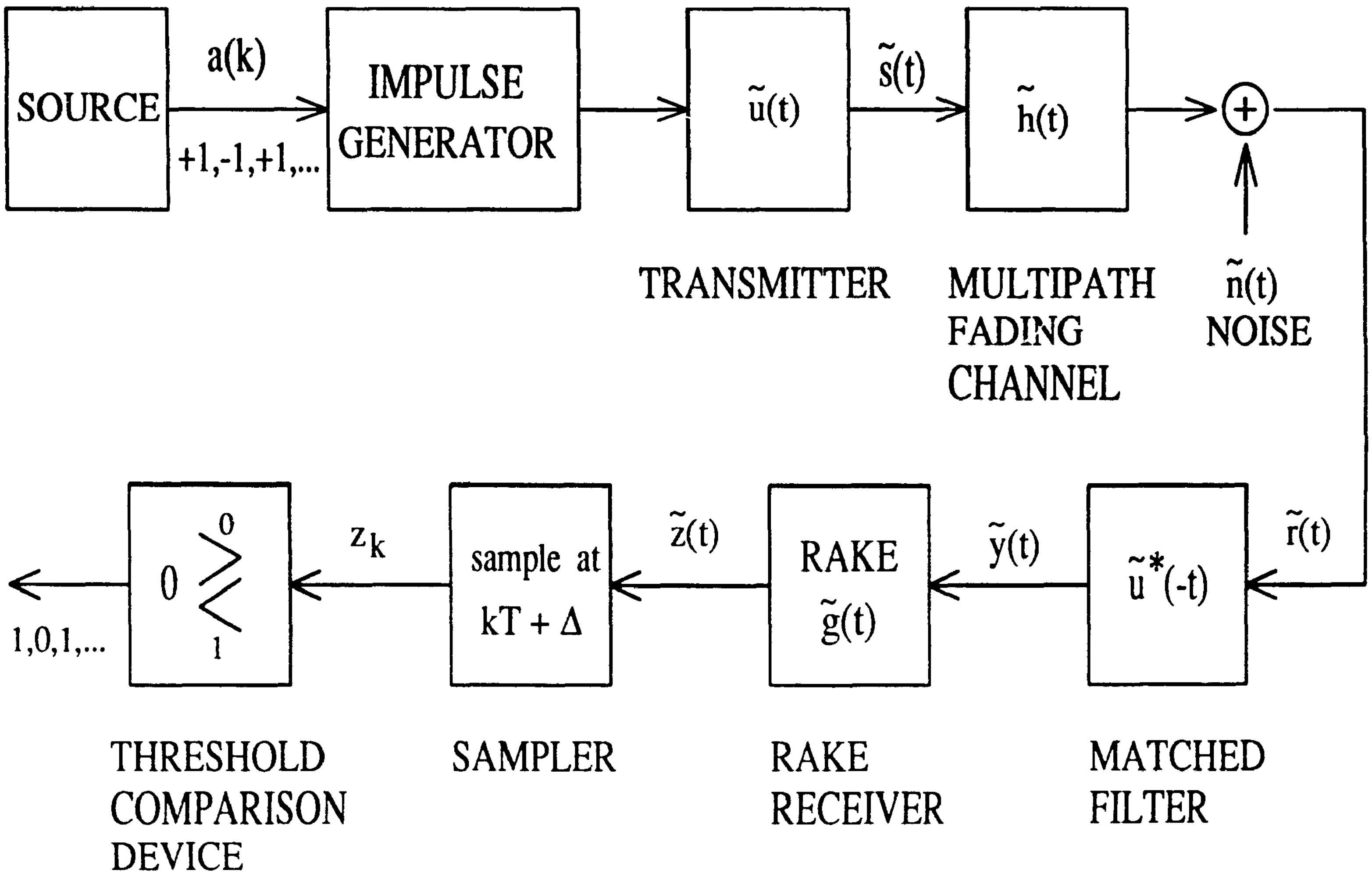

Figure 3.6: A model for a bandwidth expanding communication system with maximum gain RAKE receiver.

has an impulse response which matches to the multipath fading channel. As a result, the RAKE receiver together with the matched filter $\tilde{u}^*(-t)$ as a whole is another filter matched to both the shaping filter and the channel. Therefore, the multipath induced ISI occurred at the output of the RAKE receiver is reflected in the autocorrelation function of the received signal $\tilde{r}(t)$. In many communication systems, adaptive equalization is usually done following the matched filter in order to deal with ISI However, we claim that with sufficient bandwidth expansion, the amount of significant ISI at the output of the RAKE receiver can be made arbitrarily small. Therefore, in this model, we do not have an adaptive equalizer, but a sampler and a threshold comparison device, following the RAKE receiver.

As mentioned in section 3.1 when the signaling pulse is of bandwidth expanding type, its autocorrelation function $\Phi(t)$ is characterized by a narrow mainlobe of duration T_c and some small autocorrelation sidelobes. For a bandwidth expanding system, the property that $T_c << T$, where T is the symbol time interval, allows the RAKE receiver [14] to suppress the multipath induced ISI in the matched filter response. Because of this capability, the eye pattern at the output of the RAKE receiver as depicted in Fig. 3.7 is open at the sampling time. Thus, reasonable performance can be achieved without any additional equalization to be done following the RAKE receiver. However, this situation depends on the channel which is random and there are channel realizations which do not yield an open eye pattern. In this work, we try to upper-bound the probability of this event.

The ISI at the RAKE receiver output can be generated by:

1. The mainlobe of $\Phi(t)$. This results in significant ISI which degrades the system performance considerably, unless effective equalization is used.

2. The sidelobes of $\Phi(t)$. Since for a well designed bandwidth expanding signaling scheme, these sidelobes are low, this type of ISI is not significant and there is no need for equalization.

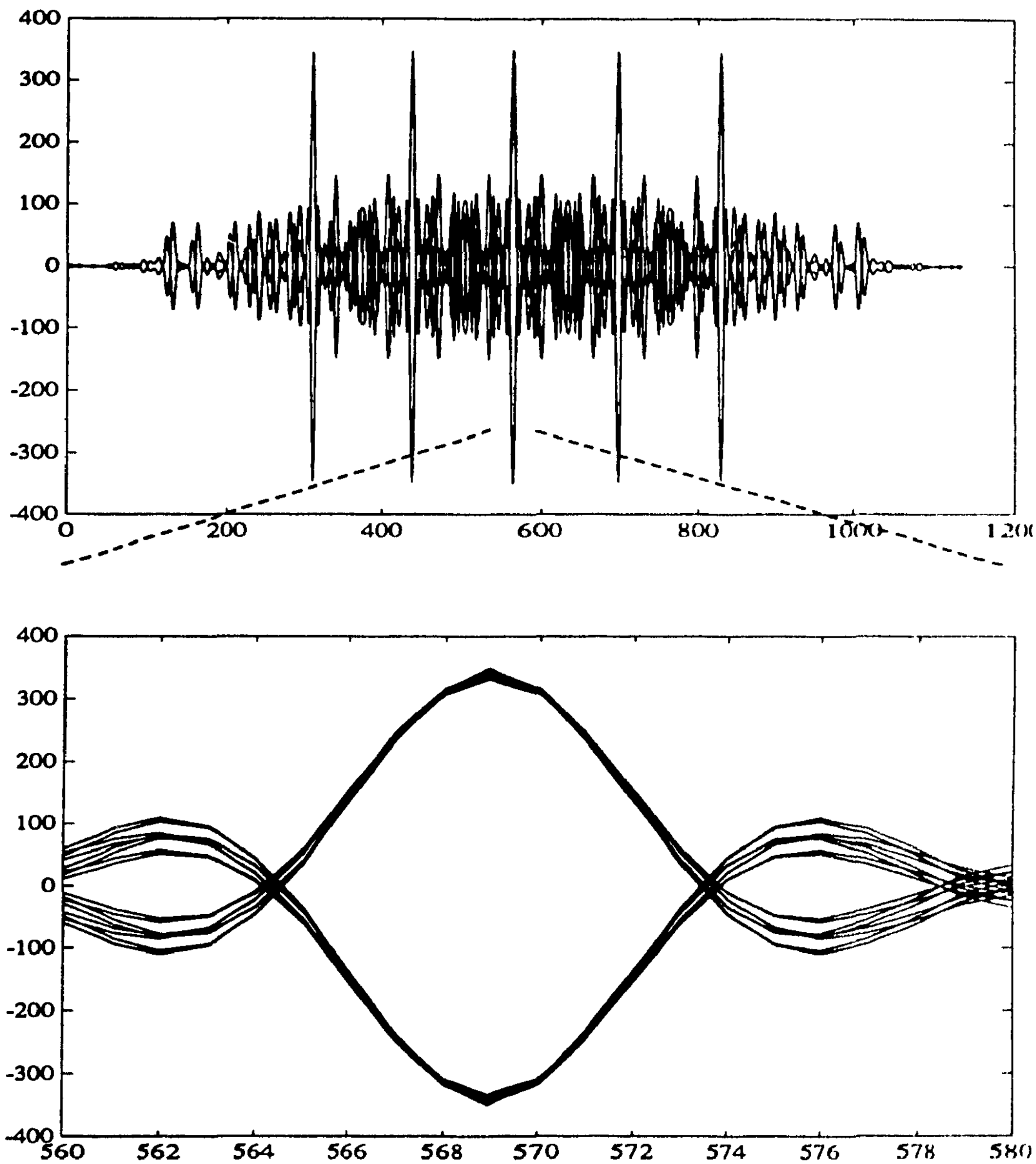

Figure 3.7: Eye pattern at the RAKE receiver output

The type of ISI that is present at the RAKE receiver output depends on the channel realization and thus it is a random event. We will examine the effects of multipath induced ISI on the data detection process by considering the upper-bound of the event of having significant ISI over a random multipath channel.

We consider a single pulse transmission over the system of Fig. 3.6 with the transmitted signal given by:

$$\tilde{s}(t) = \tilde{u}(t) \tag{3.3}$$

where $\tilde{u}(t)$ is the CE of the signaling pulse. The complex, low-pass impulse response of the multipath fading channel as given in (2.1) is:

$$\tilde{h}(t) = \sum_{i=0}^{\infty} \alpha(i)\delta(t - \tau_i) \tag{3.4}$$

where the term $\alpha_i e^{j\theta_i}$ in (2.1) is replaced by $\alpha(i)$ in (3.4) for simplicity. It follows from (3.3) and (3.4) that the received signal is simply the time convolution of $\tilde{s}(t)$ and $\tilde{h}(t)$. and is given as follows:

$$\tilde{r}(t) = \tilde{s}(t) * \tilde{h}(t) = \sum_{i=0}^{\infty} \alpha(i)\tilde{u}(t - \tau_i) \tag{3.5}$$

As our analysis considers the effects of multipath induced ISI only, the additive noise is neglected in the received signal. The output of the matched filter which is the convolution of $\tilde{r}(t)$ and $\tilde{u}^*(-t)$ is given by:

$$\begin{aligned} \tilde{y}(t) &= \tilde{r}(t) * \tilde{u}^*(-t) = \sum_{i=0}^{\infty} \alpha(i)\tilde{u}(t - \tau_i) * \tilde{u}^*(-t) \\ &= \sum_{i=0}^{\infty} \alpha(i) \int_0^T \tilde{u}(\tau)\, \tilde{u}^*(\tau - t + \tau_i)\, d\tau \\ &= \sum_{i=0}^{\infty} \alpha(i)\Phi_u(t - \tau_i) \end{aligned} \tag{3.6}$$

where $\Phi_u(t) = \int_0^T \tilde{u}(\tau)\tilde{u}^*(\tau - t)d\tau$ is the autocorrelation function of the signaling pulse $\tilde{u}(t)$.

As the RAKE receiver in this model is a filter matched to the multipath fading channel, the impulse response of this maximum gain RAKE combining receiver is:

$$\tilde{g}(t) = \tilde{h}^*(-t) = \sum_{l=0}^{\infty} \alpha^*(l)\delta(t+\tau_l) \tag{3.7}$$

The output of the RAKE receiver is the convolution of $\tilde{y}(t)$ and $\tilde{g}(t)$ given as follows:

$$\begin{aligned} \tilde{z}(t) &= \tilde{y}(t) * \tilde{g}(t) = \sum_{i=0}^{\infty} \alpha(i)\Phi_u(t-\tau_i) * \sum_{l=0}^{\infty} \alpha^*(l)\delta(t+\tau_i) \\ &= \sum_{i=0}^{\infty}\sum_{l=0}^{\infty} \alpha(i)\,\alpha^*(l)\Phi_u(t-\tau_i+\tau_l) \end{aligned} \tag{3.8}$$

Since the filter $\tilde{u}^*(-t)$ is matched to the signaling pulse and the RAKE receiver is matched to the multipath fading channel, the output of the RAKE receiver, $\tilde{z}(t)$ is simply the autocorrelation function $\Phi_r(t)$ of the received signal $\tilde{r}(t)$, that is.

$$\Phi_r(t) = \tilde{z}(t) = \int_0^T \tilde{r}(\tau)\tilde{r}^*(\tau - t)d\tau = \sum_{i=0}^{\infty}\sum_{l=0}^{\infty} \alpha(i)\alpha^*(l)\Phi_u(t-\tau_i+\tau_l) \tag{3.9}$$

Therefore, the multipath induced ISI is reflected in $\Phi_r(t)$ not satisfying Nyquist's first criterion. We can see from (3.9) that the autocorrelation function $\Phi_r(t)$ is a sum of many scaled autocorrelation functions $\Phi_u(t)$ of different delays.

A typical plot of the autocorrelation function $\Phi_r(t)$ is depicted in Fig. 3.8. In order to have minimum ISI, the values at discrete points $t = kT$, where k is an integer and $k \neq 0$, should be zero or minimized. This implies that $\Phi_r(t)$ must satisfy Nyquist's first criterion. Although the delayed paths are naturally occurred in random, we can see from Fig. 3.8 that the narrower the peaks are, the smaller the chance of having them occurred at the discrete times $t = kT$ causing significant ISI. Therefore, in order to get smaller probability of having significant ISI, we need to use a signaling pulse $\tilde{u}(t)$ which has a narrow mainlobe in its autocorrelation function. This can be obtained at the expense of bandwidth.

At discrete points $t = kT$, for $k = 0$, we have:

$$\Phi_r(0) = \Phi_u(0)\sum_{i=0}^{\infty}|\alpha(i)|^2 + \sum_{i=0}^{\infty}\sum_{l=0, l\neq i}^{\infty} \alpha(i)\alpha^*(l)\Phi_u(-\tau_i+\tau_l) \tag{3.10}$$

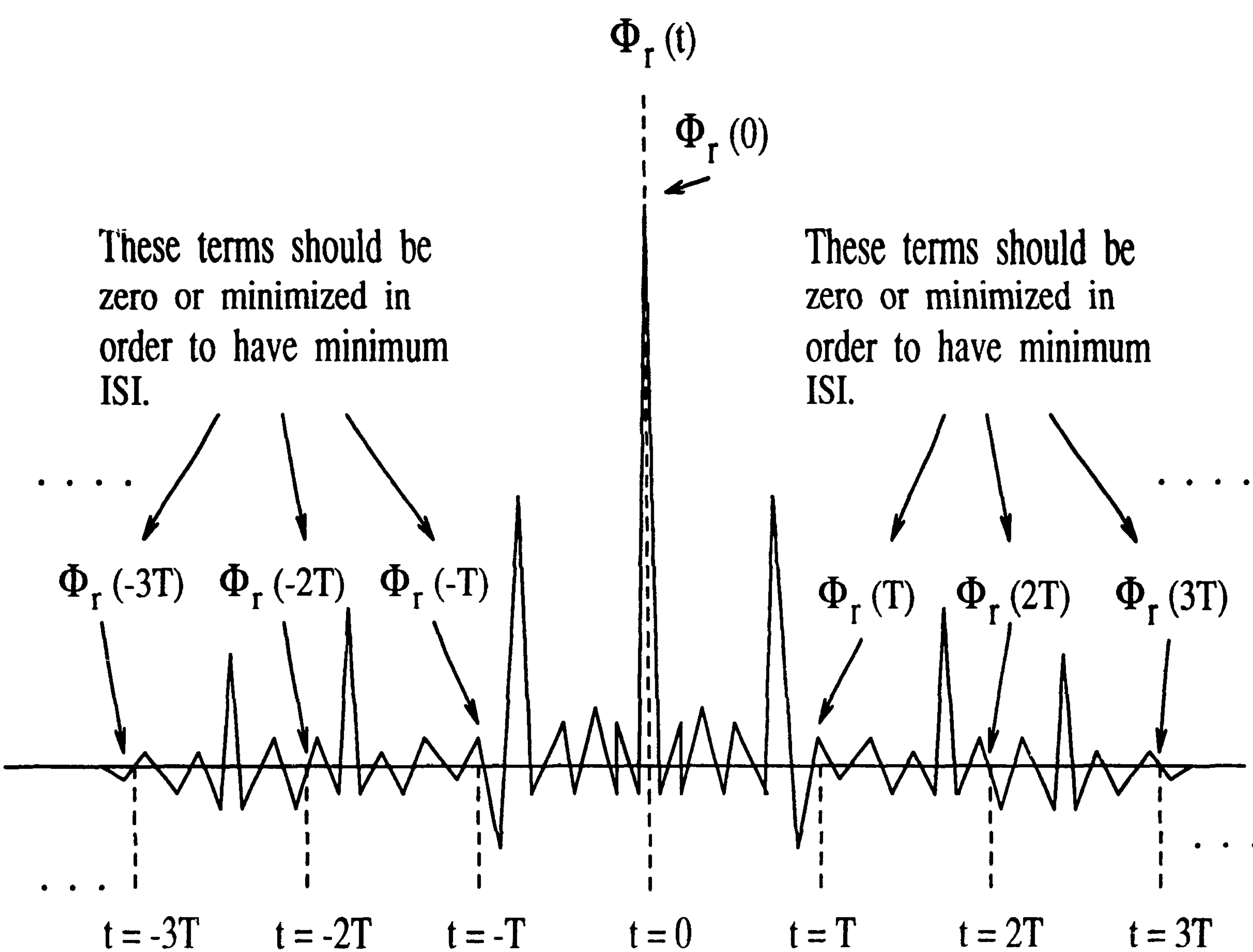

Figure 3.8: The autocorrelation function of the received signal.

and for $k \neq 0$,

$$\Phi_{\mathbf{r}}(kT) = \Phi_{\mathbf{u}}(kT)\sum_{i=0}^{\infty}|\alpha(i)|^2 + \underbrace{\sum_{i=0}^{\infty}\sum_{l=0,l\neq i}^{\infty}\alpha(i)\alpha^*(l)\Phi_{\mathbf{u}}(kT-\tau_i+\tau_l)}_{\eta(kT)} \tag{3.11}$$

The mainlobe of $\Phi_{\mathbf{u}}(t)$ affects the interference term $\eta(kT)$ when $|kT-\tau_i+\tau_l| \leq T_c$ and the corresponding path gains $\alpha(i)$ and $\alpha(l)$ are not vanishing. The probability that the mainlobe of $\Phi_{\mathbf{u}}(t)$ is included in the ISI term can be upper-bounded by the union-bound. Let P be the probability of having significant ISI occurred at the output of the maximum gain RAKE combiner. By union-bounding, it can be bounded by.

$$P \leq \sum_{l=0}^{\infty}\sum_{i=0,i\neq l}^{\infty}\sum_{k\neq 0,k=-\infty}^{\infty} Pr\left[\,|kT-\tau_i+\tau_l| \leq T_c \;\mid\; |\alpha(i)| > \theta, |\alpha(l)| > \theta\,\right] \tag{3.12}$$

where θ is a threshold that defines the level of the path gains where the interference becomes significant. In general, the path delays are estimated from channel impulse measurements. Therefore, all the paths which are less than the maximum observed delay spread have path gains which are above the threshold θ. In other words, the two events $|\alpha(i)| > \theta$ and $\tau_i < \Delta$ are equivalent, where Δ denotes the maximum observed delay spread, we then have:

$$P \leq \sum_{l=0}^{\infty}\sum_{i=0,i\neq l}^{\infty}\sum_{k\neq 0,k=-\infty}^{\infty} Pr\left[\,|kT-\tau_i+\tau_l| \leq T_c \;\mid\; \tau_i < \Delta, \tau_l < \Delta\,\right] \tag{3.13}$$

In order to evaluate (3.13), we need a probabilistic model for the multipath delays τ_i. To get an insight into the problem, a simple Poisson model will be enough. Let us assume that $\tau_0 = 0$ and the path delays $\tau_1 < \tau_2 < \tau_3 \ldots$, when considered ordered random variables, are the arrival times of a Poisson process with rate λ characterized by the exponential probability density function $p(\tau_i|\tau_{i-1}) = \lambda e^{-\lambda(\tau_i - \tau_{i-1})}$. Let I be the number of arrivals with $\tau_i \leq \Delta$ and the probability of having I arrivals in the period of Δ is:

$$Pr[I=n] = e^{-\lambda\Delta}\frac{(\lambda\Delta)^n}{n!} \tag{3.14}$$

If I is fixed, (3.13) becomes:

$$P(I) \leq \sum_{l=0}^{I}\sum_{i=0,i\neq l}^{I}\sum_{k\neq 0,k=-\infty}^{\infty} Pr\left[\,|kT-\tau_i+\tau_l| \leq T_c \;\mid\; \tau_i < \Delta, \tau_l < \Delta\,\right] \tag{3.15}$$

When I is fixed, then $\tau_1, \tau_2, \ldots, \tau_I$ are distributed as the ordered statistics of I mutually independent random variables uniformly distributed in $[0,\Delta]$ [33, pp. 191]. However, the bound to $P(I)$ is not changed if we remove the restriction that $\tau_1, \tau_2, \ldots, \tau_I$ are ordered and thus they must be only independent and uniformly distributed in $[0,\Delta]$. Therefore, (3.15) can be further reduced to:

$$P(I) \leq \sum_{l=0}^{I} \sum_{i=0, i\neq l}^{I} \sum_{k\neq 0, k=-\infty}^{\infty} Pr\left[\,|kT - \tau_{il}| \leq T_c \mid \tau_i < \Delta, \tau_l < \Delta\,\right] \tag{3.16}$$

where $\tau_{il} = \tau_i - \tau_l$. With the assumption that $\tau_0 = 0$, the random variables $-\tau_{0l}$ and τ_{i0}, where $i, l \geq 1$, have a uniform distribution with the probability density function as shown in Fig. 3.9 while the random variables τ_{il}, where $i, l \geq 1$, have a triangular distribution with the probability density function as shown in Fig. 3.10. To evaluate (3.16), we first consider the case when either i or l is zero. For $l = 0$, the random variable $\tau_{il} = \tau_{i0} = \tau_i$ is uniformly distributed, we have

$$\begin{aligned} Pr\left[\,|kT - \tau_{i0}| \leq T_c \mid \tau_i < \Delta\,\right] &= Pr\left[\,|kT - \tau_i| \leq T_c \mid \tau_i < \Delta\,\right] \\ &= Pr\left[\,kT - T_c \leq \tau_i \leq kT + T_c \mid \tau_i < \Delta\,\right] \\ &= 2T_c\, P_{\tau_i}[kT \mid \tau_i < \Delta] = \frac{2T_c}{\Delta} \end{aligned} \tag{3.17}$$

where $0 < kT < \Delta$. Since $T_c \ll T$, therefore k assumes positive values from 1 to $\lceil \Delta/T \rceil$. Similarly, for $i = 0$, the random variable $\tau_{il} = \tau_{0l} = -\tau_l$ is also uniformly distributed, we have

$$\begin{aligned} Pr\left[\,|kT - \tau_{0l}| \leq T_c \mid \tau_l < \Delta\,\right] &= Pr\left[\,|kT + \tau_l| \leq T_c \mid \tau_l < \Delta\,\right] \\ &= Pr\left[\,-kT - T_c \leq \tau_l \leq -kT + T_c \mid \tau_l < \Delta\,\right] \\ &= 2T_c\, P_{\tau_l}[-kT \mid \tau_l < \Delta] = \frac{2T_c}{\Delta} \end{aligned} \tag{3.18}$$

where $0 < -kT < \Delta$, so k assumes negative values from -1 to $-\lceil \Delta/T \rceil$. As there are $2I$ terms which have either $i = 0$ or $l = 0$, this gives the sum:

$$2I \sum_{k=1}^{\lceil \Delta/T \rceil} \frac{2T_c}{\Delta} \tag{3.19}$$

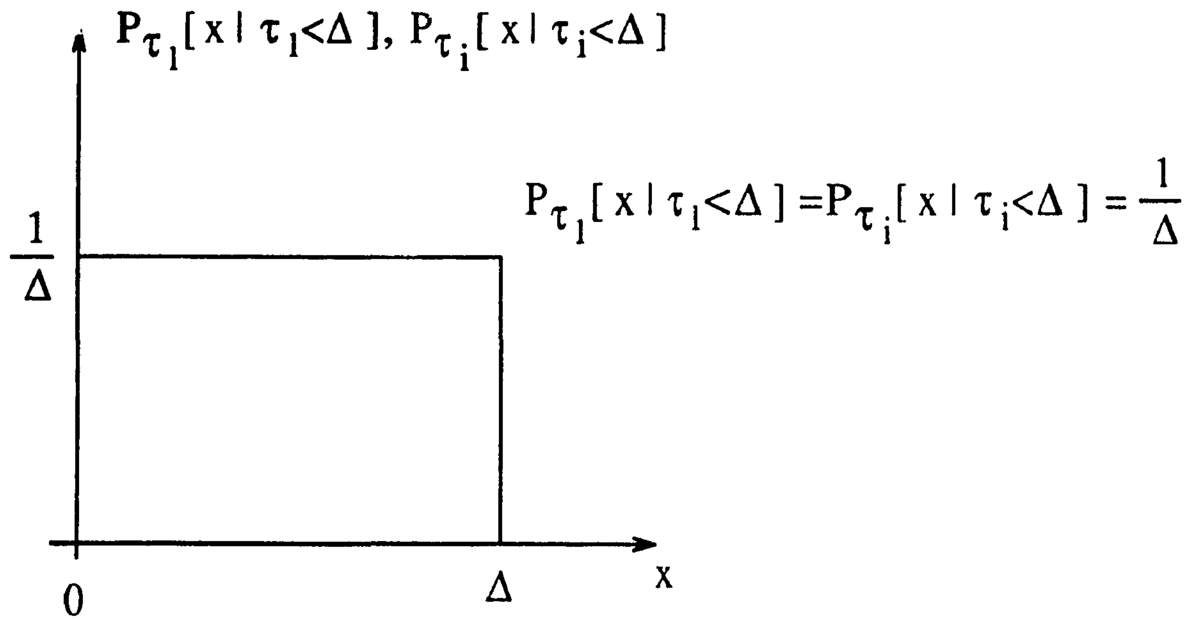

Figure 3.9: Probability density function of the random variables τ_l and τ_i

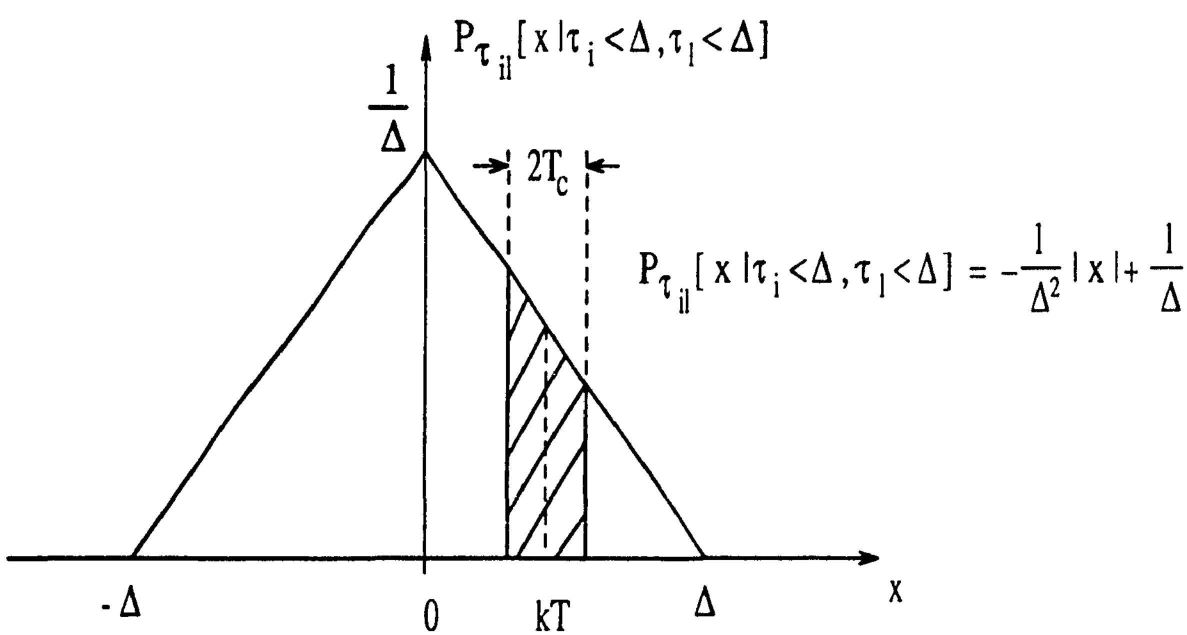

Figure 3.10: Probability density function of the random variable τ_{il}.

In the case when both i and l are nonzero, the random variable τ_{il} is triangularly-distributed, we have

$$\begin{aligned}
Pr\left[\,|kT-\tau_{il}|\le T_c \mid \tau_i<\Delta,\tau_l<\Delta\,\right] &= Pr\left[\,-T_c-kT\le\tau_{il}\le T_c-kT \mid \tau_i<\Delta,\tau_l<\Delta\,\right]\\
&= Pr\left[\,kT-T_c\le\tau_{il}\le kT+T_c \mid \tau_i<\Delta,\tau_l<\Delta\,\right]\\
&= 2T_c\,P_{\tau_{il}}[kT\mid \tau_i<\Delta,\tau_l<\Delta]\\
&= \frac{2T_c}{\Delta}-\frac{2T_c\,|kT|}{\Delta^2}
\end{aligned} \tag{3.20}$$

where $0<|kT|<\Delta$. In this case, k can be either positive or negative, and it assumes values between $-\lceil\Delta/T\rceil$ and $\lceil\Delta/T\rceil$, except 0. Since there are $I(I-1)$ terms which have nonzero i and l, this gives the sum:

$$I(I-1)\sum_{k=-\lceil\Delta/T\rceil,k\neq 0}^{\lceil\Delta/T\rceil}\frac{2T_c}{\Delta}[1-\frac{|kT|}{\Delta}] \tag{3.21}$$

Therefore, (3.16) becomes:

$$P(I)\le I(I-1)\sum_{k=-\lceil\Delta/T\rceil,k\neq 0}^{\lceil\Delta/T\rceil}\frac{2T_c}{\Delta}[1-\frac{|kT|}{\Delta}]+2I\sum_{k=1}^{\lceil\Delta/T\rceil}\frac{2T_c}{\Delta} \tag{3.22}$$

Let $K=\lceil\Delta/T\rceil$, then:

$$\begin{aligned}
P(I) &\le I(I-1)\sum_{k=-K,k\neq 0}^{K}\frac{2T_c}{\Delta}[1-\frac{|k|T}{\Delta}]+2I\sum_{k=1}^{K}\frac{2T_c}{\Delta}\\
&= 4I^2K\frac{T_c}{\Delta}-4I(I-1)T\frac{T_c}{\Delta^2}\frac{(1+K)K}{2}\\
&= 4I^2K\frac{T_c}{\Delta}[1-\frac{T}{\Delta}\frac{(1+K)}{2}]+4IK\frac{T_c}{\Delta}\frac{T}{\Delta}\frac{(1+K)}{2}
\end{aligned} \tag{3.23}$$

Define

$$\frac{1}{G}=K\frac{T_c}{\Delta}=\lceil\Delta/T\rceil\frac{T_c}{\Delta} \tag{3.24}$$

Substituting (3.24) into (3.23) yields:

$$P(I)\le\frac{4}{G}\,[I^2(1-\frac{T}{\Delta}\frac{(1+K)}{2})+\frac{IT}{\Delta}\frac{(1+K)}{2}] \tag{3.25}$$

When averaging over I, we have $\overline{I} = \lambda\Delta$ and $\overline{I^2} = \lambda^2\Delta^2 + \lambda\Delta$, then

$$\begin{aligned} P = \overline{P(I)} &\leq \frac{4}{G}[\overline{I^2}(1 - \frac{T}{\Delta}\frac{(1+K)}{2}) + \frac{\overline{I}T}{\Delta}\frac{(1+K)}{2}] \\ &= \frac{4}{G}[(\lambda^2\Delta^2 + \lambda\Delta)(1 - \frac{T}{\Delta}\frac{(1+K)}{2}) + \lambda T\frac{(1+K)}{2}] \\ &= \frac{4}{G}[\lambda^2\Delta^2 + \lambda\Delta - \lambda^2\Delta T\frac{(1+K)}{2}] \\ &= \frac{4}{G}\lambda\Delta[1 + \lambda\Delta - \lambda T\frac{(1+K)}{2}] \end{aligned} \tag{3.26}$$

Let us define $\tilde{\Delta} = KT = \lceil \Delta/T \rceil T$, then

$$\frac{1}{G} = \frac{\tilde{\Delta}}{T}\frac{T_c}{\Delta} \tag{3.27}$$

or

$$G = \frac{T}{T_c}\frac{\Delta}{\tilde{\Delta}} = G_p\frac{\Delta}{\tilde{\Delta}} \tag{3.28}$$

where $G_p = \frac{T}{T_c}$ is the bandwidth expansion factor or the processing gain. Therefore

$$\begin{aligned} P &\leq \frac{4}{G_p}\lambda\tilde{\Delta}[1 + \lambda\Delta - \lambda T\frac{(1+\tilde{\Delta}/T)}{2}] \\ &= \frac{4}{G_p}\lambda\tilde{\Delta}[1 + \lambda(\Delta - \frac{\tilde{\Delta}}{2} - \frac{T}{2})] \end{aligned} \tag{3.29}$$

or

$$P \leq \max\ \{\ 0,\ \frac{4}{G_p}\lambda\tilde{\Delta}[1 + \lambda(\Delta - \frac{\tilde{\Delta}}{2} - \frac{T}{2})]\ \} \tag{3.30}$$

where the use of max $(0, \cdot)$ takes into account that when (3.29) is negative, then there is no ISI. Normally, $\Delta \leq \tilde{\Delta}$, and therefore a less tight upper bound is:

$$P < \frac{4}{G_p}\lambda\tilde{\Delta}[1 + \frac{\lambda}{2}(\tilde{\Delta} - T)] = \tilde{P} \tag{3.31}$$

When $\tilde{P} \geq 1$, then (3.31) is useless and the tighter bound(3.30) should be used

The upper-bound of (3.31) shows that the probability of having significant ISI over a random multipath channel decreases with increasing the bandwidth expansion factor. Therefore, with sufficient bandwidth expansion, the multipath induced ISI does not have any significant effect on the system performance. Rearranging (3.31), we can express the processing gain as:

$$G_p = \frac{4\tilde{I}_{max}}{\tilde{P}} [1 + \frac{\tilde{I}_{max}}{2}(1 - \frac{1}{R\tilde{\Delta}})] \tag{3.32}$$

where $\tilde{I}_{max} = \lambda\tilde{\Delta}$ and $R = 1/T$. Equation (3.32) gives an estimate to the required processing gain which ensures a certain upper bound $\tilde{P}$ to the probability of having significant ISI.

If L order antenna diversity is used, the probability that all L diversity channels are bad simultaneously is reduced considerably. The strategy that the receiver uses for this diversity technique is to choose the best signal among the L diversity channels. If $\tilde{P}$ is the upper bound of having significant ISI in one diversity channel, then $\tilde{P}^L$ is the upper bound of having significant ISI in all L channels and thus we cannot avoid ISI With this antenna selection diversity technique, the required processing gain becomes.

$$G_p = \frac{4\tilde{I}_{max}}{\tilde{P}^{\frac{1}{L}}} [1 + \frac{\tilde{I}_{max}}{2}(1 - \frac{1}{R\tilde{\Delta}})] \tag{3.33}$$

A graph of the processing gain G_p as a function of $R\tilde{\Delta}$ with $\tilde{P} = 0.01$ and different values of $\tilde{I}_{max}$ and L is shown in Fig. 3.11. It is seen that the required processing gain. G_p, increases with $R\tilde{\Delta} = \lceil\Delta/T\rceil$, the multipath delay spread normalized to the symbol time. However, there is a saturation effect in the sense that above a certain processing gain, any additional increase in $R\tilde{\Delta}$ can be accomodated with only a small further increase in G_p. For a relatively small multipath spread, $\Delta \leq T$ and $R\tilde{\Delta} = 1$. In this case,

$$G_p = \frac{4\tilde{I}_{max}}{\tilde{P}^{\frac{1}{L}}} \tag{3.34}$$

showing that the required processing gain increases linearly with the number of channel paths. When $\Delta \ll T$, (3.33) is not tight and therefore (3.30) should be used showing that if the symbol time is sufficiently large, there is no ISI ($P \leq 0$). The other extreme is $R\tilde{\Delta}$ approaches ∞. In this case,

$$G_p \approx \frac{4\tilde{I}_{max}}{\tilde{P}^{\frac{1}{L}}}(1 + \frac{\tilde{I}_{max}}{2}) \tag{3.35}$$

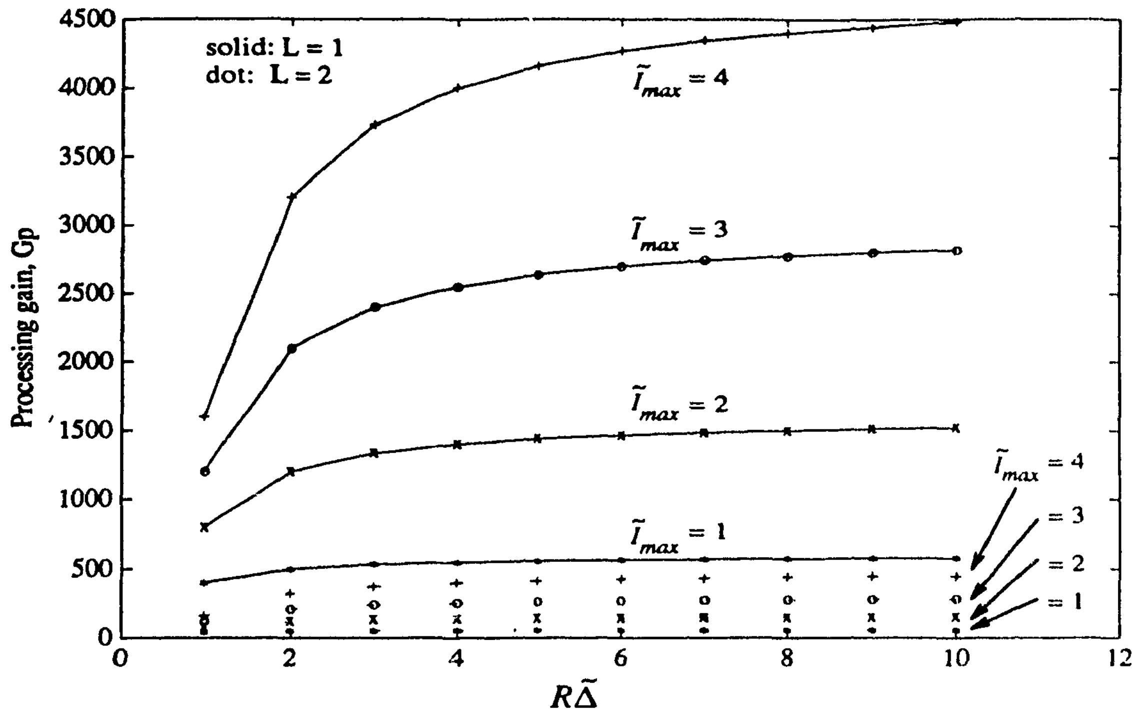

Figure 3.11: Graph of processing gain G_p as a function of $R\Delta$ with $\tilde{P} = 0.01$.

which shows that the required processing gain increases as the square of the number of channel paths.

The bandwidth expansion required is large when $\tilde{P}$ is small because of the inversely proportional relationship between G_p and $\tilde{P}$ which can be inferred from (3.33) With the current state of the art in SAW, digital and SAW convolver technologies, pseudonoise matched filters or correlators with processing gain as large as 30 dB are achievable [34]. However, the necessary processing gain is greatly reduced when antenna diversity is employed. The required processing gain is reduced significantly even when $L = 2$. In fact, for $\tilde{l}_{max} = 1$ and $\tilde{P} = 0.01$, the required processing gain is reduced by a factor of 10 when $L = 2$. It will further be reduced when L increases, this result can be seen in Fig. 3.12.

From the above analysis, we conclude that with sufficient bandwidth expansion

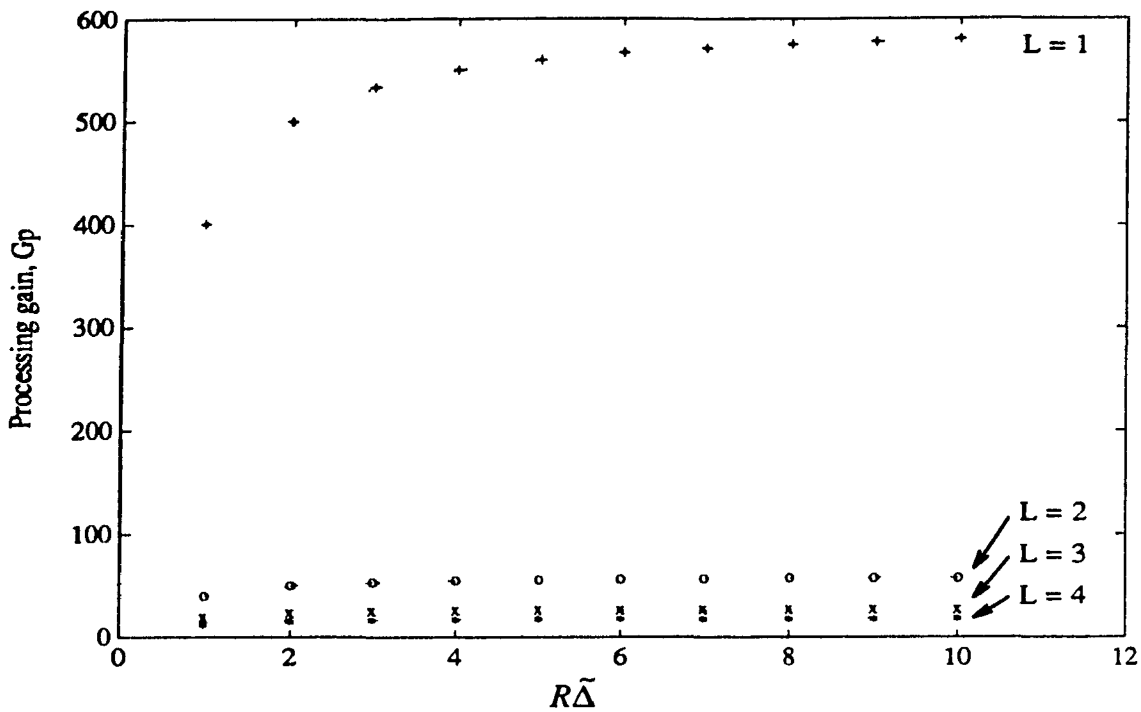

Figure 3.12: Graph of processing gain G_p as a function of $R\Delta$ with $\tilde{P} = 0.01$ and $\tilde{I}_{max} = 1$.

in digital communication over random multipath channels, the probability of having significant ISI can be made arbitrarily small and thus an adaptive equalizer following the RAKE receiver is unnecessary. Furthermore, the necessary bandwidth expansion required is tremendously reduced in the case when antenna diversity techniques are employed.

This analysis can be modified to apply also to the GL receiver of section 2.2 which is composed of a matched filter followed by a square-law nonlinearity and equal weight RAKE combiner. The difficulty here is the presence of the nonlinearity, and therefore the first step is to examine to what extent a single pulse analysis can be used for ISI investigation. The model of this system is shown in Fig. 3.13. The output of the

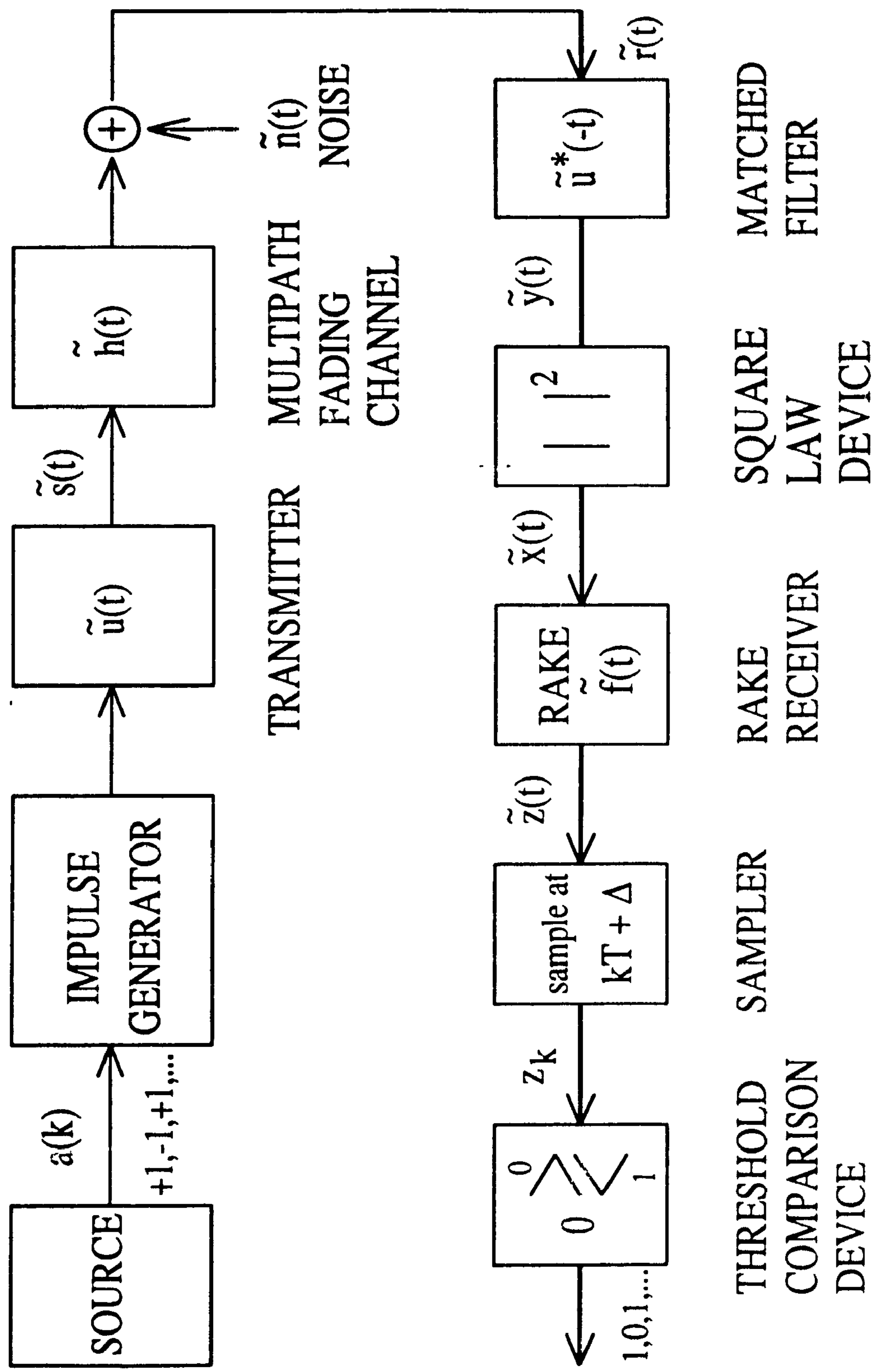

Figure 3.13: A model for a bandwidth expanding communication system with square-law equal weight RAKE receiver.

matched filter for a single pulse transmission as obtained in (3.6) is:

$$\tilde{y}(t) = \sum_{i=0}^{\infty} \alpha(i)\Phi_u(t - \tau_i) \tag{3.36}$$

where $\Phi_u(t) = \int_0^T \tilde{u}(\tau)\tilde{u}^*(\tau - t)d\tau$. For sequential transmissions, the output of the matched filter becomes:

$$\tilde{v}(t) = \sum_{p=-\infty}^{\infty} a(p)\tilde{y}(t - pT) \tag{3.37}$$

where $a(p)$'s are the transmitted data sequences. The output of the squared-law device is given by:

$$\tilde{x}(t) = |\tilde{v}(t)|^2 \tag{3.38}$$

and the output of the equal weight RAKE combiner with impulse response $\tilde{f}(t)$ is:

$$\begin{aligned} \tilde{z}(t) &= \tilde{x}(t) * \tilde{f}(t) \\ &= \int |\tilde{v}(\tau)|^2 \cdot \tilde{f}(t - \tau)\, d\tau \end{aligned} \tag{3.39}$$

With the substitution of (3.37), we have:

$$\begin{aligned} \tilde{z}(t) &= \int \sum_{p=-\infty}^{\infty} \sum_{q=-\infty}^{\infty} a(p)a(q)\tilde{y}(\tau - pT)\tilde{y}^*(\tau - qT)\tilde{f}(t - \tau)\, d\tau \\ &= \sum_{p=-\infty}^{\infty} \sum_{q=-\infty}^{\infty} \int a(p)a(q)\tilde{y}(\tau - pT)\tilde{y}^*(\tau - qT)\tilde{f}(t - \tau)\, d\tau \\ &= \sum_{p=-\infty}^{\infty} \int a^2(p)|\tilde{y}(\tau - pT)|^2\tilde{f}(t - \tau)\, d\tau + \sum_{p=-\infty}^{\infty} \sum_{q=-\infty, q\neq p}^{\infty} \int \tilde{y}(\tau - pT)\tilde{y}^*(\tau - qT)\tilde{f}(t - \tau)\, d\tau \end{aligned} \tag{3.40}$$

A typical plot of $\tilde{y}(t)$ is depicted earlier in Fig. 3.2, it shows that the multipath mainlobes of $\tilde{y}(t)$ are of different amplitudes and are spreaded over the interval $t = T$ and $t = T + \Delta$. Unless the multipath mainlobes are occurred at the integral number of T, then $\tilde{y}(\tau - pT)$ and $\tilde{y}^*(\tau - qT)$, where $p \neq q$, do not overlap. Therefore, the second term in the right side of (3.40) is small comparing to the first term, and thus we have:

$$\begin{aligned} \tilde{z}(t) &\approx \sum_{p=-\infty}^{\infty} \int a^2(p)|\tilde{y}(\tau - pT)|^2\tilde{f}(t - \tau)d\tau \\ &\approx \sum_{p=-\infty}^{\infty} a^2(p)|\tilde{y}(t - pT)|^2 * \tilde{f}(t) \end{aligned} \tag{3.41}$$

This shows that essentially the RAKE combiner acts linearly on $\sum_{p=-\infty}^{\infty} a^2(p)|\tilde{y}(t-pT)|^2$, and therefore a single pulse analysis can be used.

The output of the square-law device for a single pulse transmission is given by:

$$\tilde{x}(t) = |\tilde{y}(t)|^2 = \tilde{y}(t) \cdot \tilde{y}^*(t) \tag{3.42}$$

By using (3.6), we have:

$$\tilde{x}(t) = \sum_{i=0}^{\infty}\sum_{l=0}^{\infty} \alpha(i)\alpha^*(l)\Phi_u(t-\tau_i)\,\Phi_u^*(t-\tau_l) \tag{3.43}$$

As the impulse response of the equal weight RAKE combiner is:

$$\tilde{f}(t) = \sum_{j=0}^{\infty} \delta(t+\tau_j) \tag{3.44}$$

we then have the output of the equal weight RAKE combiner as follows:

$$\tilde{z}(t) = \tilde{x}(t) * \tilde{f}(t) = \sum_{i=0}^{\infty}\sum_{j=0}^{\infty}\sum_{l=0}^{\infty} \alpha(i)\alpha^*(l)\,\Phi_u(t-\tau_i+\tau_j)\,\Phi_u^*(t-\tau_l+\tau_j) \tag{3.45}$$

After sampling $\tilde{z}(kT)$, the mainlobe of $\Phi_u(t)$ and $\Phi_u^*(t)$ affect the interference term when $|kT-\tau_i+\tau_j| \leq T_c$ and $|kT-\tau_l+\tau_j| \leq T_c$ and the corresponding path gains $\alpha(i)$ and $\alpha^*(l)$ are not vanishing. Since τ_j appears in both random variables $|kT-\tau_i+\tau_j|$ and $|kT-\tau_l+\tau_j|$, these two are not independent.

To find the upper bound to the probability of having significant ISI occurred at the output of the equal weight RAKE combiner, we expand (3.45) as follows:

$$\begin{aligned}\tilde{z}(t) &= \sum_{i=0}^{\infty}\sum_{j=0}^{\infty}|\alpha(i)|^2\,|\Phi_u(t-\tau_i+\tau_j)|^2 + \sum_{i=0}^{\infty}\sum_{l=0,l\neq i}^{\infty}\sum_{j=0}^{\infty}\alpha(i)\alpha^*(l)\Phi_u(t-\tau_i+\tau_j)\Phi_u^*(t-\tau_l+\tau_j) \\ &= z_1(t) + z_2(t) \end{aligned} \tag{3.46}$$

where

$$z_1(t) = \sum_{i=0}^{\infty}\sum_{j=0}^{\infty}|\alpha(i)|^2\,|\Phi_u(t-\tau_i+\tau_j)|^2 \tag{3.47}$$

and

$$z_2(t) = \sum_{i=0}^{\infty}\sum_{l=0,l\neq i}^{\infty}\sum_{j=0}^{\infty}\alpha(i)\alpha^*(l)\Phi_u(t-\tau_i+\tau_j)\Phi_u^*(t-\tau_l+\tau_j) \tag{3.48}$$

If we define P_1 and P_2 to be the probability of having significant ISI in $z_1(t)$ and $z_2(t)$ respectively, then we have $P \leq P_1 + P_2$. The bounding of P_1 is similar to the analysis for maximum gain RAKE receiver as done earlier; thus, from (3.12), we have:

$$P_1 \leq \sum_{i=0}^{\infty} \sum_{j=0,j\neq i}^{\infty} \sum_{k\neq 0,k=-\infty}^{\infty} Pr\,[\,|kT - \tau_i + \tau_j| \leq T_c{}' \mid |\alpha(i)| > \theta, |\alpha(j)| > \theta\,] \tag{3.49}$$

where $T_c{}'$ is the width of $|\Phi_u(t)|^2$. Since the multiplication of two functions in the time domain is equivalent to the convolution of their spectral densities in the frequency domain, so the convolution of the spectral density of $\Phi_u(t)$ with itself results in a spectrum of bandwidth $2W$, where W is the bandwidth of $u(t)$. Therefore, as opposed to $T_c \approx \frac{1}{W}$, $T_c{}' \approx \frac{1}{2W}$, and $T_c \approx 2T_c{}'$. Since $G_p = \frac{T}{T_c}$, from (3.30), we then have:

$$P_1 \leq \max \{\, 0,\ \frac{2}{G_p}\lambda\tilde{\Delta}[1 + \lambda(\Delta - \frac{\tilde{\Delta}}{2} - \frac{T}{2})]\,\} \tag{3.50}$$

The bounding of P_2 is slightly complicated because the random variables $|kT - \tau_i + \tau_j|$ and $|kT - \tau_l + \tau_j|$ which are dependent due to τ_j. However, when we first fix τ_j, the two random variables are independent. Therefore,

$$\begin{aligned} P_2 \ \leq\ & \sum_{i=0}^{\infty} \sum_{l=0,l\neq i}^{\infty} \sum_{j=0}^{\infty} \sum_{k\neq 0,k=-\infty}^{\infty} \int_0^{\infty} Pr\,[\,|\,kT - \tau_i + \tau_j\,| \leq T_c \mid |\alpha(i)| > \theta, |\alpha(j)| > \theta, \tau_j\,] \\ & \cdot Pr\,[\,|\,kT - \tau_l + \tau_j\,| \leq T_c \mid |\alpha(l)| > \theta, |\alpha(j)| > \theta, \tau_j\,] \cdot P\,[\tau_j \mid |\alpha(j)| > \theta\,]\, d\tau_j \end{aligned} \tag{3.51}$$

Since the two events $|\alpha(i)| > \theta$ and $\tau_i < \Delta$ are equivalent, we then have:

$$\begin{aligned} P_2 \ \leq\ & \sum_{i=0}^{\infty} \sum_{l=0,l\neq i}^{\infty} \sum_{j=0}^{\infty} \sum_{k\neq 0,k=-\infty}^{\infty} \int_0^{\infty} Pr\,[\,|\,kT - \tau_i + \tau_j\,| \leq T_c \mid \tau_i < \Delta, \tau_j < \Delta, \tau_j\,] \\ & \cdot Pr\,[\,|\,kT - \tau_l + \tau_j\,| \leq T_c \mid \tau_l < \Delta, \tau_j < \Delta, \tau_j\,] \cdot P\,[\tau_j \mid \tau_j < \Delta\,]\, d\tau_j \end{aligned} \tag{3.52}$$

where $P\,[\tau_j \mid \tau_j < \Delta]$ is uniformly-distributed with the probability density function as shown in Fig. 3.14. Since

$$\begin{aligned} & Pr\,[\,|\,kT - \tau_i + \tau_j\,| \leq T_c \mid \tau_i < \Delta, \tau_j < \Delta, \tau_j\,] \\ = \ & Pr\,[\,kT + \tau_j - T_c \leq \tau_i \leq kT + \tau_j + T_c \mid \tau_i < \Delta, \tau_j < \Delta, \tau_j\,] \\ = \ & \frac{2T_c}{\Delta} \end{aligned} \tag{3.53}$$

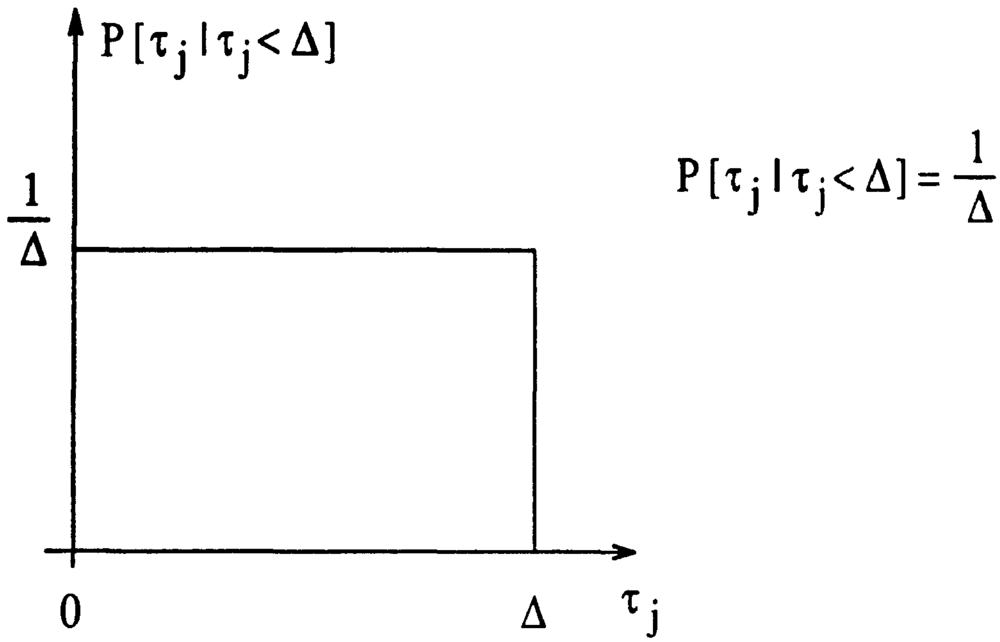

Figure 3.14: Probability density function of the random variable $P\left[\tau_j \mid \tau_j < \Delta\right]$.

where k must satisfy $0 < kT + \tau_j < \Delta$ for every τ_j. Since k assumes values from $-\infty$ to ∞, thus it always has $\lceil \frac{\Delta}{T} \rceil$ values which satisfy $0 < kT + \tau_j < \Delta$ regardless of what τ_j is. Therefore, after conditioning on the number of paths I, (3.52) becomes:

$$P_2(I) \leq \sum_{i=0}^{I} \sum_{l=0,l\neq i}^{I} \sum_{j=0}^{I} \lceil \frac{\Delta}{T} \rceil \int_0^{\Delta} (\frac{2T_c}{\Delta}) \cdot (\frac{2T_c}{\Delta}) \cdot \frac{1}{\Delta}\, d\tau_j \tag{3.54}$$

Let us define $K = \lceil \frac{\Delta}{T} \rceil$, then

$$\begin{aligned} P_2(I) &\leq \sum_{i=0}^{I} \sum_{l=0,l\neq i}^{I} \sum_{j=0}^{I} \int_0^{\Delta} \frac{4KT_c^2}{\Delta^3}\, d\tau_j \\ &= \sum_{i=0}^{I} \sum_{l=0,l\neq i}^{I} \frac{4K(I+1)T_c^2}{\Delta^2} \\ &= \frac{4KT_c^2(I^2+I)(I+1)}{\Delta^2} \end{aligned} \tag{3.55}$$

When averaging over I, we have $\overline{I} = \lambda\Delta$, $\overline{I^2} = \lambda^2\Delta^2 + \lambda\Delta$ and $\overline{I^3} = \lambda^3\Delta^3 + 3\lambda^2\Delta^2 + \lambda\Delta$, then:

$$\begin{aligned} P_2 = \overline{P_2(I)} &\leq \frac{4KT_c^2}{\Delta^2}(\overline{I}^3 + 2\overline{I}^2 + \overline{I}) \\ &\leq \frac{4KT_c^2}{\Delta^2}(\lambda^3\Delta^3 + 5\lambda^2\Delta^2 + 4\lambda\Delta) \end{aligned} \tag{3.56}$$

With the definitions of (3.24), (3.27) and (3.28), (3.56) becomes:

$$P_2 \leq \frac{4\lambda\tilde{\Delta}}{G_p^{\,2}(R\Delta)}\,(\lambda^2\Delta^2 + 5\lambda\Delta + 4) \tag{3.57}$$

where $G_p = \frac{T}{T_c}$. This shows that P_2 is inversely proportional to the square of the bandwidth expansion factor. With (3.50) and (3.57), we have:

$$\begin{aligned} P &\leq P_1 + P_2 \\ &\leq \max\{\,0, \frac{2}{G_p}\lambda\tilde{\Delta}[1 + \lambda(\Delta - \frac{\tilde{\Delta}}{2} - \frac{T}{2})] + \frac{4\lambda\tilde{\Delta}}{G_p^{\,2}(R\Delta)}\,(\lambda^2\Delta^2 + 5\lambda\Delta + 4)\,\} \end{aligned} \tag{3.58}$$

Comparing (3.58) to (3.30), it shows that with square-law equal weight RAKE combiner. an improvement of at least 3 dB over maximum gain RAKE receiver is achieved. Since $\Delta \leq \tilde{\Delta}$, and therefore a less tight upper bound is:

$$\begin{aligned} P &\leq \frac{2}{G_p}\lambda\tilde{\Delta}[1 + \frac{\lambda}{2}(\tilde{\Delta} - T)] + \frac{4\lambda\tilde{\Delta}}{G_p^{\,2}(R\Delta)}\,(\lambda^2\tilde{\Delta}^2 + 5\lambda\tilde{\Delta} + 4) \\ &\leq \frac{2\tilde{I}_{max}}{G_p}[1 + \frac{\tilde{I}_{max}}{2}(1 - \frac{1}{\lceil R\Delta\rceil})] + \frac{4\tilde{I}_{max}}{G_p^{\,2}(R\Delta)}\,(\tilde{I}^2_{max} + 5\tilde{I}_{max} + 4) = \tilde{P} \end{aligned} \tag{3.59}$$

where $\tilde{I}_{max} = \lambda\tilde{\Delta}$, $R = 1/T$ and $\lceil R\Delta\rceil = R\tilde{\Delta}$. For large G_p, $P_1 \gg P_2$, so we have:

$$P \leq \frac{2\tilde{I}_{max}}{G_p}[1 + \frac{\tilde{I}_{max}}{2}(1 - \frac{1}{\lceil R\Delta\rceil})] \tag{3.60}$$

For fixed $\tilde{P} > 0$, (3.59) can be rearranged into the following form:

$$\tilde{P}(R\Delta)G_p^{\,2} - 2\tilde{I}_{max}(R\Delta)\,[1 + \frac{\tilde{I}_{max}}{2}(1 - \frac{1}{\lceil R\Delta\rceil})]G_p - 4\,(\tilde{I}^3_{max} + 5\tilde{I}^2_{max} + 4\tilde{I}_{max}) = 0 \tag{3.61}$$

Since the processing gain G_p is always positive, it can be expressed as follows:

$$\begin{aligned} G_p &= \frac{\tilde{I}_{max}}{\tilde{P}}[1 + \frac{\tilde{I}_{max}}{2}(1 - \frac{1}{\lceil R\Delta\rceil})] \\ &+ \frac{\sqrt{\tilde{I}^2_{max}\,[1 + \frac{\tilde{I}_{max}}{2}(1 - \frac{1}{\lceil R\Delta\rceil})]^2 + \frac{4\tilde{P}}{(R\Delta)}\,(\tilde{I}^3_{max} + 5\tilde{I}^2_{max} + 4\tilde{I}_{max})}}{\tilde{P}} \end{aligned} \tag{3.62}$$

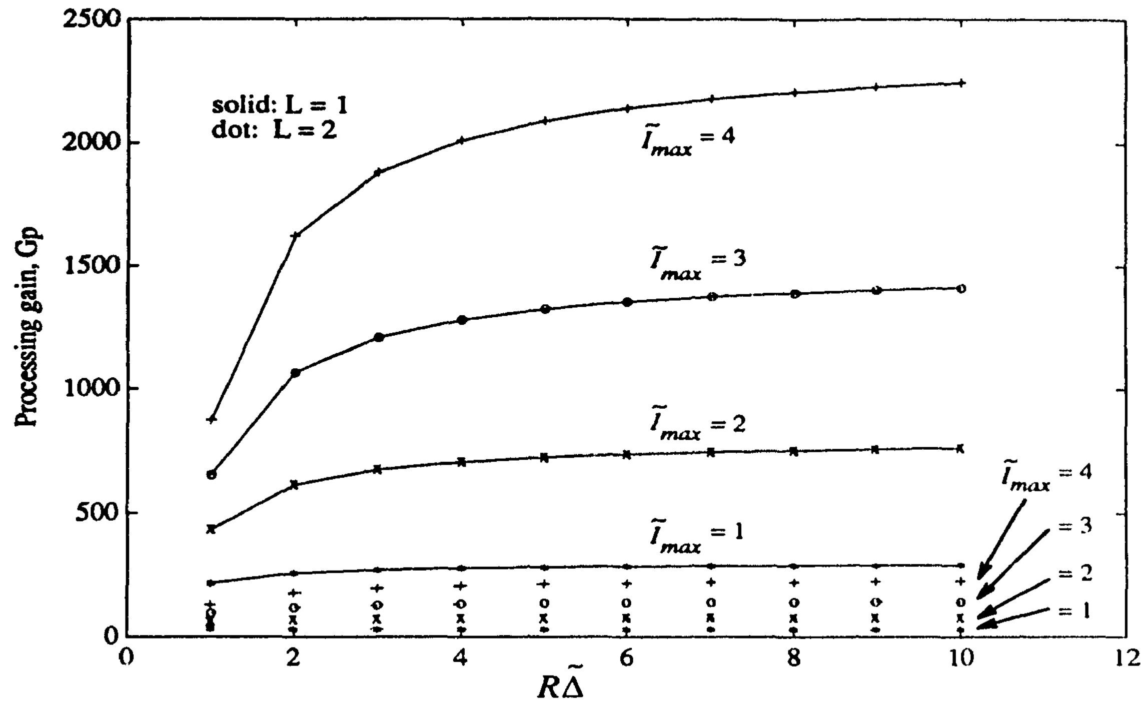

Figure 3.15: Graph of processing gain G_p as a function of $R\Delta$ with $\tilde{P} = 0.01$.

With L antenna diversity, the required processing gain becomes:

$$\begin{aligned} G_p &= \frac{\tilde{I}_{max}}{(\tilde{P})^{\frac{1}{L}}}[1 + \frac{\tilde{I}_{max}}{2}(1 - \frac{1}{\lceil R\Delta \rceil})] \\ &+ \frac{\sqrt{\tilde{I}^2_{max}[1 + \frac{\tilde{I}_{max}}{2}(1 - \frac{1}{\lceil R\Delta \rceil})]^2 + \frac{4(\tilde{P})^{\frac{1}{L}}}{(R\Delta)}(\tilde{I}^3_{max} + 5\tilde{I}^2_{max} + 4\tilde{I}_{max})}}{(\tilde{P})^{\frac{1}{L}}} \end{aligned} \quad (3.63)$$

The relationship between the processing gain G_p and $R\tilde{\Delta}$ with $\tilde{P} = 0.01$ and different values of $\tilde{I}_{max}$ and L is shown in Fig. 3.15. The behaviour of G_p for the square-law equal weight RAKE combiner is similar to that of the maximum gain RAKE combiner as shown earlier in Fig. 3.11 The required processing gain increases with the number of delayed paths in the channel impulse response and it also increases with $R\tilde{\Delta}$. However, the saturation effect indicates that above a certain processing gain, any additional increase in $R\tilde{\Delta}$ results in only a small increase in G_p. In addition, the required

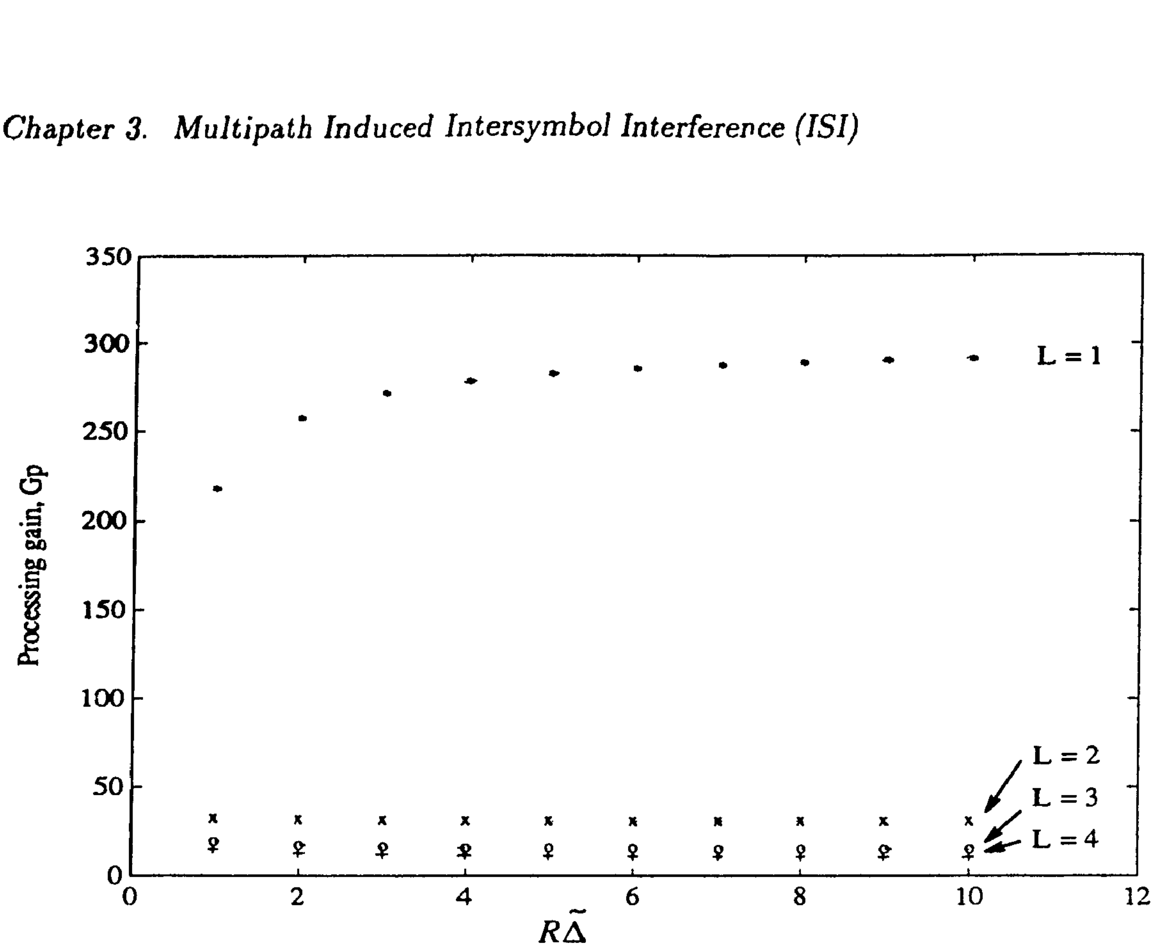

Figure 3.16: Graph of processing gain G_p as a function of $R\Delta$ with $\tilde{P}$ = 0.01 and $\tilde{I}_{max}$ = 1.

amount of bandwidth expansion for ISI suppression is greatly reduced when antenna diversity is employed, which can be seen in Fig. 3.16. One advantage of using the square-law equal weight RAKE combiner is that for a given $\tilde{P}$, the necessary processing gain is approximately half of that as required for the maximum gain RAKE combiner. This can be seen by comparing Fig. 3.11 and Fig. 3.15. In the next section, we extend the above ISI analysis to the maximum gain RAKE combiner and the square-law equal weight RAKE combiner when commutation signaling is used.

3.3 ISI Effects on Commutation Signaling

In this section, we consider the effects of multipath induced ISI on the data detection process in a system where commutation signaling scheme is employed. As mentioned in section 3.1 that $M \times N$ signaling relied on switching N distinct M-ary signal sets. None of the N signal sets is used again until the ringing of its previous transmission has diminished. As a result, the sampling time of each matched filter with commutation signaling scheme is no longer kT, but kNT, where T is the symbol time interval Therefore, all the results of the ISI analysis obtained in section 3.2 can be applied to commutation signaling with T replaced by NT.

For maximum gain RAKE combiner with commutation signaling, by using the the result as obtained in (3.30), the probability of having significant ISI is

$$P \leq \max \{ \, 0, \; \frac{4}{G_p} \lambda \tilde{\Delta} [1 + \lambda(\Delta - \frac{\tilde{\Delta}}{2} - \frac{NT}{2})] \, \} \tag{3.64}$$

where the processing gain is now $G_p = \frac{NT}{T_c}$ and $\tilde{\Delta} = \lceil \frac{\Delta}{NT} \rceil NT$. In order to have zero ISI, we need:

$$\begin{aligned} 1 + \lambda(\Delta - \frac{\tilde{\Delta}}{2} - \frac{NT}{2}) \;&\leq\; 0 \\ 1 - \lambda\Delta(\frac{NT}{2\Delta} + \frac{NT}{2\Delta}\lceil \frac{\Delta}{NT} \rceil - 1) \;&\leq\; 0 \\ (\frac{NT}{2\Delta} + \frac{NT}{2\Delta}\lceil \frac{\Delta}{NT} \rceil - 1) \;&\geq\; \frac{1}{\lambda\Delta} \end{aligned} \tag{3.65}$$

Now, since $\lceil \frac{\Delta}{NT} \rceil \frac{NT}{\Delta} \geq 1$, thus, the condition for zero ISI is:

$$\begin{aligned} \frac{NT}{2\Delta} + \frac{1}{2} - 1 \;&>\; \frac{1}{\lambda\Delta} \\ \frac{NT}{\Delta} \;&>\; 1 + \frac{2}{\lambda\Delta} \end{aligned} \tag{3.66}$$

Therefore, a sufficient condition for zero ISI for the maximum gain RAKE combiner with commutation signaling is:

$$N > \frac{\Delta}{T} + \frac{2}{\lambda T} \tag{3.67}$$

or

$$N \geq \lceil R\Delta + \frac{2}{\lambda T} \rceil \tag{3.68}$$

where λT is the average number of paths within the symbol time interval.

As explained in section 3.1 that in order to have no ISI for binary commutation signaling, the number of binary signal sets required is $N = \lceil R\Delta \rceil$, which is less than the condition derived in (3.68). The discrepancy is due to the exact implication of the parameter Δ. In section 3.1, the parameter Δ is defined as the *time delay spread* within which all the delayed paths are presented. That is, there is no delayed path with time delay larger than this *time delay spread.* Therefore, we use a heuristic approach to show that no ISI exists when the number of binary signal sets is $N = \lceil R\Delta \rceil$. However, the condition in (3.68) is derived using a probabilistic channel model. The path delays are modelled as a Poisson process with constant rate λ. The parameter Δ is considered as the maximum observed delay spread and any delayed path, within this time interval, results in a peak at the matched filter output with its amplitude exceeding the threshold. There are two possibilities that a peak is not considered as a delayed path. One of which is that the peak is being attenuated such that its amplitude does not exceed the threshold, and this peak does not cause significant ISI. The other possibility is that the delayed path appears outside the interval of the maximum observed delay spread, this happens when the rate λ is so small that the arrival time of the delayed path falls beyond the maximum observed delay spread. Depending on the amplitude of this delayed path, it may cause significant ISI. As a result, the term $\frac{2}{\lambda T}$ in (3.68) is a safety factor which takes into account of the occurrence of the latter possibility. When the rate λ is small or the average number of delayed paths within the symbol time interval, λT is much smaller than 2, that is, $\lambda T \ll 2$, then the safety factor is much greater than 1. Therefore, (3.68) is the condition for zero ISI in the maximum gain RAKE combiner with commutation signaling. This implies that more signal sets than $\lceil R\Delta \rceil$ are needed when taking into consideration of the possibility of having some paths of significant ampitude with time delays larger than the maximum observed delay spread. In the case when the rate λ is large such that $\lambda T \gg 2$, the safety factor is comparatively small to $\lceil R\Delta \rceil$ and can be neglected. Thus, the condition for zero ISI with commutation signaling and maximum gain RAKE combiner reduces to the one as follows:

$$N \geq \lceil R\Delta \rceil \tag{3.69}$$

where N is, in general, larger than $\lceil R\Delta \rceil$. How close N is to $\lceil R\Delta \rceil$ depends on the chance of having delayed paths with delays larger than Δ and with amplitudes above the threshold. The more confident we are that there are no such paths, the more close N can be to $\lceil R\Delta \rceil$.

Let us now consider commutation signaling with square-law equal weight RAKE combining. The probability of having significant ISI can be upper-bounded by $P \leq P_1 + P_2$ where:

$$P_1 \leq \max\{0, \frac{2}{G_p}\lambda\tilde{\Delta}[1 + \lambda(\Delta - \frac{\tilde{\Delta}}{2} - \frac{NT}{2})]\} \tag{3.70}$$

$$P_2 \leq \frac{4\lambda\tilde{\Delta}NT}{{G_p}^2\Delta}(\lambda^2\Delta^2 + 5\lambda\Delta + 4) \tag{3.71}$$

and $G_p = \frac{NT}{T_c}$, $\tilde{\Delta} = \lceil \frac{\Delta}{NT} \rceil NT$. When N satisfies (3.67), then $P_1 = 0$ and the probability of having significant ISI is determined only by P_2. With $\tilde{I}_{max} = \lambda\tilde{\Delta}$, we have

$$P_2 \leq \frac{4\tilde{I}_{max}NT}{{G_p}^2\Delta}(\tilde{I}_{max}^2 + 5\tilde{I}_{max} + 4) = \tilde{P}_2 \tag{3.72}$$

For a fixed $\tilde{P}_2 > 0$, (3.72) can be rearranged into the following:

$$T/T_c = \sqrt{\frac{4\tilde{I}_{max}}{(R\Delta)N\tilde{P}_2}(\tilde{I}_{max}^2 + 5\tilde{I}_{max} + 4)} \tag{3.73}$$

where $R = 1/T$. With L-order space diversity, we have:

$$T/T_c = \sqrt{\frac{4\tilde{I}_{max}}{(R\Delta)N\tilde{P}_2^{\frac{1}{L}}}(\tilde{I}_{max}^2 + 5\tilde{I}_{max} + 4)} \tag{3.74}$$

Since N satisfies (3.67), we have:

$$N > R\Delta + \frac{2}{\lambda T} \tag{3.75}$$

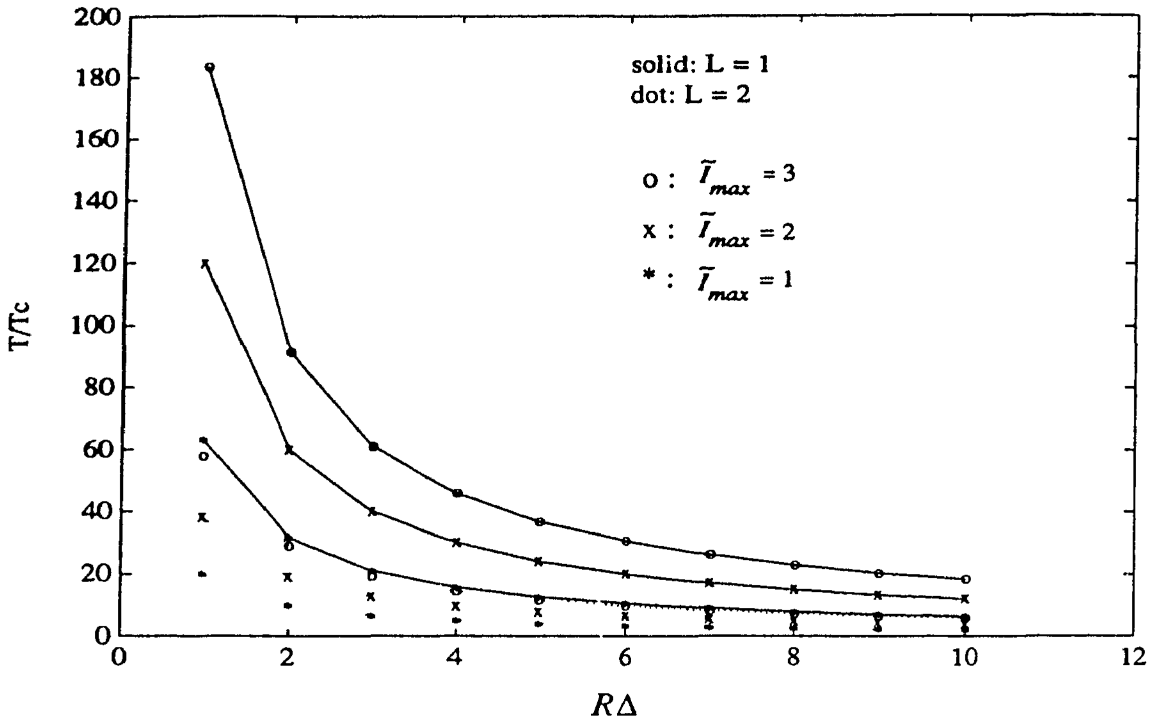

Figure 3.17: Graph of bandwidth expansion T/T_c as a function of $R\Delta$ with $\tilde{P}_2 = 0.01$

and an upper bound of (3.74) is obtained as follows:

$$T/T_c \leq \sqrt{\frac{4\tilde{I}_{max}}{(R\Delta)^2\tilde{P}_2^{\frac{1}{L}}}(\tilde{I}_{max}^2 + 5\tilde{I}_{max} + 4)} \tag{3.76}$$

A graph of the bandwidth expansion factor T/T_c versus $R\Delta$ with $\tilde{P}_2 = 0.01$ and different values of $\tilde{I}_{max}$ and L is shown in Fig. 3.17. We observe that for a fixed $\tilde{P}_2$, the required bandwidth expansion T/T_c increases with the number of channel paths, but decreases with $R\Delta$. However, the required N has to be increased also when $R\Delta$ is increased so that (3.75) is satisfied. In the case when $R\Delta$ is very large or approaching ∞, the bandwidth expansion factor T/T_c is small, however N must be large. Because of the condition as imposed by (3.67), it is seen that the required bandwidth expansion T/T_c decreases with N, the number of commutation signals to be used.

When comparing Fig. 3.17 with Fig. 3.15, it shows that for the same probability

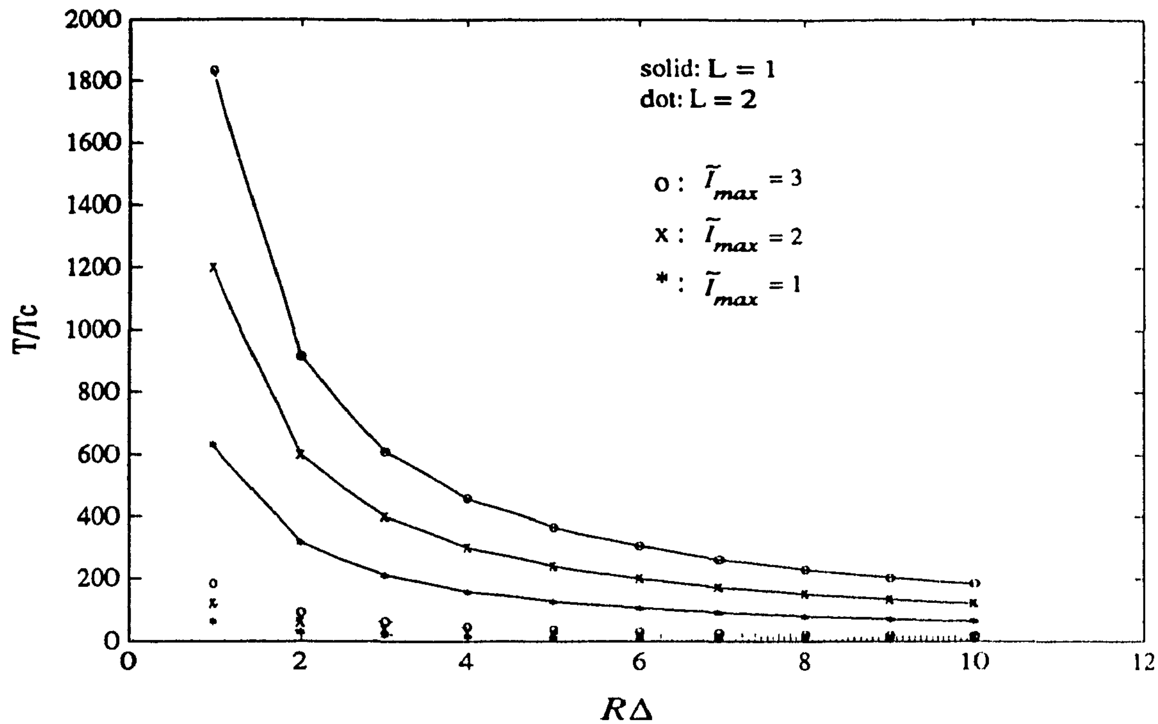

Figure 3.18: Graph of bandwidth expansion T/T_c as a function of $R\Delta$ with $\tilde{P}_2 = 0.0001$

of having significant ISI, the square-law equal weight RAKE combiner with commutation signaling requires a smaller bandwidth expansion than that without commutation signaling. For $R\Delta = 2$, $L = 1$, and $\tilde{I}_{max} = 3$, the required bandwidth expansion, as obtained from Fig. 3.17, for the square-law equal weight RAKE combiner with commutation signaling is about 90, but from Fig. 3.15, a bandwidth expansion as large as about 1000 is required if commutation signaling is not used.

More bandwidth expansion is required in the case when $\tilde{P}_2$ is small. Fig 3.18 depicts a graph of the bandwidth expansion factor T/T_c as a function of $R\Delta$ with $\tilde{P}_2 = 0.0001$ and different values of $\tilde{I}_{max}$ and L. When $R\Delta = 2$, $L = 1$ and $\tilde{I}_{max} = 3$, the required bandwidth expansion is about 900. In addition, it can be seen from Fig 3.17 and Fig. 3.18 that the required amount of bandwidth expansion is reduced greatly when antenna diversity is possible.

As explained earlier that zero ISI could be achieved for the maximum gain RAKE combiner with commutation signaling when N satisfied (3.67). However, when commutation signaling is incorporated with square-law equal weight RAKE combiner, there is ISI and the probability of having significant ISI is mainly determined by P_2 as given in (3.72) even when (3.67) holds. From section 3.2, P_2 is defined as the probability of having significant ISI in $z_2(t)$ where:

$$z_2(t) = \sum_{i=0}^{\infty} \sum_{l=0, l\neq i}^{\infty} \sum_{j=0}^{\infty} \alpha(i)\alpha^*(l)\Phi_u(t-\tau_i+\tau_j)\Phi_u^*(t-\tau_l+\tau_j) \tag{3.77}$$

Since $z_2(t)$ is primarily a sum of the multiplication of the autocorrelation function $\Phi_u(t)$ with its conjugate of different delays, there are two possibilities that a strong mainlobe is formed after the multiplication causing significant ISI at the sampling time. One of them is when two large mainlobes align together. The other possibility is when one large mainlobe aligns with one small sidelobe. All these possibilities increase the chance of having significant ISI at the output of the square-law equal weight RAKE combiner. As a result, unlike the situation for maximum gain RAKE combiner with commutation signaling which has zero ISI when N satisfies (3.67), ISI may exist at the output of square-law equal weight RAKE combiner even with commutation signaling, and this is reflected by P_2 from (3 71) not being identically zero. However, P_2 can be made very small.

Using commutation signaling with N satisfying the zero ISI condition, the probability of having significant ISI for the square-law equal weight RAKE combiner as obtained earlier is given by (3.72):

$$P_2 \leq \frac{4\tilde{I}_{max}NT}{{G_p}^2\Delta}(\tilde{I}_{max}^2 + 5\tilde{I}_{max} + 4) \tag{3.78}$$

When N satisfies (3.67), we have:

$$N > R\Delta + \frac{2}{\lambda T} \tag{3.79}$$

An approximate bound of P_2 is therefore obtained when $N \approx R\Delta$ and is given as follows:

$$P_2 \approx \frac{4\tilde{I}_{max}}{{G_p}^2}(\tilde{I}_{max}^2 + 5\tilde{I}_{max} + 4) \tag{3.80}$$

This shows that the amount of multipath induced ISI at the output of the square-law equal weight RAKE combiner can be made arbitrarily small and is negligible when:

$$G_p{}^2 \gg 4\tilde{I}_{max}(\tilde{I}^2_{max} + 5\tilde{I}_{max} + 4) \tag{3.81}$$

or

$$G_p = \frac{NT}{T_c} \gg 2\sqrt{\tilde{I}_{max}(\tilde{I}^2_{max} + 5\tilde{I}_{max} + 4)} \tag{3.82}$$

The advantage of using commutation signaling is reflected in (3.82) since the processing gain can be increased not only by increasing T/T_c, but also by increasing N. Although zero ISI can be achieved in the maximum gain RAKE combiner when commutation signaling is employed, maximum gain combining, as mentioned in Section 2.2, required not only the estimation of the multipath delays, but also the estimates on the amplitude and phase of the received signal. However, the phase estimation is not an easy task in many communication systems especially over multipath fading channels. Therefore, the square-law equal weight RAKE combiner with commutation signaling seems to be appropriate for indoor channels since it only requires the estimates on the multipath delays. By properly designing commutation signaling scheme, the amount of multipath induced ISI at the output of the square-law equal weight RAKE combiner can be made negligibly small. In the next section, we will combine commutation signaling with differentially encoding and will consider how the signaling scheme can be used with the GL receiver.

Chapter 4

GL Receiver for Differentially Encoded Binary Commutation Signaling

The subject of this chapter is the combination of binary commutation signaling with differentially encoding. In section 4.1, we incorporate the differential encoding scheme with commutation signaling and apply the Generalized Likelihood concept as described in section 2.2 to obtain the simplified GL receiver structure for implementing the signaling scheme. Section 4.2 describes how the scheme can be implemented via differential phase shift keyed (DPSK) modulation. It is shown that DPSK modulation offers many advantages, one of which is significant reduction of the autocorrelation sidelobes of the signal to be processed by the RAKE combiner.

4.1 Differentially Encoded Binary Commutation Signaling

In this section, we combine binary commutation signaling with differentially encoding. Differentially encoding structures the signal such that the reference required for detecting a symbol is carried by the previous symbol, thus eliminating problems associated with phase or polarity ambiguity. With commutation signaling, the reference symbol and the data symbol belong to different shift quasi-orthogonal signaling alphabets and thus their mutual multipath induced interference is significantly reduced.

The binary data sequence $a(k) = \pm 1$ where $k = 0,1,..$ to be transmitted is differentially encoded into another binary data sequence according to the following relation.

$$b(k) = b(k-1) \cdot a(k) \qquad ; \ k = 0, 1, \ .. \tag{4.1}$$

where $b(k)$'s are of values +1 or -1, and $b(-1) = 1$. To incorporate this differential encoding scheme with $2 \times N$ commutation signaling or we simply call N commutation signaling. N commutation signaling waveforms $\tilde{u}_0(t), \tilde{u}_1(t), .., \tilde{u}_{N-1}(t)$ are employed. These waveforms are assumed to be wideband signals and are T duration shift quasi-orthogonal. With this modulation scheme, the transmitted signal over $0 \leq t \leq 2T$

$$\begin{aligned}
\tilde{s}_m(t) &= b(0)\tilde{u}_{m-1}(t) + b(1)\tilde{u}_m(t-T) \\
&= b(0)[\tilde{u}_{m-1}(t) + \frac{b(1)}{b(0)}\tilde{u}_m(t-T)] \\
&= b(0)[\tilde{u}_{m-1}(t) + a(1)\tilde{u}_m(t-T)]
\end{aligned} \tag{4.2}$$

where m can assume the values $1, .., N$ and $\tilde{u}_N(t) = \tilde{u}_0(t)$. The receiver must employ a synchronization strategy which also keeps track of which commutation waveform is currently in use. Thus, we can assume that m is known. The term $b(0)$ which assumes value +1 or -1 can be included in the coefficient $e^{-j\theta_i}$ in (2.13) and therefore an equivalent problem is to consider the signal:

$$\tilde{s}_m(t) = \tilde{u}_{m-1}(t) + a(1)\tilde{u}_m(t-T) \qquad ; m = 1, .., N \tag{4.3}$$

Since $a(1) = \pm 1$, the detection of $a(1)$ when m is known is a binary hypothesis problem. With the transmitted signal $\tilde{s}_m(t)$, the CE of the received signal according to (2.13) is:

$$\begin{aligned} \tilde{r}(t) &= \sum_{i=0}^{I-1} \alpha_i e^{j\theta_i} \tilde{s}_m(t-\tau_i) + \tilde{n}(t) \quad ,0 \le t \le T_o \quad ,m = 1,..,N \\ &= \sum_{i=0}^{I-1} \alpha_i e^{j\theta_i} [\tilde{u}_{m-1}(t-\tau_i) + a(\imath)\tilde{u}_m(t-\tau_i - T)] + \tilde{n}(t) \end{aligned} \quad (4.4)$$

where $a(\imath) = \pm 1$ are the data symbols and I is the number of delayed paths. Using (2.21), the decision variable, for a known m, of the GL receiver for this differential encoded binary commutation signaling scheme is:

$$Z_m = \sum_{i=0}^{I-1} \left| \int_0^{T_o} \tilde{r}(t)\tilde{s}_m^*(t-\hat{\tau}_i)\, dt \right|^2 \quad ; m = 1,..,N. \quad (4.5)$$

By substituting (4.3) into (4.5), we have the decision variables for the two hypotheses as follows:

For H_0 $(a(1) = -1)$, the decision variable is:

$$\begin{aligned} Z_m^- &= \sum_{i=0}^{I-1} \left| \int_0^{T_o} \tilde{r}(t)\tilde{u}_{m-1}^*(t-\hat{\tau}_i^-)\, dt - \int_0^{T_o} \tilde{r}(t)\tilde{u}_m^*(t-\hat{\tau}_i^- - T)\, dt \right|^2 \quad ; m = 1,...N. \\ &= \sum_{i=0}^{I-1} \left| z_{m-1}(\hat{\tau}_i^-) - z_m(\hat{\tau}_i^- + T) \right|^2 = \sum_{i=0}^{I-1} z_m^-(\hat{\tau}_i^-) \end{aligned} \quad (4.6)$$

and for H_1 $(a(1) = 1)$, the decision variable is:

$$\begin{aligned} Z_m^+ &= \sum_{i=0}^{I-1} \left| \int_0^{T_o} \tilde{r}(t)\tilde{u}_{m-1}^*(t-\hat{\tau}_i^+)\, dt + \int_0^{T_o} \tilde{r}(t)\tilde{u}_m^*(t-\hat{\tau}_i^+ - T)\, dt \right|^2 \quad ; m = 1,..,N. \\ &= \sum_{i=0}^{I-1} \left| z_{m-1}(\hat{\tau}_i^+) + z_m(\hat{\tau}_i^+ + T) \right|^2 = \sum_{i=0}^{I-1} z_m^+(\hat{\tau}_i^+) \end{aligned} \quad (4.7)$$

where $\hat{\tau}_i^-$ and $\hat{\tau}_i^+$ are the estimated time delays under hypothesis H_0 and H_1 respectively, and

$$\begin{aligned} z_m(t) &= \int_0^{T_o} \tilde{r}(\tau)\tilde{u}_m^*(\tau - t)\, d\tau, \\ z_m^-(t) &= \left| z_{m-1}(t) - z_m(t+T) \right|^2, \\ z_m^+(t) &= \left| z_{m-1}(t) + z_m(t+T) \right|^2 \end{aligned}$$

The corresponding GL receiver is depicted in Fig. 4.1. The path delays $\hat{\tau}_i^-$ and $\hat{\tau}_i^+$, where $i = 0, .., I-1$, are estimated from the output of the square-law device. During the channel estimation process and in each observation interval, the time delays of I largest peaks, of $z_m^-(t)$ for H_0, and of $z_m^+(t)$ for H_1, are estimated and the corresponding delay taps on the RAKE combiner are activated with equal weight of unity. An equivalent form of the receiver is presented in Fig. 4.2. From (4.6) and (4.7), the decision variables for both hypotheses can be expanded as follows.

$$\begin{aligned} Z_m^{\pm} &= \sum_{i=0}^{I-1} \left| \int_0^{T_o} \tilde{r}(t)\tilde{u}_{m-1}^*(t-\hat{\tau}_i^{\pm})\,dt \pm \int_0^{T_o} \tilde{r}(t)\tilde{u}_m^*(t-\hat{\tau}_i^{\pm}-T)\,dt \right|^2 \quad ; m = 1, .., N. \\ &= \sum_{i=0}^{I-1} \left| \int_0^{T_o} \tilde{r}(t)\tilde{u}_{m-1}^*(t-\hat{\tau}_i^{\pm})\,dt \right|^2 + \sum_{i=0}^{I-1} \left| \int_0^{T_o} \tilde{r}(t)\tilde{u}_m^*(t-\hat{\tau}_i^{\pm}-T)\,dt \right|^2 \\ &\pm\; 2\sum_{i=0}^{I-1} Re\{\, [\int_0^{T_o} \tilde{r}(t)\tilde{u}_{m-1}^*(t-\hat{\tau}_i^{\pm})\,dt\,] \cdot [\int_0^{T_o} \tilde{r}(t)\tilde{u}_m^*(t-\hat{\tau}_i^{\pm}-T)\,dt\,]^* \} \end{aligned} \tag{4.8}$$

The first two terms

$$\sum_{i=0}^{I-1} \left| \int_0^{T_o} \tilde{r}(t)\tilde{u}_{m-1}^*(t-\hat{\tau}_i^{\pm})\,dt \right|^2 + \sum_{i=0}^{I-1} \left| \int_0^{T_o} \tilde{r}(t)\tilde{u}_m^*(t-\hat{\tau}_i^{\pm}-T)\,dt \right|^2 \tag{4.9}$$

are common for both hypotheses. If the estimation of the path delays $\hat{\tau}_i^-$ for H_0 is exactly the same as that of the path delays $\hat{\tau}_i^+$ for H_1, an equivalent decision rule for the GL receiver is then given by:

$$Z_m \underset{H_0}{\overset{H_1}{\gtrless}} 0$$

where $m = 1, .., N$ and

$$Z_m = \sum_{i=0}^{I-1} Re\{\, [\int_0^{T_o} \tilde{r}(t)\tilde{u}_{m-1}^*(t-\hat{\tau}_i)\,dt\,] \cdot [\int_0^{T_o} \tilde{r}(t)\tilde{u}_m^*(t-\hat{\tau}_i-T)\,dt\,]^* \} \tag{4.10}$$

where $\hat{\tau}_i = \hat{\tau}_i^+ = \hat{\tau}_i^-$. The realization of the GL receiver using this decision rule for both hypotheses is depicted in Fig. 4.2. When deriving the decision variable Z_m in (4.10), we assume that the estimated path delays in both hypotheses are exactly the same, therefore, the structure of the GL receiver in Fig. 4.2 can further be simplified

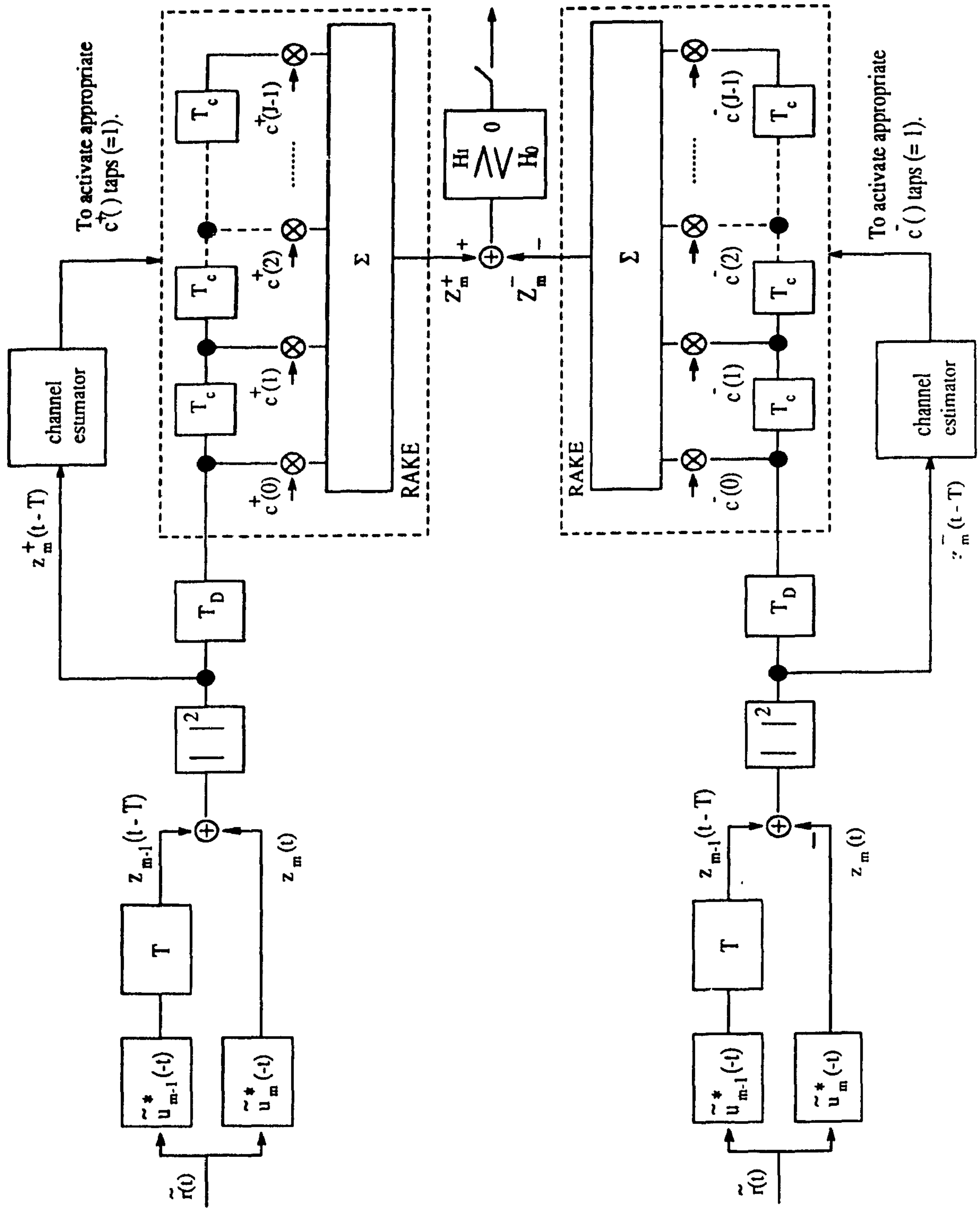

Figure 4.1: The GL receiver for differentially encoded binary commutation signaling

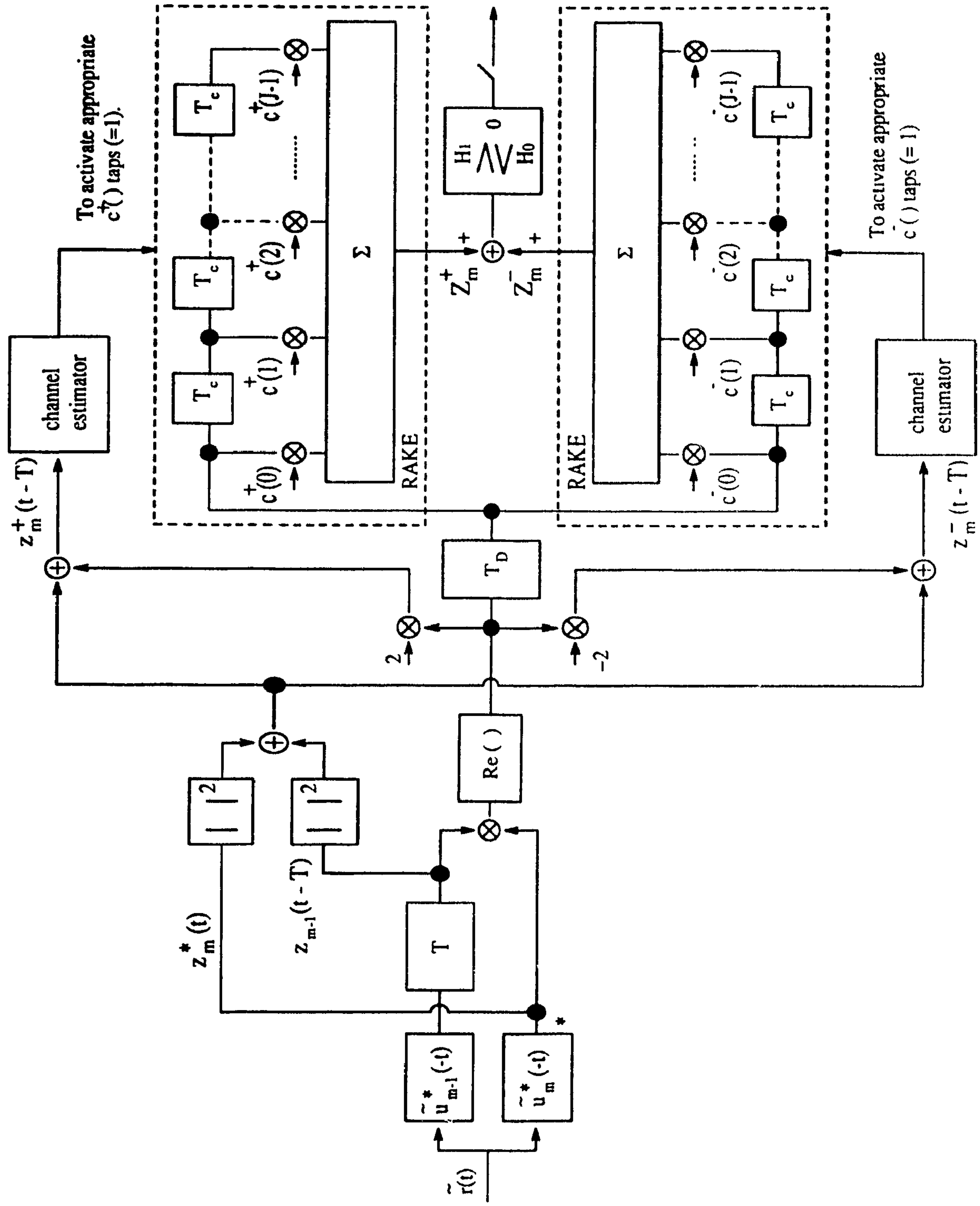

Figure 4.2: Equivalent GL receiver for differentially encoded binary commutation signaling.

into the one, as shown in Fig. 4.3, which requires only a single set of channel estimator and equal weight RAKE combiner.

The performance of this simplified GL receiver depends on the path delays estimates acquired in the channel estimation process. To understand the relationship between the optimality of the simplified GL receiver of Fig. 4.3 and path delay estimation, we must first consider the optimal GL receiver of Fig. 4.1. This receiver uses conditional path delays estimates under each of the hypothesis H_0 and H_1. If we assume ideal commutation signaling, that is, zero autocorrelation sidelobes and zero crosscorrelation, then under the adverse hypothesis, the output of the matched filter contains noise only. Therefore, the path delays estimates are purely random resulting in a random activation of the corresponding RAKE taps Therefore, any I activated RAKE taps under the adverse hypothesis will yield the same performance. Under the correct hypothesis, however, the output of the matched filter contains a signal component. It is this signal component that the corresponding RAKE combiner tends to enhanced by summation of its activated taps. To ensure optimal performance, the activated taps should correspond to the signal components at the matched filter output. Therefore, in order to have optimal performance, the channel estimate under the correct hypothesis should be exact. If this estimate is used also as the adverse hypothesis estimate, no loss in performance should occur. The problem is that the receiver does not know in advance which hypothesis is correct. However, due to the signal component under the correct hypothesis, the matched filter output peaks corresponding to the path delays are more likely to be larger than the corresponding peaks under the adverse hypothesis. This feature can be used to form a single set of path delays estimates for the two hypotheses, which enables the operation of the simplified GL receiver of Fig. 4.3 with minimal degradation. The single set of path delays estimates to be used is obtained by choosing the location of the I largest peaks of the two matched filters squared outputs peaks $z_m^-(t)$ and $z_m^+(t)$ over the estimation interval. In the next section, we discuss how the signaling scheme can be implemented via differential phase shift keyed modulation.

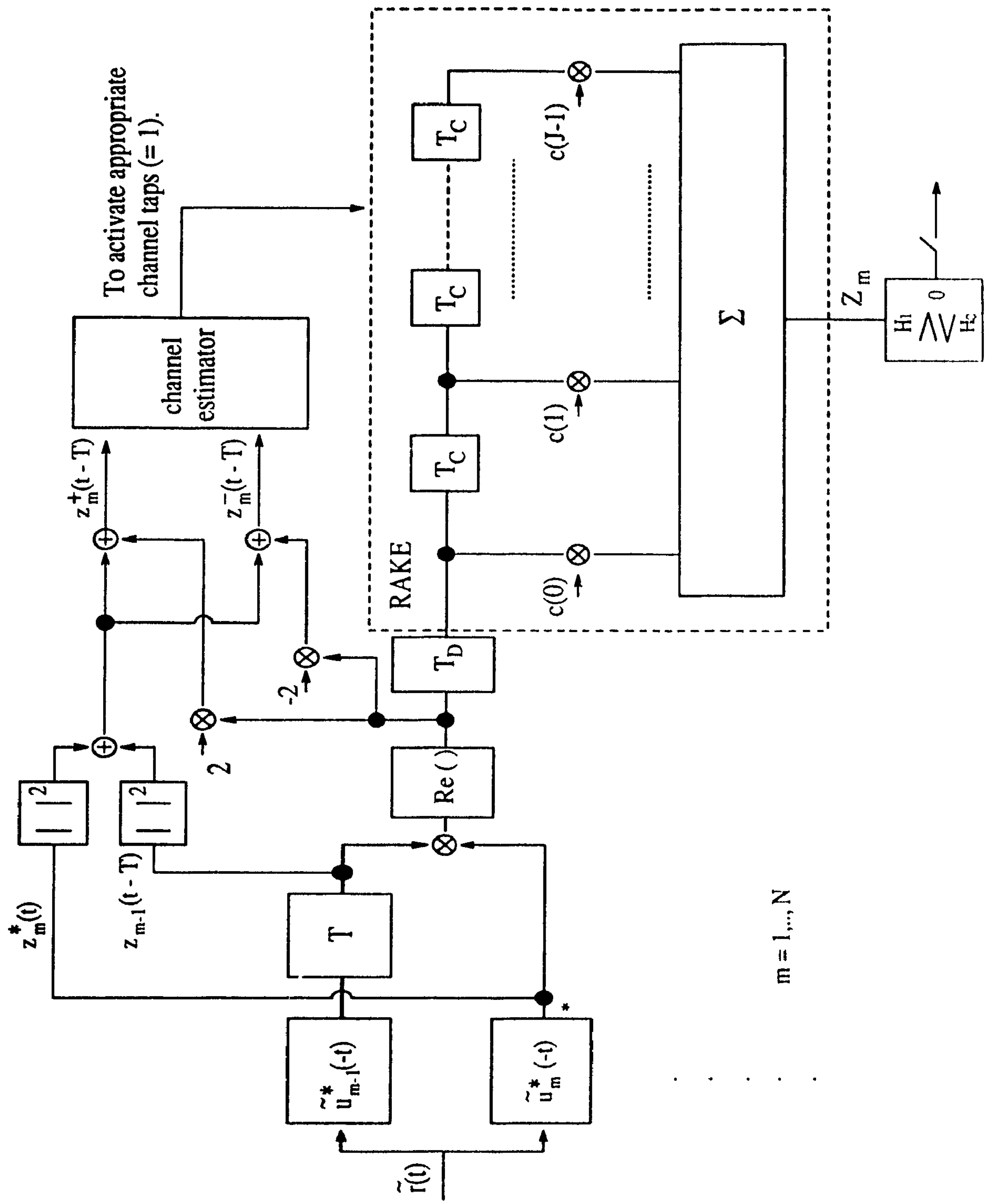

Figure 4.3: The simplified GL receiver for differentially encoded binary commutation signaling.

4.2 Commutation Differential Coherent Phase Shift Keying

In the previous section, we considered binary commutation signaling combined with differentially encoding. In this section, we consider how this scheme can be implemented via binary differential phase shift keyed (DPSK) modulation.

The modulation scheme is shown in Fig. 4.4. The original binary data sequence $a(k) = \pm 1$ is differentially encoded into another binary data sequence $b(k)$ where $b(k) = b(k-1) \cdot a(k)$. This encodes the information into different phase shifts between successive transmissions. Prior to the transmission, each encoded data bit $b(k)$ modulates a particular commutation signal. These commutation signals are bandwidth spreading sequences which can be generated by using maximum-length shift registers and are T duration shift quasi-orthogonal. In the case of $2 \times N$ commutation signaling, the same commutation signal is repeated again every N symbol periods.

The demodulation of DPSK requires that the received signal in any given signaling interval is compared to the phase of the received signal in the previous signaling interval, therefore, the estimation of the carrier phase is not necessary. As we can see from Fig. 4.3, the signal to be combined in the equal weight RAKE combiner is obtained by delaying the received signal by the symbol period T and using the delayed signal to multiply with the received signal.

The advantage of using commutation signaling with DPSK is that it can greatly reduce the sidelobes of the signal to be combined in the equal weight RAKE combiner As mentioned in section 3.1 the autocorrelation sidelobes of the signaling pulse may cause ISI unless the signaling pulse was well designed such that its autocorrelation sidelobes were small. For ideal commutation signaling, the autocorrelation sidelobes and cross-correlation sidelobes should be zero in order to have minimum multipath induced ISI. Although pseudorandom sequences, which possess excellent autocorrelation properties,

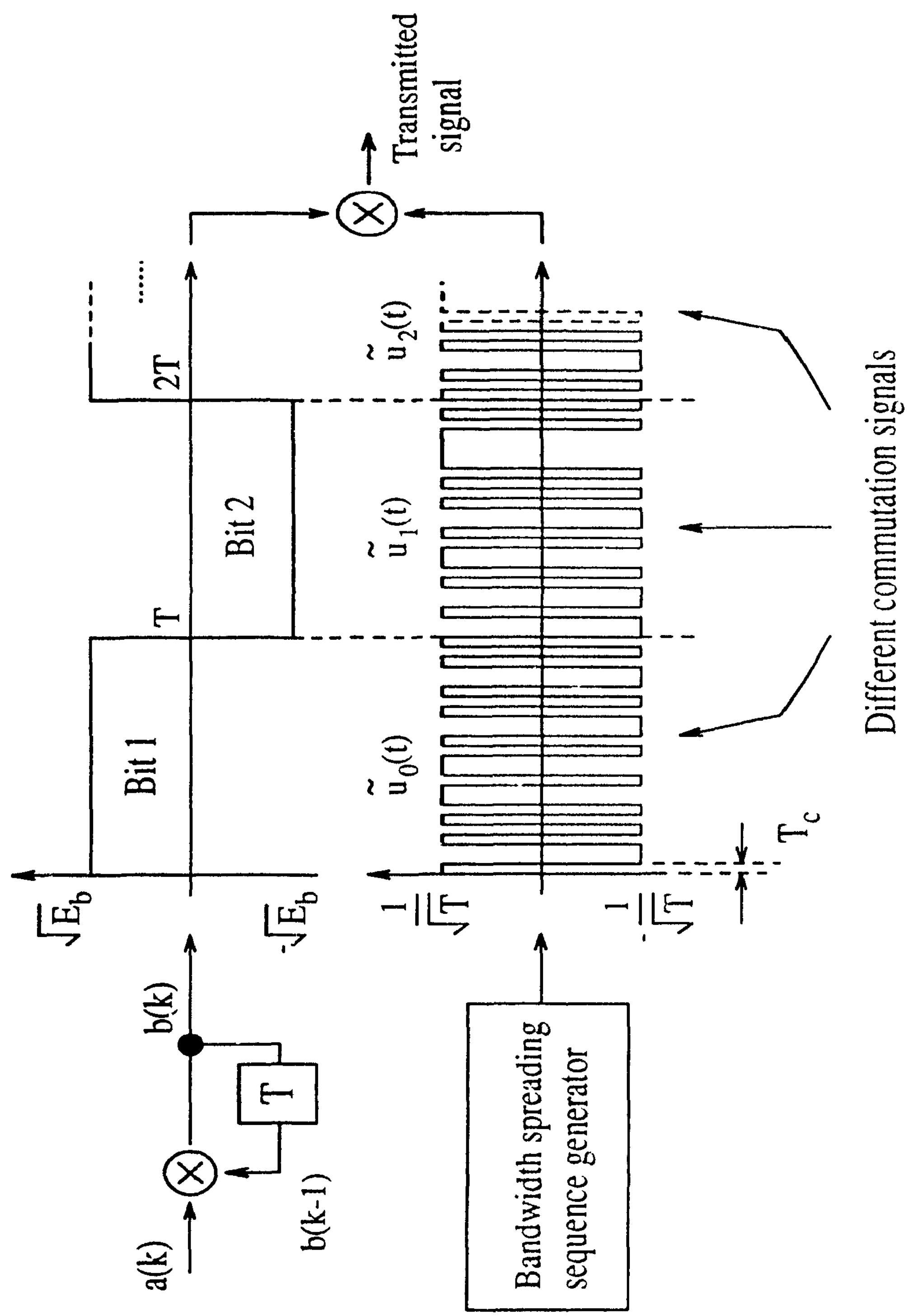

Figure 4.4: Binary differential phase shift keyed modulation with commutation signaling

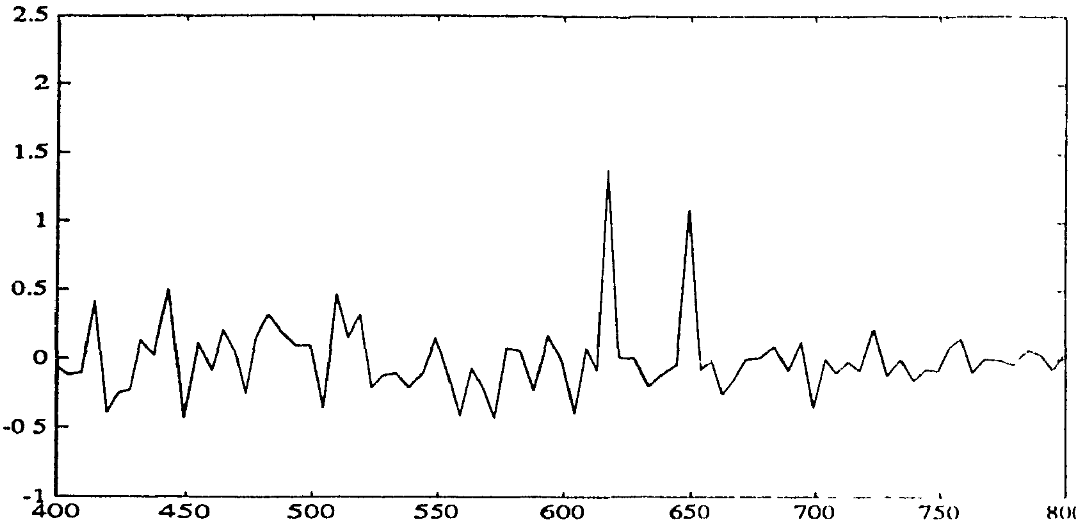

Figure 4.5: The output of the matched filter $\tilde{u}_m^*(-t)$ when one data symbol is transmitted over a multipath fading channel with two delayed paths.

have been employed in bandwidth expanding signaling schemes, they do not give zero autocorrelation sidelobes. In this work, we consider Gold sequences [35] for expanding the bandwidth of the transmitted signal.

To understand how commutation signaling with the DPSK scheme reduces the sidelobes of the signal at the input of the equal weight RAKE combiner, we consider the demodulation of DPSK in the simplified GL receiver as given in Fig. 4.3, and examine the outputs of the two matched filters and the signal at the input of the equal weight RAKE combiner. Suppose that the commutation signals are obtained from Gold sequences. Fig. 4.5 shows the output of matched filter $\tilde{u}_m^*(-t)$ and Fig. 4.6 depicts the output of the matched filter $\tilde{u}_{m-1}^*(-t)$ after delaying by the symbol period T when one data symbol is transmitted over a multipath fading channel with two delayed paths. Because of the autocorrelation property of Gold sequences, the autocorrelation sidelobes in each of the outputs are relatively small comparing to the mainlobes.

The demodulation of DPSK requires to multiply one matched filter output with

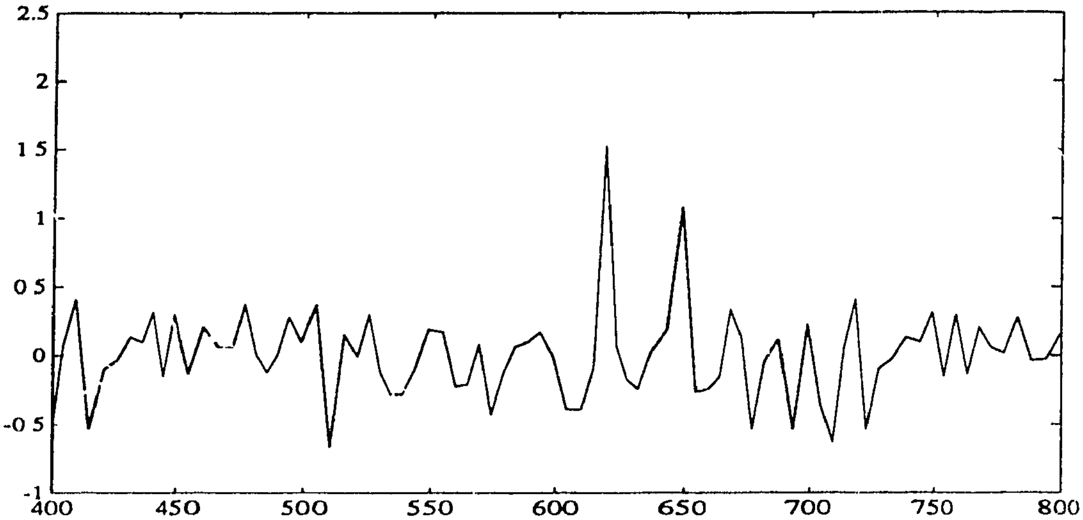

Figure 4.6: The output of the matched filter $\tilde{u}^*_{m-1}(-t)$ after delaying by the symbol period T.

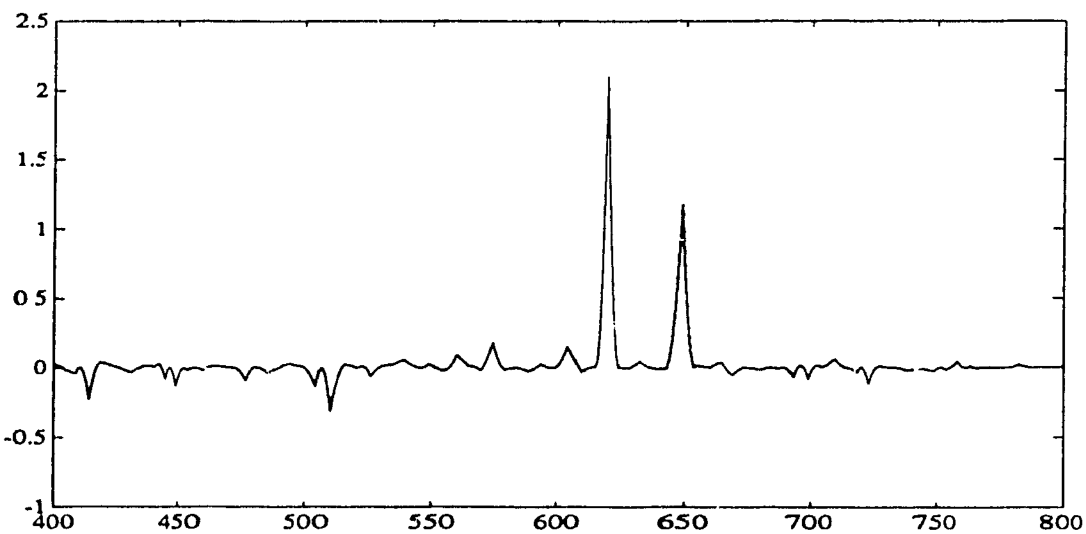

Figure 4.7: The signal at the input of the equal weight RAKE combiner.

the other matched filter output delayed by the symbol period T. The signal after the multiplication, which is the input to the equal weight RAKE combiner, is depicted in Fig. 4.7. Since the autocorrelation functions of different Gold sequences have the main lobes located at the same position but the sidelobes spreaded over different locations, appropriate sequences can be chosen as commutation signals such that the autocorrelation mainlobes are aligned at the same position, but the autocorrelation sidelobes are being cancelled or reduced to a minimum after the multiplication. It can be seen in Fig. 4.7 that the mainlobes are aligned together resulting in an enhancement in the magnitude of the mainlobe after the multiplication. On the other hand, it clearly shows that the sidelobes are significantly reduced because of the cancellation of the autocorrelation sidelobes after the multiplication.

The cancellation of the autocorrelation sidelobes not only lowers the multipath induced ISI, but also improves the system performance in the sense that when the channel estimation is done incorrectly causing wrong RAKE taps to be activated, the signals being combined in the equal weight RAKE combiner are the autocorrelation sidelobes; therefore, the smaller the sidelobes, the smaller the degradation will be. This advantage further advocates the use of DPSK in implementing differentially encoded binary commutation signaling scheme in the simplified GL receiver, and the performance will be considered in the next chapter.

Chapter 5

Performance of the Simplified GL Receiver

This chapter analyses the probability of error performance of the differentially encoded binary commutation signaling for the simplified GL receiver Section 5.1 considers the performance of the simplified GL receiver over multipath Rayleigh fading channel under the assumption that the channel estimation is done correctly. In addition, we focus on the diversity improvement. In section 5.2, we examine the performance of the simplified GL receiver when operating over multipath Lognormal fading channel with perfect channel estimation. Finally, section 5.3 considers the effects of incorrect channel estimation on the simplified GL receiver. The performance degradation due to wrong activated RAKE taps is investigated by comparing the computer simulation results under practical channel estimation with the error performance with perfect channel estimation

5.1 Performance of Simplified GL Receiver over Multipath Rayleigh Fading Channel

From the previous chapter, it was seen that the GL receiver with differentially encoded binary commutation signaling resulted in a simple structure when one set of path delays estimates was used for the two hypotheses. As a result, the receiver required only a single set of channel estimator and equal weight RAKE combiner. In this section, we consider the performance of this simplified GL receiver with differentially encoded binary commutation signaling over a multipath Rayleigh fading channel. We assume here that the channel path delays estimates are correct, that is, ideal channel estimation, and concentrate on the diversity improvement. With this assumption, the simplified and the exact GL receivers yield identical performances. Degradation due to practical channel estimation with errors will be considered in section 5.3.

With the use of commutation signaling which gives minimum autocorrelation sidelobes and crosscorrelations, the effects of ISI on the simplified GL receiver in the data detection process are insignificant and are neglected. In addition, since the channel estimation is assumed to be performed perfectly, all necessary RAKE taps are properly activated. In order for differential phase shift keyed (DPSK) modulation to be a feasible signaling technique, we also assume that the channel variations are sufficiently slow such that the channel phase shifts do not vary significantly over two consecutive signaling intervals.

We first consider the performance of binary DPSK for a nonfading channel. If the CE of the transmitted signal is $\tilde{s}(t)$, the received signal in one signaling interval is

$$\tilde{r}(t) = \alpha e^{j\theta}\tilde{s}(t) + \tilde{n}(t) \qquad ;0 \le t \le T \tag{5.1}$$

where $\tilde{n}(t)$ represents the zero mean additive Gaussian noise with two-sided power spectral density $\frac{N_o}{2}$ [Watt/Hz], α is a fixed attenuation and θ is the phase shift. The error probability of binary DPSK for a nonfading channel is [19, pp. 270]:

$$P_b(\gamma_b) = \frac{1}{2} exp\,(-\,\gamma_b) \tag{5.2}$$

where $\gamma_b = \alpha^2 \frac{E_b}{N_o}$ is the signal-to-noise ratio (SNR) per bit and E_b is the signal energy per bit.

To evaluate the error performance of binary DPSK for a single-path fading channel, we consider (5.2) as conditional error probability with α being fixed. When α is random, the error probability is obtained by averaging (5.2) over the probability density function (pdf) of γ_b, by evaluating the following integral

$$P_e = \int_0^\infty P_b(\gamma_b)\, p(\gamma_b)\, d\gamma_b \tag{5.3}$$

where $p(\gamma_b)$ is the pdf of γ_b when α is random. In this section, α is assumed to be Rayleigh-distributed, then α^2 has a chi-square probability distribution with 2 degrees of freedom [19, pp. 29]. Therefore, γ_b is also chi-square-distributed and has the following pdf:

$$p(\gamma_b) = \frac{1}{\overline{\gamma}_b}\, exp\,(-\gamma_b/\overline{\gamma}_b) \qquad : \gamma_b \geq 0 \tag{5.4}$$

where $\overline{\gamma}_b$ is the average SNR ratio given by:

$$\overline{\gamma}_b = \frac{E_b}{N_o}\, \mathrm{E}\,[\alpha^2] \tag{5.5}$$

and $\mathrm{E}\,[\alpha^2]$ is the average value of α^2 or the second moment of α. By substituting (5.2) and (5.4) into (5.3), the error probability of binary DPSK for a single-path Rayleigh fading channel is:

$$\begin{aligned} P_e &= \int_0^\infty P_b(\gamma_b)\, p(\gamma_b)\, d\gamma_b \\ &= \frac{1}{2\overline{\gamma}_b} \int_0^\infty exp\,[-\,\gamma_b(1 + \frac{1}{\overline{\gamma}_b})\,]\, d\gamma_b \\ &= \frac{1}{2(\overline{\gamma}_b + 1)} \end{aligned} \tag{5.6}$$

The probabilities of error performance of the simplified GL receiver for binary DPSK over a nonfading channel and a single-path Rayleigh fading channel are illustrated in

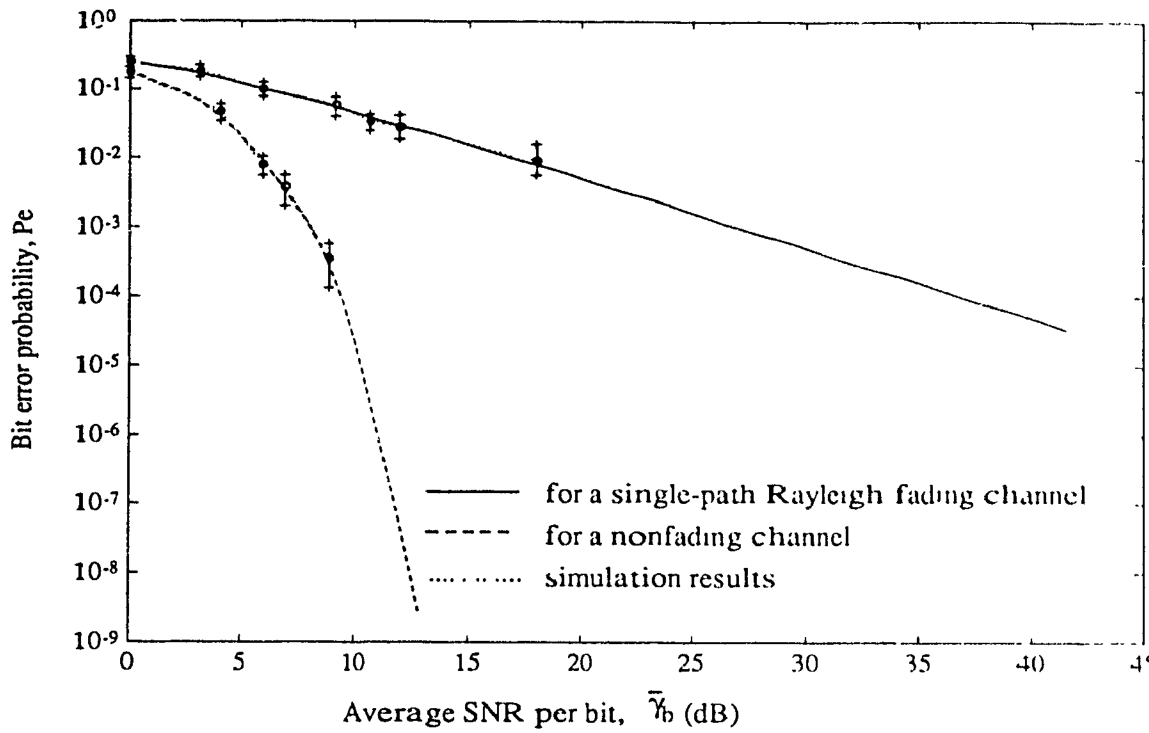

Figure 5.1: The error performance of the simplified GL receiver for binary DPSK over a single-path Rayleigh fading channel and a nonfading channel.

Fig. 5.1. The figure also shows the computer simulation results. The simulations are described in Appendix A. It can be seen that the performance of the simplified GL receiver degrades significantly when the receiver is operating over a fading channel. From (5.2), we observe that the error probability for a nonfading channel decreases exponentially with SNR. However, from (5.6), it shows that the error rate on a single-path Rayleigh fading channel decreases only inversely with SNR. This implies that in order to maintain a low probability of error on a fading channel, the transmitter needs to transmit a large amount of power, and thus the system is SNR inefficient. A better SNR performance on a fading channel can be achieved by means of diversity techniques.

As mentioned in section 2.2 the square-law equal weight RAKE combiner in the GL receiver was capable of combining the resolved signal components received over multiple channel paths. Its operation is one form of diversity combining techniques which provides the receiver with several replicas of the same transmitted signal. Therefore, the performance of the simplified GL receiver over a multipath fading channel is equivalent to that over a single-path fading channel with diversity of order L, where L is the number of resolvable delay paths in the channel. With the assumptions that the fading processes among the L diversity channels are mutually statistically independent and the average SNR per channel is identical for all channels, the pdf $p(\gamma_b)$ of the Rayleigh fading channel statistics is [19, pp. 723]:

$$p(\gamma_b) = \frac{1}{(L-1)!\,\overline{\gamma}_c^L}\,\gamma_b^{L-1} exp\,(-\gamma_b/\overline{\gamma}_c) \tag{5.7}$$

where $\overline{\gamma}_c$ is the average SNR per channel given as:

$$\overline{\gamma}_c = \frac{E_b}{N_o}\,\mathrm{E}\,[\alpha_i{}^2] \qquad ; i = 0, .., L-1 \tag{5.8}$$

and the SNR per bit γ_b is defined as:

$$\gamma_b = \frac{E_b}{N_o}\sum_{i=0}^{L-1} \alpha_i{}^2 \tag{5.9}$$

Since we assume that the average SNR per channel is identical for all L channels, we have the average SNR per bit:

$$\overline{\gamma}_b = L\overline{\gamma}_c \tag{5.10}$$

The conditional error probability of binary DPSK transmitted over L time-invariant channels with equal weight combining is [19, pp. 725]:

$$P_b(\gamma_b) = \frac{1}{2^{2L-1}} exp\,(-\gamma_b)\sum_{k=0}^{L-1} b_k {\gamma_b}^k \tag{5.11}$$

where γ_b is given by (5.9) and

$$b_k = \frac{1}{k!}\sum_{n=0}^{L-1-k} \binom{2L-1}{n} \tag{5.12}$$

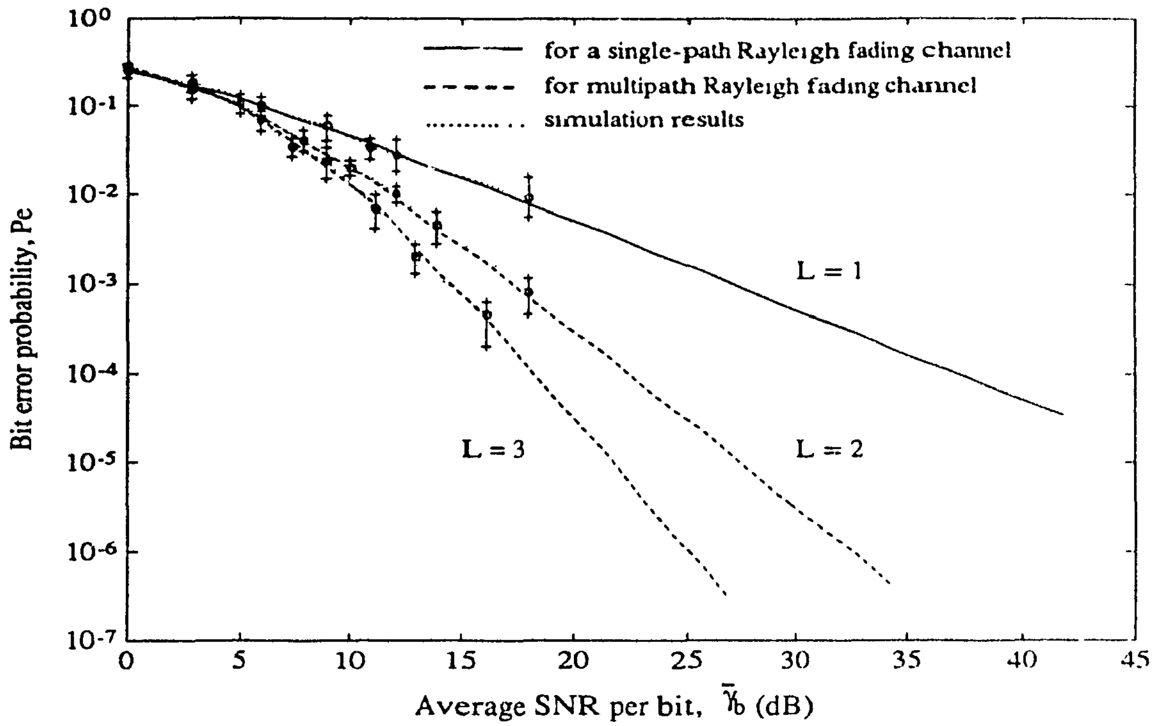

Figure 5.2: The error performance of the simplified GL receiver for binary DPSK over multipath Rayleigh fading channel.

where $\begin{pmatrix} p \\ q \end{pmatrix} = \frac{p!}{q!(p-q)!}$. Therefore, the probability of error of the simplified GL receiver for binary DPSK over a multipath Rayleigh fading channel is obtained by averaging (5.11) over the fading channel statistics given by $p(\gamma_b)$ in (5.7) and the result is [19, pp 725]:

$$P_e = \frac{1}{2^{2L-1}(L-1)!\,(1+\frac{\bar{\gamma}_b}{L})^L} \sum_{k=0}^{L-1} b_k(L-1+k)!\,(\frac{\bar{\gamma}_b}{L+\bar{\gamma}_b})^k \tag{5.13}$$

For $L = 2$, the probability of error is:

$$\begin{aligned} P_e &= \frac{1}{8\,(1+\frac{\bar{\gamma}_b}{2})^2} \sum_{k=0}^{1} b_k(1+k)!\,(\frac{\bar{\gamma}_b}{2+\bar{\gamma}_b})^k \\ &= \frac{1}{2\,(2+\bar{\gamma}_b)^2}[\,4 \;+\; 2(\frac{\bar{\gamma}_b}{2+\bar{\gamma}_b})\,] \end{aligned} \tag{5.14}$$

Similarly, for $L = 3$, the probability of error is:

$$\begin{aligned}
P_e &= \frac{1}{2^6\,(1+\frac{\bar{\gamma}_b}{3})^3}\sum_{k=0}^{2} b_k(2+k)!\,(\frac{\bar{\gamma}_b}{3+\bar{\gamma}_b})^k \\
&= \frac{1}{2^6\,(1+\frac{\bar{\gamma}_b}{3})^3}[\,32 \;+\; 36(\frac{\bar{\gamma}_b}{3+\bar{\gamma}_b}) \;+\; 12(\frac{\bar{\gamma}_b}{3+\bar{\gamma}_b})^2\,] \\
&= \frac{27}{(3+\bar{\gamma}_b)^3}[\,\frac{1}{2} \;+\; \frac{9}{16}(\frac{\bar{\gamma}_b}{3+\bar{\gamma}_b}) + \frac{3}{16}(\frac{\bar{\gamma}_b}{3+\bar{\gamma}_b})^2\,] \qquad (5.15)
\end{aligned}$$

The probabilities of error performance of the simplified GL receiver for binary DPSK over a Rayleigh multipath fading channel with $L = 2$ and $L = 3$ are shown in Fig. 5.2. The error performance is plotted as a function of the average SNR per bit $\bar{\gamma}_b$ The results clearly show the advantage of employing equal weight RAKE combiner for the exploitation of multipath diversity to overcome the severe penalty in SNR due to fading. However, there is also a diminishing returns effect which increases with the error rate. A two fold diversity seems to give a measurable performance improvement over non-diversity up to an error rate close to 10^{-1}. A three fold diversity gives measurable improvement over two fold only up to an error rate of 10^{-2}. Therefore, the higher is the operational error rate of the system, the less effective is diversity. It seems that a three fold diversity is most appropriate for error rates between 10^{-3} and 10^{-2}, under independent Rayleigh fading. However, if much lower error rates are required, a higher diversity order can be more effective.

5.2 Performance of Simplified GL Receiver over Multipath Lognormal Fading Channel

In this section, we consider the performance of the simplified GL receiver with differentially encoded binary commutation signaling over a multipath Lognormal fading channel. We also assume that the channel estimation is perfectly performed and all necessary RAKE taps are activated correctly. Unlike the case for multipath Rayleigh fading channels, the error performance of the simplified GL receiver over Lognormal fading channels does not result in closed-form solutions. Therefore, we need to use bounds and numerical integrations to obtain the error probabilities.

We begin with the error performance of binary DPSK for a nonfading channel given in (5.2) as:

$$P_b(\gamma_b) = \frac{1}{2} exp(-\gamma_b) \tag{5.16}$$

where $\gamma_b = \alpha^2 \frac{E_b}{N_o}$ is the signal-to-noise ratio (SNR) per bit and E_b is the signal energy per bit. For a fading channel, α is random. In this section, α is assumed to be Lognormally distributed, therefore, we have:

$$\alpha = exp(x) \tag{5.17}$$

where x is normally-distributed with mean μ and variance σ^2. The pdf of x is then given as:

$$p(x) = \frac{1}{\sqrt{2\pi\sigma^2}} exp\left[-\frac{(x-\mu)^2}{2\sigma^2}\right] \tag{5.18}$$

The error performance of binary DPSK for a single-path Lognormal fading channel is obtained by averaging (5.16) over the pdf of x, that is.

$$P_e = \int_{-\infty}^{\infty} \frac{1}{2} exp\left(-\frac{E_b}{N_o} e^{2x}\right) p(x)\, dx \tag{5.19}$$

By substituting (5.18) into (5.19), we have:

$$P_e = \frac{1}{2} \int_{-\infty}^{\infty} \frac{1}{\sqrt{2\pi\sigma^2}} exp\left[-\frac{(x-\mu)^2}{2\sigma^2}\right] exp\left(-\frac{E_b}{N_o} e^{2x}\right) dx$$

$$= \frac{1}{\sqrt{8\pi\sigma^2}} \int_{-\infty}^{\infty} exp\,[-\frac{(x-\mu)^2}{2\sigma^2} - \frac{E_b}{N_o} e^{2x}\,]\,dx \tag{5.20}$$

From (5.5),

$$\overline{\gamma}_b = \frac{E_b}{N_o}\,\mathrm{E}\,[\alpha^2] \tag{5.21}$$

and when α is Lognormally-distributed,

$$\mathrm{E}\,[\alpha^2] = exp\,(2\sigma^2 + 2\mu) \tag{5.22}$$

Substituting (5.22) into (5.21) gives

$$\frac{E_b}{N_o} = \overline{\gamma}_b\, exp\,(-2\sigma^2 - 2\mu) \tag{5.23}$$

Therefore, by substituting (5.23) into (5.20), the error probability of binary DPSK for a single-path Lognormal fading channel is.

$$P_e = \frac{1}{\sqrt{8\pi\sigma^2}} \int_{-\infty}^{\infty} exp\,[-\frac{(x-\mu)^2}{2\sigma^2} - \overline{\gamma}_b\, e^{-2\sigma^2 - 2\mu + 2x}\,]\,dx \tag{5.24}$$

Unfortunately, (5.24) cannot be further simplified into a closed form, and thus it can only be evaluated by numerical integration. However, we can derive the bounds to the error probability

5.2.1 Bounds

The bounds to the error probability in (5.24) can be obtained by considering (5.19).

$$\begin{aligned} P_e &= \int_{-\infty}^{\infty} \frac{1}{2}\, exp\,(-\frac{E_b}{N_o} e^{2x})\, p(x)\, dx \\ &= \frac{1}{2}\,\mathrm{E}\,[\, exp\,(-\frac{E_b}{N_o}\, e^{2x})\,] \\ &= \frac{1}{2}\,\mathrm{E}\,[\, exp\,(-c\, e^{2x})\,] \end{aligned} \tag{5.25}$$

where $c = \frac{E_b}{N_o} > 0$ is a constant, x is a random variable with pdf given in (5.18) and $\mathrm{E}[\cdot]$ is the expectation with respect to x. Figure 5.3 depicts the function e^{2x} and a tangential line to this function. Now, let

$$f(x) = ax + b \tag{5.26}$$

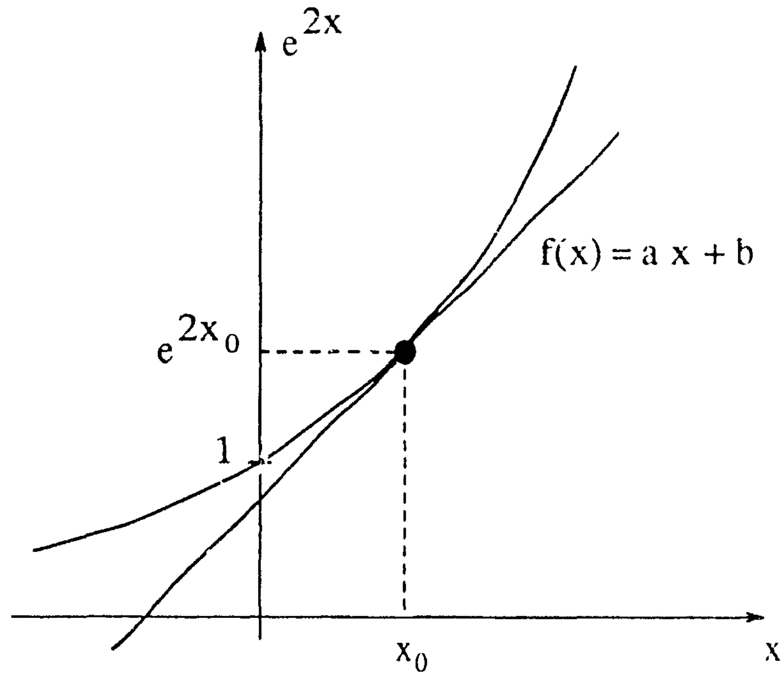

Figure 5.3: The tangential line to the function e^{2x}

be the equation of the tangential line to the function e^{2x} at $x = x_o$. So, the slope at $x = x_o$ is given by:

$$a = \frac{d\,e^{2x}}{d\,x}\Big|_{x=x_o} = 2e^{2x_o} \tag{5.27}$$

The value of $f(x)$ at $x = x_o$ is:

$$e^{2x_o} = a x_o + b \tag{5.28}$$

From (5.27) and (5.28), we have:

$$b = (1 - 2x_o)\, e^{2x_o} \tag{5.29}$$

By substituting (5.27) and (5.29) into (5.26), the equation of the tangential line is

$$f(x) = 2e^{2x_o} x + (1 - 2x_o)\, e^{2x_o} \tag{5.30}$$

For any x_o, we have $f(x) \leq e^{2x}$, therefore, the upper bound to (5.25) is

$$P_e \;\leq\; \frac{1}{2}\,\mathrm{E}\,[\,exp(-cf(x))\,]$$

$$\begin{aligned} &= \frac{1}{2}\,\mathrm{E}\,[\,exp\,(-2ce^{2x_o}x - (1-2x_o)ce^{2x_o})\,] \\ &= \frac{1}{2}\,exp\,[-c(1-2x_o)e^{2x_o}]\,\mathrm{E}\,[\,exp\,(-2ce^{2x_o}x)\,] \end{aligned} \tag{5.31}$$

Since the k-moment of $exp(x)$ about the origin is [36, pp. 9]:

$$\mathrm{E}\,[\,exp\,(kx)\,] = exp\,(\,k\mu\,+\,\frac{k^2\sigma^2}{2}) \tag{5.32}$$

we have

$$\mathrm{E}\,[\,exp\,(-2ce^{2x_o}x)\,] = exp\,(\,-2c\mu e^{2x_o} +\,2c^2\sigma^2e^{4x_o}) \tag{5.33}$$

Therefore, after substituting (5.33) into (5.31), we have:

$$\begin{aligned} P_e &\le \frac{1}{2}\,exp\,[-c(1-2x_o)e^{2x_o}\,-\,2c\mu e^{2x_o} +\,2c^2\sigma^2e^{4x_o}] \\ &= \frac{1}{2}\,exp\,[-ce^{2x_o}(1+2\mu-2x_o-2c\sigma^2e^{2x_o})\,] \end{aligned} \tag{5.34}$$

In order to have the tightest bound, we must choose x_o such that:

$$g_1(x_o) = e^{2x_o}(1+2\mu-2x_o-2c\sigma^2e^{2x_o}) \tag{5.35}$$

is maximized. To maximize $g_1(x_o)$ with respect to x_o, we consider the following.

$$\frac{dg_1(x_o)}{dx_o} = 0 \tag{5.36}$$

or

$$\begin{aligned} e^{2x_o}(-2-4c\sigma^2e^{2x_o})\,+\,2e^{2x_o}(1+2\mu-2x_o-2c\sigma^2e^{2x_o}) &= 0 \\ -2-4c\sigma^2e^{2x_o}+2+4\mu-4x_o-4c\sigma^2e^{2x_o} &= 0 \\ \mu - x_o &= 2c\sigma^2e^{2x_o} \end{aligned} \tag{5.37}$$

To assure that (5.37) gives a maximum, we have to verify if the second derivative of $g_1(x_o)$ with respect to x_o is negative. Therefore,

$$\begin{aligned} \frac{d^2g_1(x_o)}{dx_o{}^2} &= e^{2x_o}(-8c\sigma^2e^{2x_o})\,+\,2e^{2x_o}(-2-4c\sigma^2e^{2x_o}) \\ &+\,2e^{2x_o}(-2-4c\sigma^2e^{2x_o})\,+\,4e^{2x_o}(1+2\mu-2x_o-2c\sigma^2e^{2x_o}) \\ &= e^{2x_o}[-32c\sigma^2e^{2x_o}-4-8(\mu-x_o)] \end{aligned} \tag{5.38}$$

As obtained in (5.37), $\mu - x_o = 2c\sigma^2 e^{2x_o}$, thus (5.38) reduces to:

$$\begin{aligned}\frac{d^2 g_1(x_o)}{dx_o{}^2} &= e^{2x_o}[-32c\sigma^2 e^{2x_o} - 4 - 16c\sigma^2 e^{2x_o}] \\ &= e^{2x_o}(-48c\sigma^2 e^{2x_o} - 4) \qquad (5.39)\end{aligned}$$

Since $e^{2x_o} > 0$ for all x_o, (5.39) is always negative showing that (5.37) is indeed maximizing (5.35). By substituting (5.37) into (5.34), the error probability is upper-bounded by:

$$\begin{aligned}P_e \leq P_U &= \frac{1}{2}\,exp\,[-ce^{2x_o}(1 + 2\mu - 2x_o - 2c\sigma^2 e^{2x_o})\,] \\ &= \frac{1}{2}\,exp\,[-ce^{2x_o}(1 + 2c\sigma^2 e^{2x_o})\,] \\ &= \frac{1}{2}\,exp\,[-\frac{(\mu - x_o)}{2\sigma^2}(1 + \mu - x_o)\,] \qquad (5.40)\end{aligned}$$

If we let

$$\beta = \mu - x_o \qquad (5.41)$$

then (5.40) becomes:

$$P_e \leq P_U = \frac{1}{2}\,exp\,[-\frac{\beta(\beta + 1)}{2\sigma^2}] \qquad (5.42)$$

From (5.37), we can derive an equation for β:

$$\begin{aligned}\mu - x_o &= 2c\sigma^2 e^{2x_o} \\ \beta &= 2c\sigma^2 e^{2(\mu-\beta)} = 2ce^{2\mu+2\sigma^2}\sigma^2 e^{-2\sigma^2} e^{-2\beta} \\ &= 2\overline{\gamma}_b\sigma^2 e^{-2\sigma^2} e^{-2\beta} \qquad (5.43)\end{aligned}$$

where, from (5.22),

$$\begin{aligned}\overline{\gamma}_b &= c\,\mathrm{E}\,[\alpha^2] = ce^{2\mu+2\sigma^2} \\ &= \frac{E_b}{N_o} e^{2\mu+2\sigma^2} \qquad (5.44)\end{aligned}$$

From (5.43), it is seen that $\beta > 0$. For $\beta \ll 1$,

$$\begin{aligned}\beta &= 2\overline{\gamma}_b\sigma^2 e^{-2\sigma^2} e^{-2\beta} \\ &\approx 2\overline{\gamma}_b\sigma^2 e^{-2\sigma^2}(1 - 2\beta)\end{aligned}$$

$$(5.45)$$

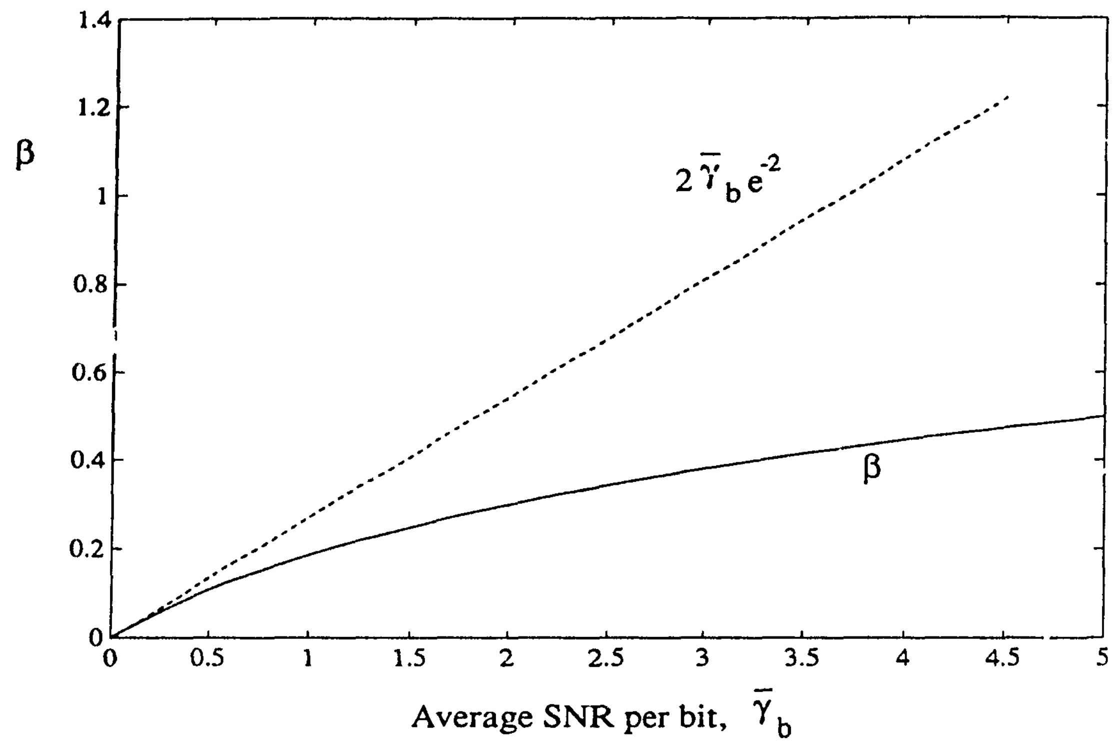

Figure 5.4: $\beta\,(\ll 1)$ as a function of average SNR per bit, $\overline{\gamma}_b$.

Therefore,

$$\begin{aligned}\beta &\approx \frac{2\overline{\gamma}_b\sigma^2 e^{-2\sigma^2}}{1+4\overline{\gamma}_b\sigma^2 e^{-2\sigma^2}} \\ &\approx 2\overline{\gamma}_b\sigma^2 e^{-2\sigma^2} \end{aligned} \tag{5.46}$$

From (5.43),

$$\ln(\beta) = \ln(2\overline{\gamma}_b\sigma^2 e^{-2\sigma^2}) - 2\beta \tag{5.47}$$

or

$$2\beta + \ln(\beta) = \ln(2\overline{\gamma}_b\sigma^2 e^{-2\sigma^2}) \tag{5.48}$$

Therefore,

$$\beta \leq \frac{1}{2}\ln(2\overline{\gamma}_b\sigma^2 e^{-2\sigma^2}) \tag{5.49}$$

and for $\beta \gg 1$, the upper bound is tight. Figures 5.4 and 5.5 show the behaviour of β when $\beta \ll 1$ and $\beta \gg 1$ respectively for $\sigma^2 = 1$ and $\mu = 0$.

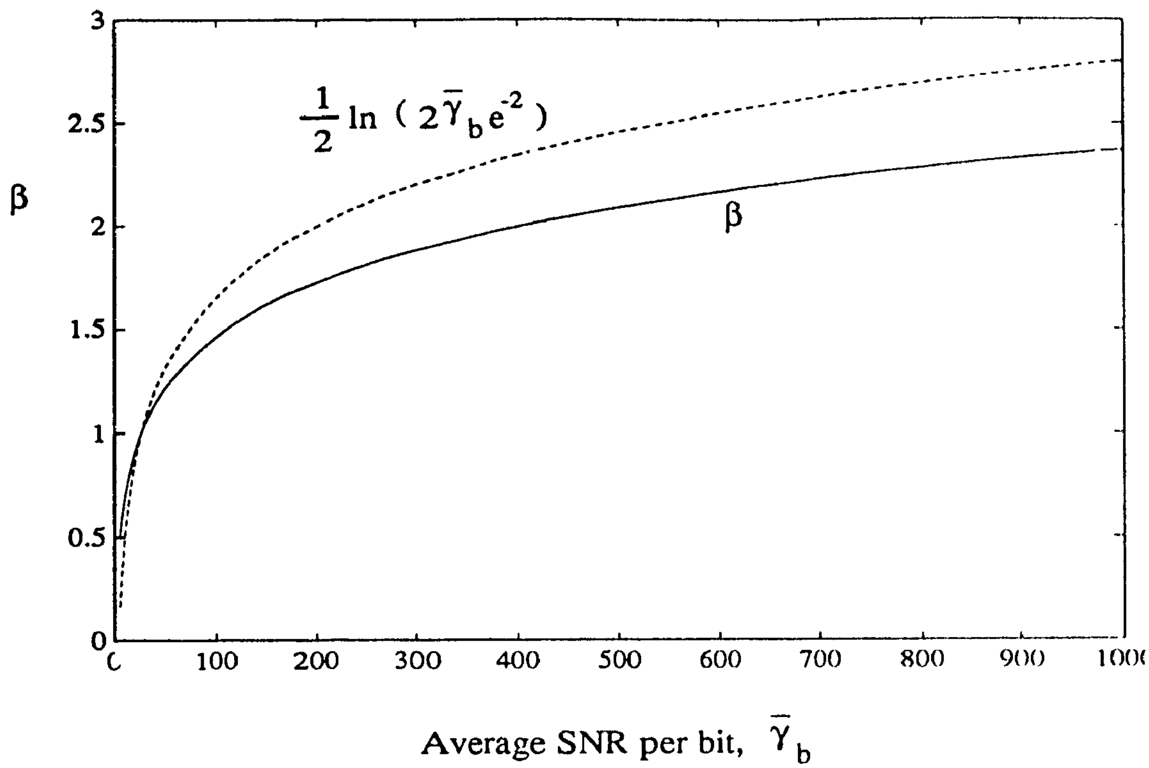

Figure 5.5: $\beta\,(\gg 1)$ as a function of average SNR per bit, $\overline{\gamma}_b$

From (5.42), we then have:

$$P_U \approx \begin{cases} \frac{1}{2}\, exp\,(-\beta/2\sigma^2) & ;\ \text{for } \beta \ll 1 \\ \frac{1}{2}\, exp\,(-\beta^2/2\sigma^2) & ;\ \text{for } \beta \gg 1 \end{cases} \tag{5.50}$$

By substituting (5.46) into (5.50), we have the upper bound for $\beta \ll 1$ as follows

$$P_U \approx \frac{1}{2}\, exp\,(-\overline{\gamma}_b e^{-2\sigma^2}) \tag{5.51}$$

This shows that the upper bound to the error probability decreases exponentially with $\overline{\gamma}_b$. Similarly, for $\beta \gg 1$, substituting (5.49) into (5.50) yields the upper bound as

$$P_U \approx \frac{1}{2}\, exp\,(-[\,\ln\,(2\overline{\gamma}_b \sigma^2 e^{-2\sigma^2})\,]^2\,/\,8\sigma^2) \tag{5.52}$$

Thus, when $\beta \gg 1$, the upper bound to the error probability decreases exponentially with the square of the natural logarithm of $\overline{\gamma}_b$.

To find the lower bound to the error probability in (5.24), we make use of Chebyshev inequality which gives the following:

$$Pr\,[\,exp\,(-ce^{2x}) \geq exp\,(-ce^{2\epsilon})\,] \;\leq\; \mathrm{E}\,[\,exp\,(-ce^{2x})\,]\,exp\,(ce^{2\epsilon}) \tag{5.53}$$

where $\epsilon > 0$. Using (5.25), (5.53) can be rearranged as:

$$\begin{aligned} \mathrm{E}\,[\,exp\,(-ce^{2x})\,] &\geq Pr\,[\,exp\,(ce^{2x}) \leq exp\,(ce^{2\epsilon})\,]\,exp\,(-ce^{2\epsilon}) \\ P_e &\geq \frac{1}{2}\,Pr\,[\,exp\,(ce^{2x}) \leq exp\,(ce^{2\epsilon})\,]\,exp\,(-ce^{2\epsilon}) \\ &\geq \frac{1}{2}\,Pr\,[\,x \leq \epsilon\,]\,exp\,(-ce^{2\epsilon}) \\ &\geq \frac{1}{2}\,Q\,(\,\frac{\mu-\epsilon}{\sigma}\,)\,exp\,(-ce^{2\epsilon}) \end{aligned} \tag{5.54}$$

where $Q\,(x)$ is the Q-function defined as follows:

$$Q\,(x) = \frac{1}{\sqrt{2\pi}} \int_x^{\infty} exp\,(-t^2/2)\,dt \tag{5.55}$$

By using a well-known inequality of the Q-function [37, pp. 247]:

$$Q\,[\,\sqrt{x}\,]\,exp\,(-y/2) \geq Q\,[\,\sqrt{x+y}\,] \qquad\qquad \text{for } x, y \leq 0 \tag{5.56}$$

we can obtain the lower bound of the error probability.

The error probability in (5.54) can be expressed as:

$$\begin{aligned} P_e &\geq \frac{1}{2}\,Q\,(\,\frac{\mu-\epsilon}{\sigma}\,)\,exp\,(-ce^{2\epsilon}) \\ &= \frac{1}{2}\,Q\,[\,\sqrt{(\frac{\mu-\epsilon}{\sigma})^2}\,]\,exp\,(-2ce^{2\epsilon}/2) \end{aligned}$$

and using (5.56), where $x = (\frac{\mu-\epsilon}{\sigma})^2$ and $y = 2ce^{2\epsilon}$, we have the lower bound of the error probability as follows:

$$P_e = P_L \geq \frac{1}{2}\,Q\,[\,\sqrt{(\frac{\mu-\epsilon}{\sigma})^2 + 2ce^{2\epsilon}}\,] \tag{5.57}$$

To have the tighest lower bound, we must find the value of ϵ which minimizes:

$$g_2(\epsilon) = (\frac{\mu-\epsilon}{\sigma})^2 + 2ce^{2\epsilon} \tag{5.58}$$

In order to minimize $g_2(\epsilon)$ with respect to ϵ, we consider

$$\frac{dg_2(\epsilon)}{d\epsilon} = 0 \tag{5.59}$$

or

$$\begin{aligned} 2\,(\frac{\mu-\epsilon}{\sigma})(-\frac{1}{\sigma}) + 4ce^{2\epsilon} &= 0 \\ -2\,(\mu-\epsilon) + 4c\sigma^2 e^{2\epsilon} &= 0 \\ \mu - \epsilon &= 2c\sigma^2 e^{2\epsilon} \end{aligned} \tag{5.60}$$

To make sure that (5.60) gives a minimum, we have to verify if the second derivative of $g_2(\epsilon)$ with respect to ϵ is positive. Therefore,

$$\frac{d^2 g_2(\epsilon)}{d\epsilon^2} = \frac{2}{\sigma^2} + 8ce^{2\epsilon} \tag{5.61}$$

Since $e^{2\epsilon} > 0$, (5.61) is always positive showing that the condition in (5.60) is minimizing (5.58). When comparing (5.60) with (5.37), they are identical. Therefore, from (5.37) and (5.41), we have

$$\beta = \mu - \epsilon = 2c\sigma^2 e^{2x_o} \tag{5.62}$$

The error probability is then lower-bounded by:

$$\begin{aligned} P_L &\geq \frac{1}{2} Q\,[\sqrt{(\frac{\beta}{\sigma})^2 + \frac{\beta}{\sigma^2}}\,] \\ &\geq \frac{1}{2} Q\,[\sqrt{\frac{\beta(\beta+1)}{\sigma^2}}\,] \end{aligned} \tag{5.63}$$

where β satisfies (5.43).

The exact, lower-bounded and upper-bounded error probabilities of the simplified GL receiver for differentially encoded binary commutation signaling over a single-path Lognormal fading (zero-mean and unit variance) channel are depicted in Fig. 5.6. The figure also shows the simulation results. The exact error probability is obtained by performing numerical integration of (5.24). By using the technique of Newton's method to solve for β in the nonlinear equation (5.43) for different values of the average SNR

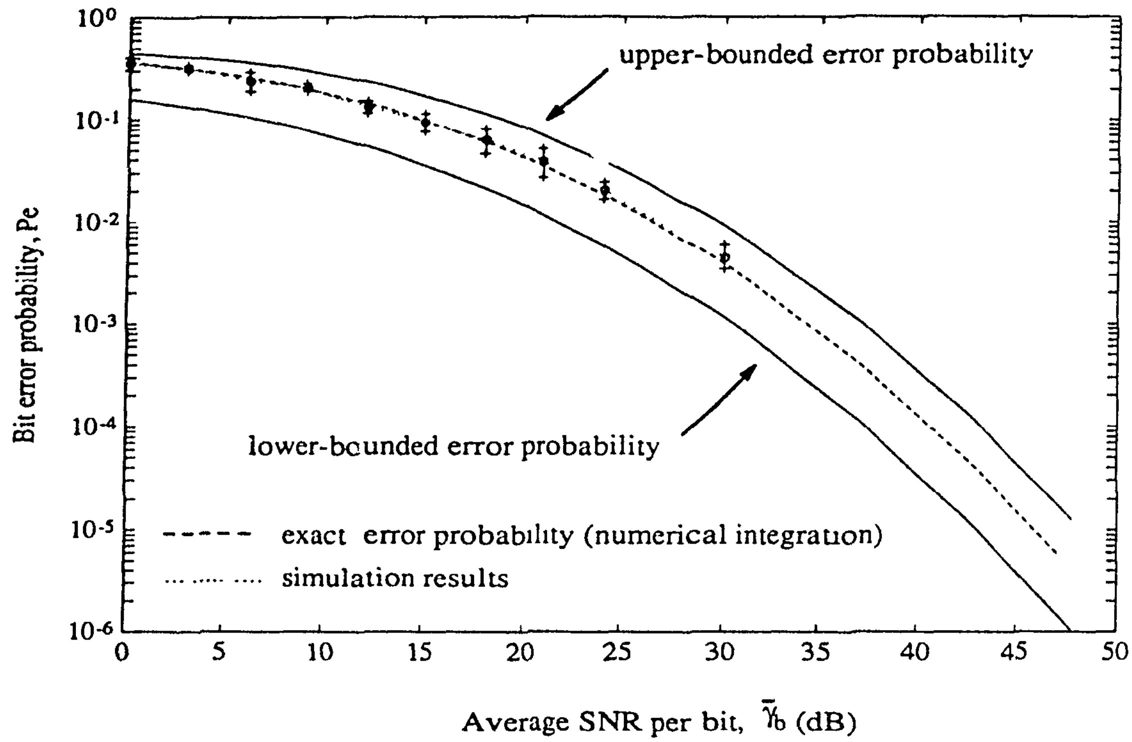

Figure 5.6: The exact, lower-bounded and upper-bounded error probabilities of the simplified GL receiver for binary DPSK over a single-path Lognormal fading channel.

per bit, the lower-bounded and upper-bounded error probabilities are then obtained according to (5.63) and (5.42) respectively. Moreover, we can see in Fig. 5.6 that when the average SNR per bit is small, the exact error probability is closer to the upper-bound error probability. When $\overline{\gamma}_b$ is large, the exact error probability curve lies between the upper-bounded and lower-bounded error probability curves. It is about 2 dB below the upper-bounded error probability curve and 3 dB above the lower-bounded error probability curve.

5.2.2 Numerical Integration

In the case of multipath Lognormal fading channel, we consider the conditional error probability of binary DPSK transmitted a time-invariant channel with L-fold equal weight combining as given in (5.11):

$$P_b(\gamma_b) = \frac{1}{2^{2L-1}} exp\,(-\gamma_b) \sum_{k=0}^{L-1} b_k {\gamma_b}^k \tag{5.64}$$

where b_k is given by (5.12) and the SNR per bit γ_b is defined as:

$$\gamma_b = \frac{E_b}{N_o} \sum_{i=0}^{L-1} {\alpha_i}^2 \tag{5.65}$$

Now, for a multipath Lognormal fading channel, $\alpha_i = e^{x_i}$, where $i = 0, .. , L-1$ and x_i is normally-distributed with mean μ_i and variance ${\sigma_i}^2$. Therefore, (5.65) becomes

$$\gamma_b = \frac{E_b}{N_o} \sum_{i=0}^{L-1} e^{2x_i} \tag{5.66}$$

Substituting (5.66) into (5.64), we have the conditional probability as:

$$P_b(x_0, x_1, .., x_{L-1}) = \frac{1}{2^{2L-1}} exp\,(-\frac{E_b}{N_o} \sum_{i=0}^{L-1} e^{2x_i})\,[\sum_{k=0}^{L-1} b_k (\frac{E_b}{N_o} \sum_{j=0}^{L-1} e^{2x_j})^k\,] \tag{5.67}$$

The probability of error of the simplified GL receiver for binary DPSK over a multipath Lognormal fading channel is then obtained by averaging (5.67) over the joint pdf $p(x_0, x_1, .., x_{L-1})$ by the following integral:

$$P_e = \int_{-\infty}^{\infty} \int_{-\infty}^{\infty} \cdot\cdot \int_{-\infty}^{\infty} P_b(x_0, x_1, .., x_{L-1})\, p(x_0, x_1, .., x_{L-1})\, dx_0\, dx_1 \cdot\cdot\cdot dx_{L-1} \tag{5.68}$$

With the assumption that the fading processes among the L diversity channels are mutually statistically independent, the joint pdf is given by:

$$p(x_0, x_1, .., x_{L-1}) = p(x_0)\, p(x_1) \cdot\cdot\cdot p(x_{L-1}) = \prod_{i=0}^{L-1} p(x_i) \tag{5.69}$$

where

$$p(x_i) = \frac{1}{\sqrt{2\pi{\sigma_i}^2}} exp\,[-\frac{(x_i - \mu_i)^2}{2{\sigma_i}^2}\,] \qquad ;\ i = 0, .., L-1 \tag{5.70}$$

Therefore, (5.68) becomes:

$$P_e = \int_{-\infty}^{\infty}\int_{-\infty}^{\infty}\cdots\int_{-\infty}^{\infty} \frac{1}{2^{2L-1}} exp\,(-\frac{E_b}{N_o}\sum_{i=0}^{L-1} e^{2x_i})\,[\sum_{k=0}^{L-1} b_k(\frac{E_b}{N_o}\sum_{j=0}^{L-1} e^{2x_j})^k\,] \cdot \prod_{i=0}^{L-1} \frac{1}{\sqrt{2\pi\sigma_i^2}} exp\,[-\frac{(x_i-\mu_i)^2}{2\sigma_i^2}\,]\; dx_0\, dx_1 \cdots dx_{L-1} \tag{5.71}$$

From (5.65), the average SNR per bit $\overline{\gamma}_b$ is:

$$\begin{aligned}\overline{\gamma}_b &= \frac{E_b}{N_o}\sum_{l=0}^{L-1} \mathrm{E}\,[\,e^{2x_l}\,] \\ &= \frac{E_b}{N_o}\sum_{l=0}^{L-1} e^{2\sigma_l^2+2\mu_l}\end{aligned} \tag{5.72}$$

or

$$\frac{E_b}{N_o} = \frac{\overline{\gamma}_b}{\sum_{l=0}^{L-1} e^{2\sigma_l^2+2\mu_l}} \tag{5.73}$$

By substituting (5.73) into (5.71), we have the error probability as follows:

$$P_e = \int_{-\infty}^{\infty}\int_{-\infty}^{\infty}\cdots\int_{-\infty}^{\infty} \frac{1}{2^{2L-1}} exp\,(-\frac{\overline{\gamma}_b\sum_{i=0}^{L-1} e^{2x_i}}{\sum_{l=0}^{L-1} e^{2\sigma_l^2+2\mu_l}})\,[\sum_{k=0}^{L-1} b_k(\frac{\overline{\gamma}_b\sum_{j=0}^{L-1} e^{2x_j}}{\sum_{l=0}^{L-1} e^{2\sigma_l^2+2\mu_l}})^k\,] \cdot \prod_{i=0}^{L-1} \frac{1}{\sqrt{2\pi\sigma_i^2}} exp\,[-\frac{(x_i-\mu_i)^2}{2\sigma_i^2}\,]\; dx_0\, dx_1 \cdots dx_{L-1} \tag{5.74}$$

However, the aboved expression cannot be simplified into a closed form, thus it can only be obtained by means of numerical integration.

For $L = 2$, the error probability is:

$$\begin{aligned}P_e &= \int_{-\infty}^{\infty}\int_{-\infty}^{\infty} \frac{1}{8} exp\,[-\frac{\overline{\gamma}_b(e^{2x_0}+e^{2x_1})}{e^{2\sigma_0^2+2\mu_0}+e^{2\sigma_1^2+2\mu_1}}] \\ &\cdot\; [\,4+\frac{\overline{\gamma}_b(e^{2x_0}+e^{2x_1})}{e^{2\sigma_0^2+2\mu_0}+e^{2\sigma_1^2+2\mu_1}}\,] \\ &\cdot\; \frac{1}{2\pi\sigma_0\sigma_1} exp\,[-\frac{(x_0-\mu_0)^2}{2\sigma_0^2}-\frac{(x_1-\mu_1)^2}{2\sigma_1^2}\,]\, dx_0\, dx_1\end{aligned} \tag{5.75}$$

Similarly, for $L = 3$, the error probability is:

$$\begin{aligned}P_e = &\int_{-\infty}^{\infty}\int_{-\infty}^{\infty}\int_{-\infty}^{\infty} \frac{1}{32} exp\,[-\frac{\overline{\gamma}_b(e^{2x_0}+e^{2x_1}+e^{2x_2})}{e^{2\sigma_0^2+2\mu_0}+e^{2\sigma_1^2+2\mu_1}+e^{2\sigma_2^2+2\mu_2}}] \\ &\cdot\; [\,16+\frac{6\overline{\gamma}_b(e^{2x_0}+e^{2x_1}+e^{2x_2})}{e^{2\sigma_0^2+2\mu_0}+e^{2\sigma_1^2+2\mu_1}+e^{2\sigma_2^2+2\mu_2}}+\frac{\overline{\gamma}_b^{\,2}(e^{2x_0}+e^{2x_1}+e^{2x_2})^2}{2(e^{2\sigma_0^2+2\mu_0}+e^{2\sigma_1^2+2\mu_1}+e^{2\sigma_2^2+2\mu_2})^2}\,] \\ &\cdot\; (\frac{1}{2\pi})^{\frac{3}{2}}\frac{1}{\sigma_0\sigma_1\sigma_2} exp\,[-\frac{(x_0-\mu_0)^2}{2\sigma_0^2}-\frac{(x_1-\mu_1)^2}{2\sigma_1^2}-\frac{(x_2-\mu_2)^2}{2\sigma_2^2}\,]\, dx_0\, dx_1\, dx_2\end{aligned} \tag{5.76}$$

The probabilities of error performance of the simplified GL receiver for differentially encoded binary commutation signaling over a multipath Lognormal fading (zero-mean and unit variance) channel with $L = 2$ and $L = 3$ as given in (5.75) and (5.76) respectively are obtained by numerical integration. The technique we use for numerical integration is Romberg integration and the routines for evaluating one-dimensional integration can be found in [38, pp. 123]. The routines can be modified and extended to evaluate higher dimensional integrations. The Romberg integration is preferred to the traditional Simpson integration because it takes fewer iterations and evaluations when the integrands are sufficiently smooth and do not have any singularity. In order to assure that Romberg integration is appropriate in this context, a plotting of the integrands of (5.75) and (5.76) was done and it was found that the integrands were smooth and no singularity was presented.

The computer simulation results are also presented in Fig. 5.7 and the error performance is plotted as a function of the average SNR per bit. The results clearly illustrate the diversity improvement on the error performance of the receiver. However, the improvement is not as good as in the case for multipath Rayleigh fading channel. The diminishing returns effect shows that a two fold diversity gives a measureable performance improvement up to an error rate of about 2×10^{-1}, and a three fold diversity gives measureable performance improvement over two fold only up to an error rate of about 10^{-1}. It seems that Lognormal fading causes a severe penalty in SNR and a three fold diversity is recommended even for error rates between 10^{-1} and 10^{-2}.

A comparison of the probability of error performance of the simplified GL receiver for differentially encoded binary commutation signaling over multipath Rayleigh fading channel and multipath Lognormal fading (zero-mean and unit variance) channel is shown in Fig. 5.8. It shows that Lognormal fading causes a more severe penalty in SNR than Rayleigh fading does. Therefore, in order to achieve the same bit error rate, larger average SNR per bit is needed for operating over multipath Lognormal fading channel.

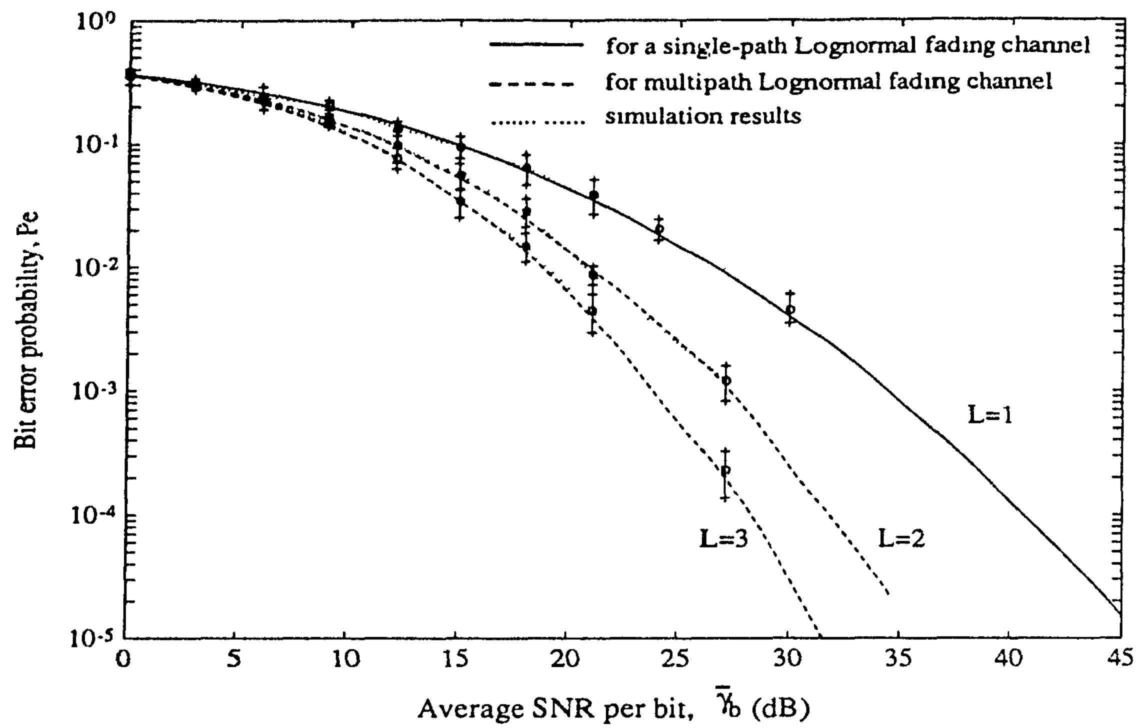

Figure 5.7: The error performance of the simplified GL receiver for binary DPSK over multipath Lognormal fading channel.

and thus diversity combining techniques should be used if possible.

So far, we have analysed the error performance of the simplified GL receiver with the assumption that the channel estimation was done perfectly. In other words, the RAKE taps were assumed to be activated properly. The effects of incorrect channel estimation on the performance of the simplified GL receiver when the RAKE taps are not correctly activated will be considered in the next section.

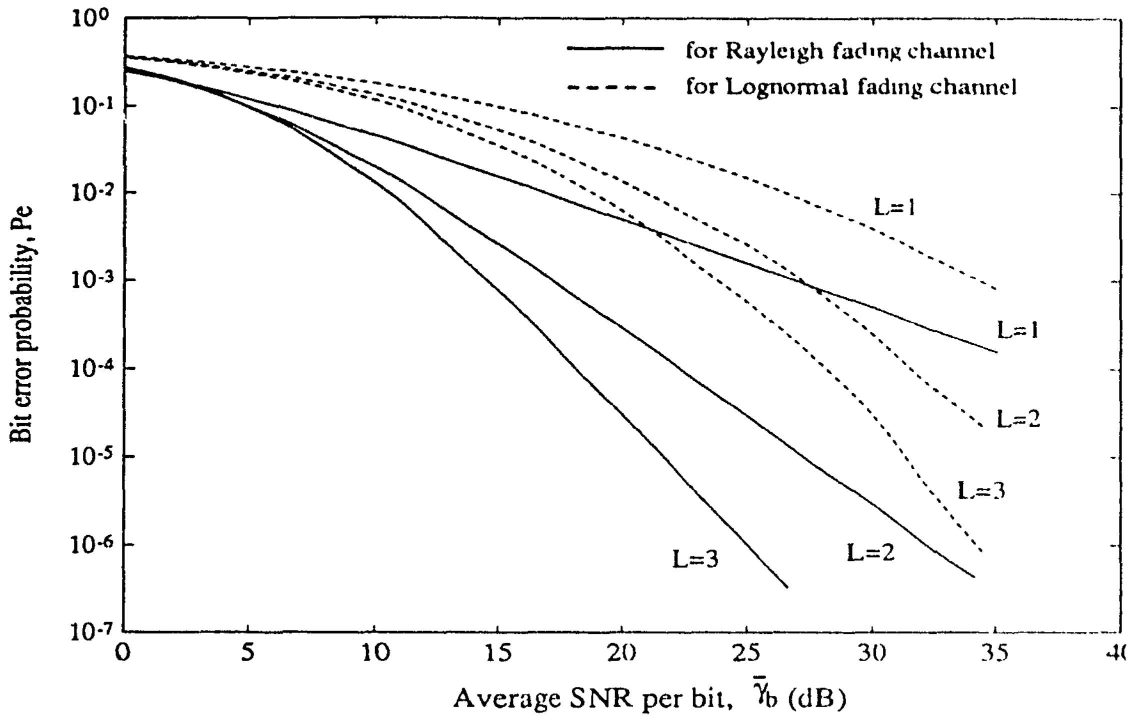

Figure 5.8: A comparison of the error performance of the simplified GL receiver for binary DPSK over multipath Rayleigh fading channel and multipath Lognormal fading channel.

5.3 Effects of Incorrect Channel Estimation

In both section 5.1 and section 5.2, our analysis on the performance of the simplified GL receiver over Rayleigh or Lognormal fading channels assumed that the channel estimation process was performed perfectly. Under such an assumption, all appropriate taps of the equal weight RAKE combiner were correctly activated. However, in practice, the channel estimation process is not perfect. Therefore, wrong activated RAKE taps due to incorrect channel estimation may cause degradation in performance. In this section, we consider the effects of incorrect channel estimation on the performance of the simplified GL receiver by computer simulations. Details on the simulation program can be found in Appendix B.

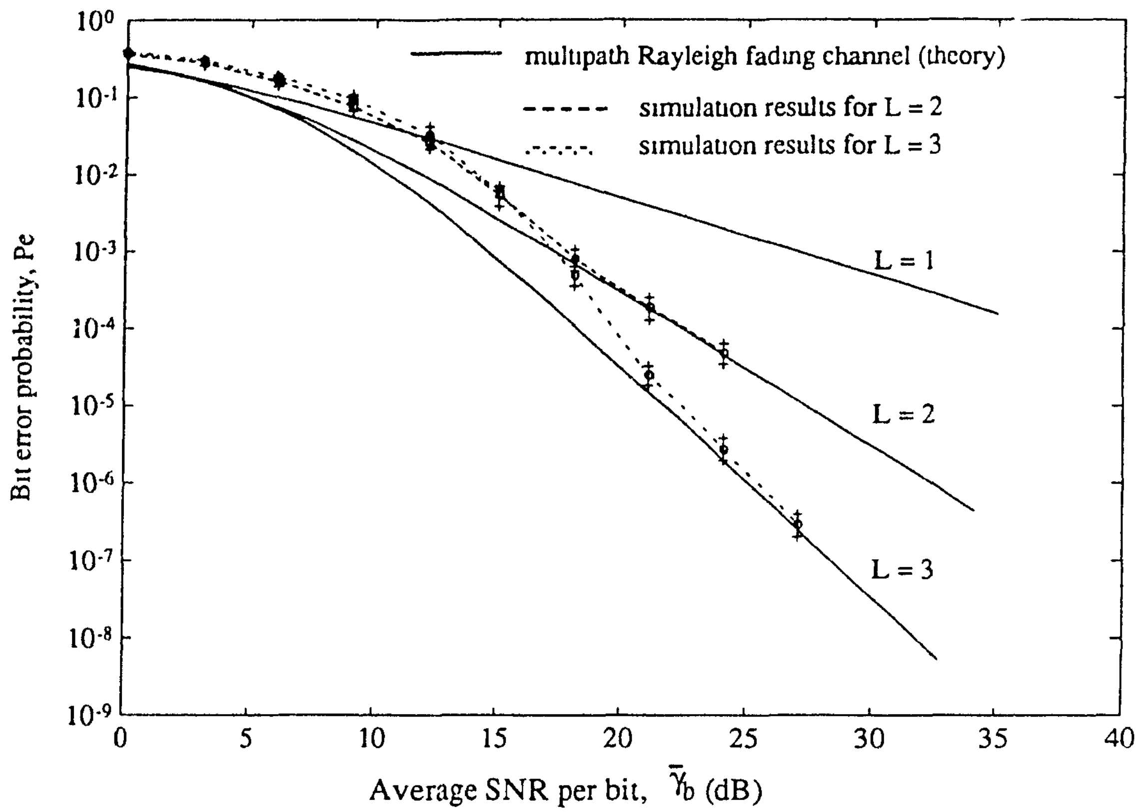

Figure 5.9: The simulation results of the simplified GL receiver over two-path and three-path Rayleigh fading channels under practical channel estimation.

Under perfect channel estimation, the equal weight RAKE combiner assumes to have a signal component to be combined at each activated tap. In the case of incorrect channel estimation, the performance will be degraded since some of the wrong activated RAKE taps not only exclude the signal components to be combined, but also contribute additional noises to the combining process. As a demonstration of the performance degradation, we show in Fig. 5.9 the simulation results of the differentially encoded binary commutation signaling for the simplified GL receiver over Rayleigh fading channel with two and three fold diversity under practical channel estimation. From these results, we observe that a performance degradation of about 3 to 4 dB occurs when the average SNR per bit is low. However, this degradation decreases as the average SNR per bit increases. The degradation is due to errors in the time delay estimation of the autocorrelation peaks. When the error is larger than the autocorrelation width, that is, the width of the peaks at the matched filter output, then incorrect RAKE taps are activated, which results in performance degradation.

For two fold diversity, the degradation is negligible when the average SNR per bit is about 18 dB, while for three fold diversity, when the average SNR per bit is about 27 dB. This threshold effect indicates that above a certain average SNR per bit, the channel estimation is close to perfect and thus the performance of the simplified GL receiver under practical channel estimation is close to that under perfect channel estimation. In addition, it can be seen that under practical channel estimation, a three fold diversity does not result in better performance over a two fold diversity when the average SNR per bit is below 15 dB. In fact, the degradation in a three fold diversity channel is even more when the average SNR per bit is below 15 dB. It seems that a three fold diversity is effective only when the operational error rate of the system is below 2×10^{-3}.

In order to have an insight into the efficiency of the channel estimation process, we also present in Fig. 5.10 and Fig 5.11 the Root Mean Square (RMS) error of the estimated path delays for the two and three paths channels respectively. The simulation program was run with the symbol period $T = 7.75\mu s$ and the autocorrelation width $T_c = 0.25\mu s$ by using 31-bit Gold sequences for bandwidth expansion. For two fold diversity, the two path delays are $\tau_0 = 0\mu s$ and $\tau_1 = 1.5\mu s$, while for three fold diversity the three path delays are $\tau_0 = 0\mu s$, $\tau_1 = 1.5\mu s$ and $\tau_2 = 3\mu s$. It is obvious that the RMS error of the estimated path delays decreases as the average SNR per bit increases. In order to activate the correct RAKE taps, the estimation error has to be less than the autocorrelation width. As shown in Fig. 5.10, the RMS errors of the two estimated path delays are both below $T_c = 0.25\mu s$ when the average SNR per bit is above 18 dB. It is the point when the channel estimation is close to perfect. The result is consistent

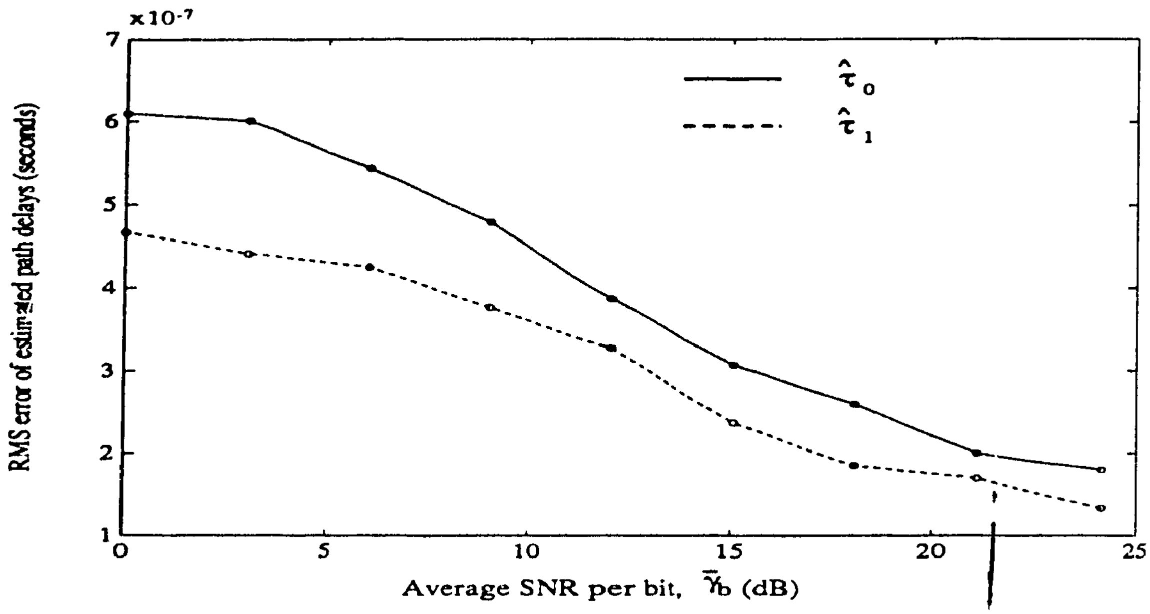

Figure 5.10: The RMS error of the estimated path delays for two-path Rayleigh fading channel.

with the error performance as obtained in Fig. 5.9. Similarly, in Fig 5.11, when the average SNR per bit is 27 dB, the RMS error of $\hat{\tau}_0$ is about $0.25\mu s$, and the RMS errors of $\hat{\tau}_1$ and $\hat{\tau}_2$ are about $0.3\mu s$, this gives a corresponding error probability about 0.5×10^{-6} as given in Fig. 5.9, which is approaching the error probability with perfect channel estimation. Error probabilities below 10^{-7} are extremely difficult to obtain from simulations, however, in Fig. 5.11, the RMS error of the three estimated path delays are all below $0.3\mu s$ when the average SNR per bit is 30 dB indicating that the channel estimation tends to be perfect above this point. From Fig. 5.10 and Fig. 5.11, we also see the threshold phenomenon associated with time delay estimation [39].

Computer simulations were also performed for Lognormal fading channel and Fig. 5.12 shows the results for the simplified GL receiver with differentially encoded binary commutation signaling. It can be seen that a performance degradation of about 3 dB occurs for low average SNR per bit. In addition, the performance for a three fold diversity is comparable to that for a two fold diversity when the average SNR per bit is

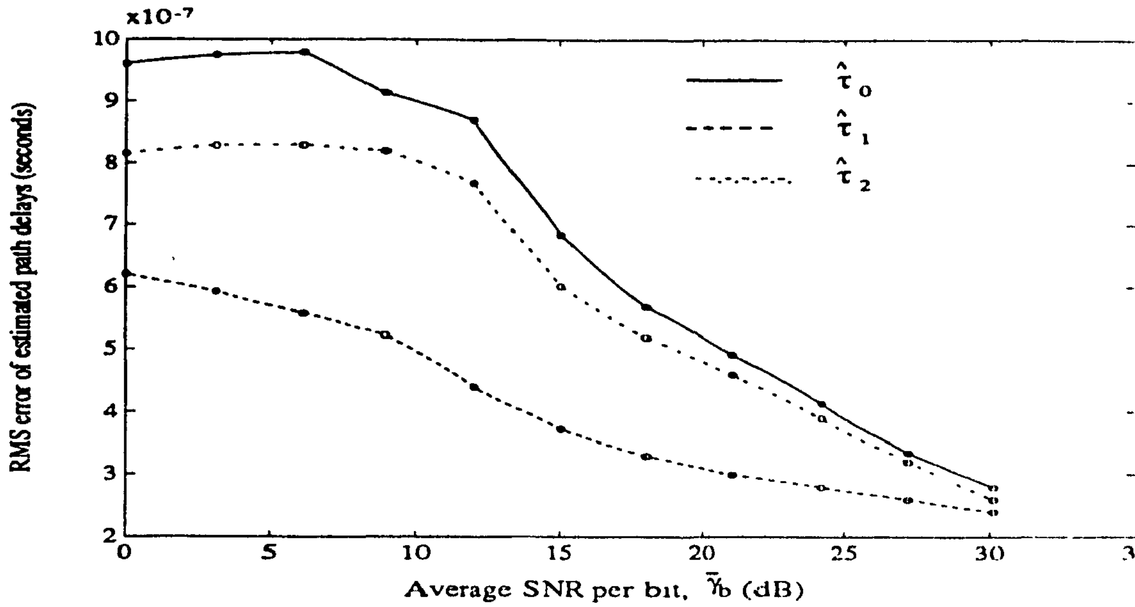

Figure 5.11: The RMS error of the estimated path delays for three-path Rayleigh fading channel.

below 15 dB. The error probability seems to converge slowly to the performance under perfect channel estimation. Fig. 5.13 and Fig. 5.14 give the corresponding RMS error of the estimated path delays of the two and three paths channels respectively. Even for two fold diversity, the channel estimation seems to be performed perfectly only when the average SNR per bit is about 36 dB at which point the RMS errors of the two estimated path delays are below $0.3\mu s$. For three fold diversity, it seems that a higher average SNR per bit is required to achieve perfect channel estimation. Even when the average SNR per bit is 36 dB, there is a performance degradation of about 1 dB. From Fig. 5.14, it can be seen that the RMS error of estimated path delays is decreasing slower than the Rayleigh fading case.

The simulation results reveal that under practical channel estimation, the simplified GL receiver suffers a performance degradation of about 3 to 4 dB when the average SNR per bit is low. However, as the average SNR per bit increases, the channel estimation process tends to perform better. This behaviour indicates that above a certain

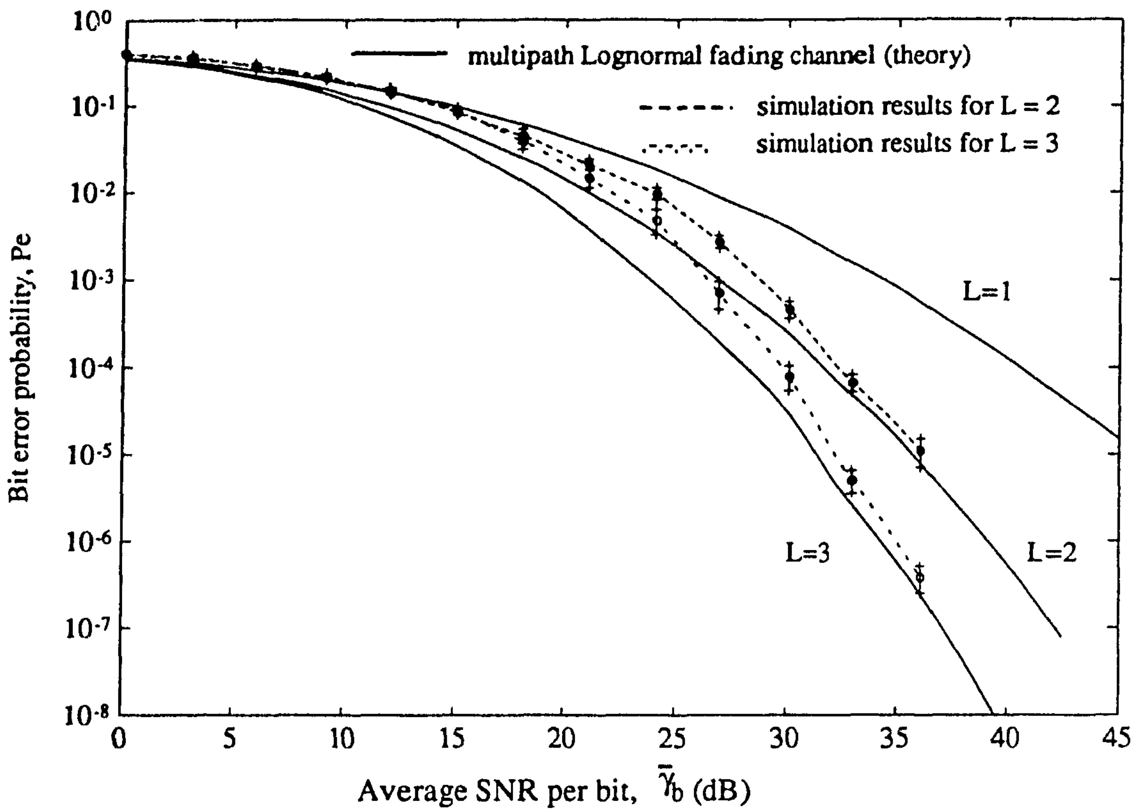

Figure 5.12: The simulation results of the simplified GL receiver over two-path and three-path Lognormal fading channel under practical channel estimation.

average SNR per bit, channel estimation error result in insignificant performance degradation. A higher order diversity requires a larger average SNR per bit for having good channel estimation.

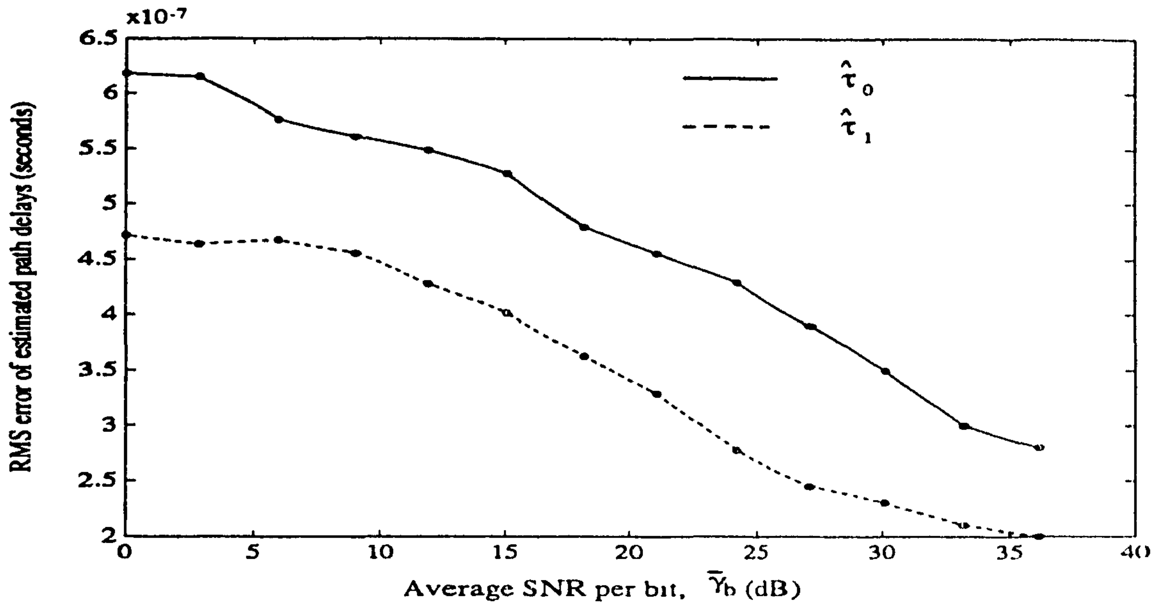

Figure 5.13: The RMS error of the estimated path delays for two-path Lognormal fading channel.

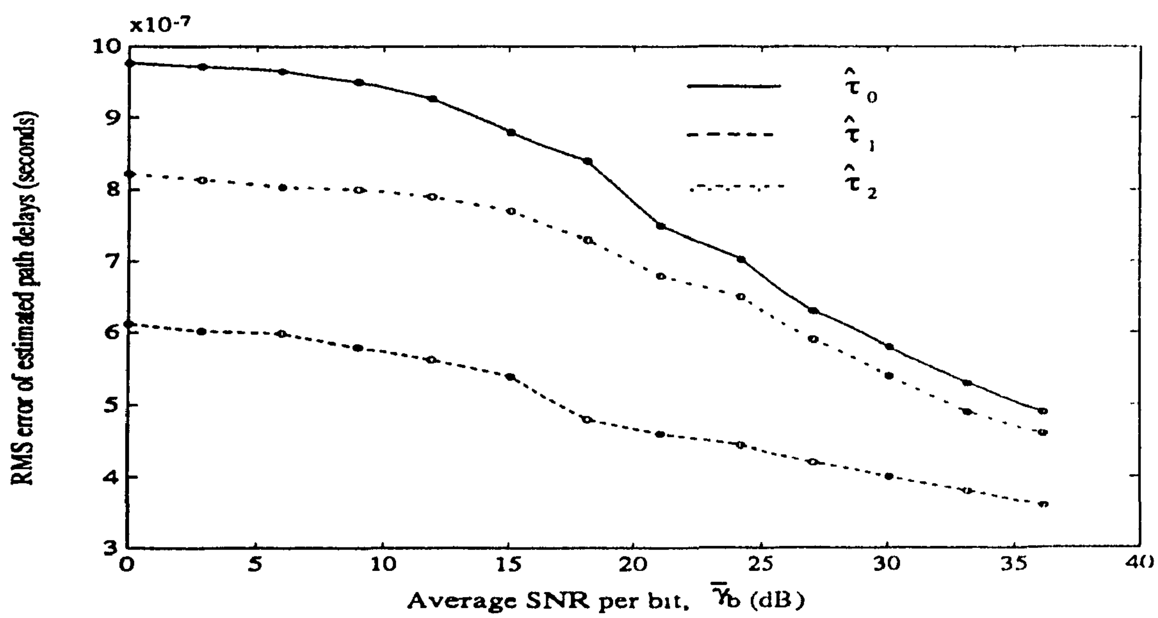

Figure 5.14: The RMS error of the estimated path delays for three-path Lognormal fading channel.

Chapter 6

Conclusions

With the use of Generalized Likelihood (GL) principle, a receiver structure of low complexity was derived for indoor wireless communication channels which were modelled as multipath fading channels. Unlike other receivers which may require an *a-priori* channel model, the GL receiver was robust against channel models. The structure of the receiver is a matched filter with square-law equal weight RAKE combining. Moreover, the GL principle combined naturally both channel parameter estimation and data detection.

The existence of multipath induced ISI caused by multipath propagations may complicate the channel estimation process. It was seen that the effects of multipath induced ISI on the channel estimation process could be reduced by employing the technique of commutation signaling. A comparison of commutation signaling with several other M-ary signaling schemes on the number of orthogonal signals and matched filter required was done. It seemed that binary commutation signaling resulted in an optimal scheme which maximized SNR performance and minimized the number of matched filters to be used.

The effects of multipath induced ISI on the data detection process has been considered by examining the amount of significant ISI at the output of the RAKE receiver. In this work, an upper bound to the event of having significant ISI at the output of the maximum gain RAKE combiner and the square-law equal weight RAKE combiner was obtained by using union bounding techiques. It was shown that with sufficient bandwidth expansion, the probability of having significant ISI could be made arbitrarily small and the multipath induced ISI effects on data detection process reduced tremendously. In addition, it was shown that using square-law equal weight RAKE receiver required 3 dB less processing gain than the maximum gain RAKE receiver. Furthermore, the required bandwidth expansion for ISI suppression was greatly reduced when antenna diversity was employed.

Although zero ISI could be achieved in the case when commutation signaling was used with maximum gain RAKE combiner, it seemed that square-law equal weight RAKE combiner was appropriate for indoor channels since it only required the path delay estimates, but not the estimation of the signal amplitude and phase as required for maximum gain RAKE combiner. With properly-designed commutation signaling, the amount of ISI in the GL receiver could be made insignificant.

Differentially encoding schemes seem to be appropriate for multipath fading channels as carrier phase tracking, which is usually difficult to perform in these channels, is not required. Therefore, in this work, the combination of binary commutation signaling with differentially phase shift keyed modulation has been considered. In this case, the GL receiver uses differentially coherent detection. It was seen that DPSK not only avoided the phase estimation difficulty, but also reduced significantly the sidelobes of the signal to be combined at the input of the equal weight RAKE combiner in the GL receiver.

The structure of a simplified GL receiver which required only one single set of channel estimator and equal weight RAKE combiner was derived. The performance of the simplified GL receiver relied also on the path delays estimates acquired in the channel estimation process. Under perfect channel estimation and assuming that the channel was multipath Rayleigh fading or Lognormal fading, the performance of the simplified GL receiver with differentially encoded binary commutation signaling scheme over these channels was analysed. The probabilities of error performance of the simplified GL receiver clearly illustrated the advantage of using equal weight RAKE combiner for the exploitation of multipath diversity to overcome the severe penalty in SNR caused by fading. Moreover, the lower the operational error rate of the system was, the more effective the diversity would be. Furthermore, it was found that Lognormal fading channel resulted in more severe penalty in SNR than Rayleigh fading channel caused

Finally, the effects of incorrect channel estimation on the simplified GL receiver have been investigated by computer simulations. The performance degradation due to incorrect activation of RAKE taps in the GL receiver was compared to the error probability under perfect channel estimation. The simulation results showed that a performance degradation of about 3 dB occurred when the average SNR per bit was low. However, the threshold effect indicated that above a certain average SNR per bit, the channel estimation was close to perfect, and the performance degradation was becoming insignificant. In addition, a higher order diversity required a larger average SNR per bit in order to have good channel estimation.

Bibliography

[1] H. H. Hoffman and D. C. Cox, "Attenuation of 900 MHz Radio Waves Propagating into a Metal Building," *IEEE Trans. on Antennas Propagat.*, Vol. AP-30, pp 808-811, July 1982.

[2] S. E. Alexander, "Radio Propagation within Building at 900 MHz," *Electron Lett.*, Vol. 18, No. 21, pp. 913-914, October 1982.

[3] S. E. Alexander, "Characterizing Buildings for Propagation at 900 MHz," *Electron. Lett.*, Vol. 19, No. 20, pp 860, September 1983.

[4] D. M. J. Devasirvatham, "Time Delay Spread Measurements of Wideband Radio Signals within a Building," *Electron. Lett.*, Vol. 20, No. 23, pp. 950-951, November 1984.

[5] D. M. J. Devasirvatham, "Time Delay Spread Measurements of 850 MHz Radio Waves in Building Environments," *GLOBECOM 85 Conf. Rec.*, Vol. 2, pp 970-973, December 1985.

[6] A. A. M. Saleh and R. A. Valenzuela, "A Statistical Model for Indoor Multipath Propagation," *IEEE J. Sel. Areas Commun.*, Vol. SAC-5, No. 2, pp. 128-137, February 1987.

[7] A. S. Bajwa, "UHF Wideband Statistical Model and Simulation of Mobile Radio Multipath Propagation Effects," *IEE Proc. F.*, Vol. 132, No. 5, pp. 327-333, 1985

[8] T. S. Rappaport, S. Y. Seidel amd K. Takamizawa, "Statistical Channel Impulse Response Models for Factory and Open Plan Building Radio Communication System Design," *IEEE Trans. on Commun.*, Vol. CS-39, No. 5, pp. 794-807, May 1991.

[9] H. L. and Van Trees, "Detection, Estimation and Modulation Theory, Part I", John Wiley & Sons, 1968.

[10] C. W. Helstrom, "Statistical Theory of Signal Detection", Pergamon Press, 1968.

[11] G. L. Turin, "Commutation Signaling - An Antimultipath Technique," *IEEE J. Select. Areas Commun.*, Vol. SAC-2, No. 4, pp. 548-562, July 1984.

[12] P. Monsen, "Fading Channel Communication," *IEEE Commun. Mag.*, pp. 16-25, January 1980.

[13] P. Monsen, "Feedback Equalization for Fading Dispersive Channels,"*IEEE Trans. on Information Theory*, pp. 56-64, January 1971.

[14] G. L. Turin, "Introduction to Spread-Spectrum Antimultipath Techniques and Their Application to Urban Digital Radio," *IEEE Proc.*, Vol. 68, No. 3, pp. 328-353, March 1980.

[15] J. D. Parsons and A. S. Bajwa, "Wideband Characterisation of Fading Mobile Radio Channels," *IEE Proc. F.*, Vol. 129, No. 2, pp. 95-101, April 1982.

[16] J. D. Parsons, D. A. Demery, and A. M. D. Turkmani, "Sounding techniques for wideband mobile radio channels: a review," *IEE Proc. F.*, Vol. 138, No. 5, pp. 437-446, October 1991.

[17] P. C. Fannin, A. Molina, S. S. Swords, and P. J. Cullen, "Digital Signal Processing Techniques Applied to Mobile Radio Channel Sounding," *IEE Proc. F.*, Vol. 138, No. 5, pp. 502-508, October 1991.

[18] D. V. Sarwate and M. B. Pursley, "Cross-correlation Properties of Pseudorandom and Related Sequences," *IEEE Proc.*, Vol. 68, pp. 593-619, May 1980

[19] J. G. Proakis, "Digital Communications", New York. McGraw-Hill, 1989, ch. 7.

[20] P. A. Bello, "Characterisation of Randomly Time-variant Linear Channels," *IEEE Trans. on Commun.*, Vol. CS-11, pp.360-393, December 1963

[21] H. Hashemi, "Simulation of the Urban Radio Propagation Channel," *IEEE Trans on Veh. Technol.*, Vol. VT-28, pp. 213-225, August 1979.

[22] G. L. Turin, F. D. Clapp, T. L. Johnston, S. B. Fine, and D. Lavry, "A Statistical Model of Urban Multipath Propagation," *IEEE Trans. on Veh. Technol.*, Vol VT-21, pp. 1-9, February 1972.

[23] A. M. D. Turkmani, D. A. Demery, J. D. Parsons, "Measurement and Modelling of Wideband Mobile Radio Channels at 900 MHz," *IEE Proc. I.*, Vol. 138, No. 5, pp 447-457, October 1991.

[24] L. Golding and A. Livne, "RALAN - A Radio Local Area Network for Voice and Data Communications," *GLOBECOM 87 Conf. Rec.*, Vol. 3, pp. 1900-1904, 1987

[25] B. Walke and R. Briechle, "A Local Cellular Radio Network (LCRN) for Digital Voice and Data Transmission at 60 GHz, *Cellular and mobile communications international*, pp.215-224, 1985.

[26] S. E. Alexander and G. Pugliese, "Cordless Communication within Buildings Results of Measurements at 900 MHz and 60 GHz," *Br. Telecom. Tech. J.*, pp 99-105, July 1983.

[27] A. R. Tharek and J. P. McGeehan, "Indoor Propagation and Bit Error Rate Measurements at 60 GHz using Phase-Locked Oscillators," *IEEE Vehicu. Tech. Conf.*, pp. 127-133, 1988.

[28] G. A. Kalivas, M. El-Tanany and S. A. Mahmoud, "Millimeter-wave Channel Measurements for Indoor Wireless Communications," *IEEE Vehicu. Tech. Conf.*, May 1992.

[29] P. F. M. Smulders and A. G. Wagemans, "Wideband Indoor Radio Propagation Measurements at 58 GHz," *Electron. Lett.*, Vol. 28, No. 13, pp.1270-1272, June 1992.

[30] P. F. M. Smulders and A. G. Wagemans, "Millimetre-wave Biconical Horn Antennas for Near Uniform Coverage Indoor Picocells," *Electron. Lett.*, Vol. 28, No. 7, pp.679-681, March 1992.

[31] J. N. Pierce, "Theoretical Diversity Improvement in Frequency-Shift-Keying," *IEEE Proc.*, Vol. 46, No. 5, pp. 903-910, May 1958.

[32] K. M. Cheung, H. Leib, and S. Pasupathy, "Multipath Induced Intersymbol Interference in Bandwidth Expanding Signaling," *Proceedings of 16th Biennial Symposium on Communications*, pp. 273-276, May 1992.

[33] H. M. Taylor, S. Karlin, "An Introduction to Stochastic Modeling", Academic Press, Inc. 1984.

[34] S. S. Rappaport and D. M. Grieco, "Spread Spectrum Signal Acquisition: Methods and Technology," *IEEE Commun. Mag.*, Vol. 22, pp. 6-21, June 1984.

[35] R. Gold, "Optimal Binary Sequences for Spread Spectrum Multiplexing", *IEEE Trans. on Information Theory*, Vol. 13, pp. 619-621, October 1967.

[36] E. L. Crow and K. Shimizu, "Lognormal Distributions", Marcel Dekker, Inc. 1988.

[37] A. J. Viterbi and J. K. Omura, "Principles of Digital Communication and Coding", McGraw-Hill, 1979.

[38] W. H. Press, B. P. Flannery, S. A. Teukolsky, and W. T. Vetterling, "Numerical Recipes in C, The Art of Scientific Computing", Cambridge University Press, 1988

[39] J. P. Ianniello, "Time Delay Estimation via Cross-correlation in the Presence of Large Estimation Errors", *IEEE Trans. on ASSP*, Vol 30, No. 6, pp. 998-1003, December 1982.

[40] G. M. Dillard, "Generating Random Numbers Having Probability Distribution Occurring in Signal Detection Problems", *IEEE Trans on Information Theory*, Vol 13, pp. 616-617, October 1967.

Appendix A

This appendix gives an overview on the simulation program of the simplified GL receiver with differentially encoded binary commutation signaling under perfect channel estimation. A complete source listings of the simulation program and some utility programs are filed into another separate document.

The computer simulation software was developed using the C programming languages and was run under the SUN Operating System. The model of the communication system that the simulation program based on is the one shown in Fig. 3.13, but the receiving side is replaced by the simplified GL receiver for differentially encoded binary commutation signaling as given in Fig. 4.3.

The program assumed a time resolution unit of $T_{res} = 5 \times 10^{-8}$ seconds. Commutation signals were obtained from 31-bit Gold sequences which were generated by using 5-bit maximum-length shift register with proper feedbacks. The appropriate feedback connections for generating 31-bit Gold sequences could be found in [19, pp. 835]. Each bit of the Gold sequence took 5 time resolution units resulting in the symbol period of $T = 5 \times 31 \times T_{res} = 7.75\mu$ s. An exhaustive search of 31-bit Gold sequences which give the smallest autocorrelation sidelobes and the narrowest autocorrelation mainlobes have been found In the simulations, two commutation signals were used, and therefore, two Gold sequences with better autocorrelation properties were chosen.

Transmitter:

On the transmitting side, the source generated the data sequence $a(k)$ of values +1 or -1 by using a random number generator. The methods for generating random numbers having different probability distributions can be found in [40] and some of the routines are provided in [38]. To assure that the random numbers to be generated are independent, the system time was used as the seed for the random number generators. A uniformly-distributed random number generator which generated values between 0 and 1 was developed and used as the data sequence generator. If the value was greater than 0.5, the data was +1, otherwise, the data was -1.

The data sequence was differentially encoded into another sequence $b(k)$ according to the relation $b(k) = b(k-1) \cdot a(k)$. Each encoded data bit was multiplied with $\sqrt{E_b}$ for normalization purpose, where E_b is the signal energy per bit, then multiplied with a 31-bit Gold sequence as commutation signal of amplitude varying between $\frac{+1}{\sqrt{T}}$ and $\frac{-1}{\sqrt{T}}$, where T is the symbol period. Since two commutation signals were used in the simulations, the same commutation signal was used again every two symbol periods. The signal was then transmitted into the indoor channel

Channel:

The indoor channel was modelled as multipath fading channel When the fading of the multipath channel was Rayleigh-distributed or Lognormally-distributed, the amplitude of each delayed path was obtained from Rayleigh-distributed or Lognormally distributed random number generator The methods for generating Rayleigh-distributed and Lognormally-distributed random numbers could be found in [40] For two-path fading channel, the two path delays were placed at 0 μs and 1.5 μs, while for three-path fading channel, the three path delays were placed at 0 μs, 1.5 μs and 3 μs Since the channel was assumed to be perturbed by additive white Gaussian noise of zero mean with two-sided power spectral density of $\frac{N_o}{2}$, a Gaussian-distributed random number generator was developed for producing the noise samples. All the required random number generators were tested rigorously to assure that they resulted in random numbers having the specific probability distributions.

Receiver:

On the receiving side, the demodulation was first performed by multiplying the output of one matched filter with the output of another matched filter delayed by the symbol period. The impulse response of the matched filters matched to the particular Gold sequences. A square-law device was then followed to square the amplitude of the signal. Under perfect channel estimation, proper tap coefficients in the equal weight RAKE combiner would be set to unity. For two-path simulation, two appropriate RAKE tap coefficients corresponding to the two path delays were set to unity while for three-path simulation, three appropriate RAKE tap coefficients were set to unity. The signals were processed by the equal weight RAKE combiner. The decision was then made at the output of the equal weight RAKE combiner at the sampling time. The sampling time was at $kT + \Delta$ where $\Delta = 1.5\mu s$ for two-path channel and $\Delta = 3\mu s$ for three-path channel. If the output was greater than zero, the data was detected as +1, otherwise, it was detected as -1

Simulation Trials:

The error probabilities of the simplified GL receiver were obtained for different values of the average SNR per bit by varying the values of E_b and N_o. For L-path Rayleigh fading channel, since the average SNR per channel was assumed to be identical for all L channels, the average SNR per bit was given by (5.10) as:

$$\overline{\gamma}_b = L\,\frac{E_b}{N_o}\,\mathrm{E}\,[\alpha^2] \qquad \text{or} \qquad 10\,log_{10}\,(\,L\,\frac{E_b}{N_o}\,\mathrm{E}\,[\alpha^2]\,)\ \text{in dB}$$

In the simulations, the Rayleigh-distributed random number generator was set such that $\mathrm{E}\,[\alpha^2] = 1$. Similarly, for L-path Lognormal fading channel, the average SNR per bit was given by (5.72) as:

$$\overline{\gamma}_b = \frac{E_b}{N_o} \sum_{l=0}^{L-1} e^{2\sigma_l{}^2+2\mu_l} \qquad \text{or} \qquad 10\, log_{10}\, (\frac{E_b}{N_o} \sum_{l=0}^{L-1} e^{2\sigma_l{}^2+2\mu_l}) \text{ in dB}$$

The Lognormally-distributed random number generator was set such that $\sigma_l{}^2 = 1$ and $\mu_l = 0$ for every l.

For every incremental 3 dB of the average SNR per bit, the corresponding values of E_b and N_o were found and a trial was performed. Each trial would generate 500 random data bits which were stored into the input data file "datain". The data bits were transmitted over the multipath fading channel which could be modelled as Rayleigh fading or Lognormal fading with two-fold or three-fold diversity. From the output of the equal weight RAKE combiner, the received 500 data bits were detected and stored into the output data file "dataout". The "datain" file then compared with the "dataout" file and the error probability was the number of wrong data bits being detected over 500. The result of the trial was then recorded into the "datares" file. Another trial was repeated in the same way. For low average SNR per bit, that is, when the ratio of E_b and N_o was small, the number of trials to be performed was 400. A utility program was employed for processing the results of different trials which were stored in the "datares" file. The average of 80 trials was evaluated and was considered as one error probability for the particular SNR Therefore, five error probabilities were obtained from 400 trials The mean and variance of the error probability corresponding to the particular average SNR per bit were calculated from those five error probabilities. The variance is indicated in the figures by solid lines with two '+' signs at both ends. In the case of high average SNR per bit, the number of trials to be simulated would be increased. It was found that when the average SNR per bit was extremely high which could result in a very low error probability, many trials should be performed.

Appendix B

This appendix gives an overview on the simulation program of the simplified GL receiver with differentially encoded binary commutation signaling under practical channel estimation. A complete source listings of the simulation program and some utility programs are filed into another separate document.

The program was identical to the one described in Appendix A. The only difference is that the system is under practical channel estimation. The activation of the taps coefficients on the equal-weight RAKE combiner depends on the result of the channel estimation process.

Channel Estimation:

The structure of the channel estimator was shown in Fig. 4.3. The channel estimation process basically required to estimate the path delays. For each delayed path, there would be a corresponding peak appeared at either one of the two matched filters squared outputs ${z_m}^-(t)$ and ${z_m}^+(t)$. During each estimation interval, that is, between kT and $kT + \Delta$, the estimation of the path delays was performed by locating where those peaks were. In the simulations, for two-path fading channel, $\Delta = 1.5\mu s$ and two largest peaks of the two matched filters squared outputs would be located. Similarly, for three-path fading channel, $\Delta = 3\mu s$ and the locations of the three largest peaks of the two matched filters squared outputs would be estimated.

The simulations assumed the autocorrelation width of 5 time resolution units giving $T_c = 0.25\mu s$. Since the number of taps along the equal weight RAKE combiner was equal to $\lceil \frac{\Delta}{T_c} \rceil + 1$, there were 7 taps in the case of two-path fading channel, but only two of them would be activated and 15 taps for three-path fading channel in which three of them would be activated.

During each estimation interval, the two matched filters squared outputs were stored into two different linear arrays which were quantized into slots of 5 time resolution units. The index of the array was the time unit within the estimation interval and the slot number corresponded to the location of the RAKE tap. The location of the first largest peak was searched by examining the contents of the two arrays. Once the largest peak was found, the estimated time delay $\hat{\tau}_0$, which was given by multiplying the index in which the largest peak occurred with T_{res}, and the slot number associated with the peak would be stored. The contents of that particular slot of the two arrays would then be masked to zero so that the next largest peak to be searched would not be on the same slot. This avoids the activation of the same RAKE tap. In addition, the contents above and below 2 time units of the index in which array the largest peak was found would also be masked to zero. This simply removes the entire autocorrelation peak of width T_c (which was equivalent to 5 time units) from the matched filters squared outputs. The same procedure was repeated by examining the two arrays to search for the next largest peak until the necessary numbers of peaks have found.

After the estimation, the stored slot numbers would be used for activating the appropriate RAKE taps and the square of the difference of the estimated path delay and the actual path delay for each delayed path would be evaluated. Suppose that the channel had three delayed paths located at τ_0, τ_1 and τ_2, where $\tau_0 < \tau_1 < \tau_2$ From the channel estimation process, the three estimated path delays were $\hat{\tau}_0$, $\hat{\tau}_1$ and $\hat{\tau}_2$. However, a sorting was done on the three estimated delays so that $\hat{\tau}_0 < \hat{\tau}_1 < \hat{\tau}_2$ The estimated path delays $\hat{\tau}_0$, $\hat{\tau}_1$ and $\hat{\tau}_2$ were then checked to see if any of them matched to any one of the actual path delays, τ_0, τ_1 or τ_2 with the delay difference less than $\frac{T_c}{2}$. If there was such a pair, small estimation error occurred and the square of their difference, ${\epsilon_j}^2$, would be evaluated and stored. The result was then associated with the j-th path delay. In the case when there was no such a pair, the estimated path delays $\hat{\tau}_0$, $\hat{\tau}_1$ and $\hat{\tau}_2$ were matched one-to-one correspondingly to the actual path delays τ_0, τ_1 and τ_2, and the square of their differences, ${\epsilon_0}^2$, ${\epsilon_1}^2$ and ${\epsilon_2}^2$ would be evaluated and stored.

Similarly, for two-path channel estimation, the estimated path delays were sorted such that $\hat{\tau}_0 < \hat{\tau}_1$. The two estimated path delays were checked if any one of them matched to any of the two actual path delays with the delay difference less than $\frac{T_c}{2}$. If no such pair existed, the two estimated path delays were matched one-to-one correspondingly to the two actual path delays τ_0 and τ_1 and the square of their differences would be evaluated and stored.

Simulation Trials:

The simulation procedures followed the same way as what was described in Appendix A. For each trial of 500 data bits, the square of the difference of the estimated path delay with the actual path delay for each delayed path in each data bit detection was evaluated and summed together. Suppose that ϵ_{ij}^2 was the square of the difference of the estimated delay with the actual delay for the j-th path delay in i-th bit detection. For each trial, the sums $S_j = \sum_{i=1}^{500} \epsilon_{ij}^2$ would also be recorded into the "datares" file. For one trial of 500 data bits, the RMS error of the j-th estimated path delay was simply $\sigma_j = \sqrt{\frac{S_j}{500}}$. A utility program was developed to process the results of different trials stored in the "datares" file. The results included the error probability and the RMS error for each estimated path delay.